AFOSR-TR- 83-0610

COLLEGE OF
EARTH AND
MINERAL
SCIENCES

Final Technical Report

LATERAL VARIATIONS IN GEOLOGIC STRUCTURE AND
TECTONIC SETTING FROM REMOTE SENSING DATA

Air Force Office of Scientific Research
Grant No. AFOSR-77-3340

Period of Performance

March 16, 1980 - September 30, 1982

Principal Investigator: Shelton S. Alexander

May 1983

The Pennsylvania
State University

University Park,
Pennsylvania
83 07 26 038

THE PENNSYLVANIA STATE UNIVERSITY

College of Earth and Mineral Sciences

UNDERGRADUATE PROGRAMS OF STUDY
Ceramic Science and Engineering, Earth Sciences, Fuel Science, Geography, Geosciences, Metallurgy, Meteorology, Mineral Economics, Mining Engineering, Petroleum and Natural Gas Engineering, and Polymer Science.

GRADUATE PROGRAMS AND FIELDS OF RESEARCH
Ceramic Science, Fuel Science, Geochemistry and Mineralogy, Geography, Geology, Geophysics, Metallurgy, Meteorology, Mineral Economics, Mineral Processing, Mining Engineering, Petroleum and Natural Gas Engineering, and Polymer Science.

UNIVERSITY-WIDE INTERDISCIPLINARY GRADUATE PROGRAMS INVOLVING E&MS FACULTY AND STUDENTS
Earth Sciences, Ecology, Environmental Pollution Control Engineering, Mineral Engineering Management, Operations Research, Regional Planning, and Solid State Science.

ASSOCIATE DEGREE PROGRAMS
Metallurgical Engineering Technology and Mining Technology.

INTERDISCIPLINARY RESEARCH GROUPS WITHIN THE COLLEGE
Coal Research Section, Mineral Conservation Section, Ore Deposits Research Section, and Mining and Mineral Resources Research Institute.

ANALYTICAL AND STRUCTURE STUDIES
Classical chemical analysis of metals and silicate and carbonate rocks; X-ray crystallography; electron microscopy and diffraction; electron microprobe analysis; atomic absorption analysis; spectrochemical analysis.

SECURITY CLASSIFICATION OF THIS PAGE *(When Data Entered)*

REPORT DOCUMENTATION PAGE	READ INSTRUCTIONS BEFORE COMPLETING FORM

1 REPORT NUMBER AFOSR-TR- 83-0610	2 GOVT ACCESSION NO. AD-A130758	3 RECIPIENT'S CATALOG NUMBER

4 TITLE *(and Subtitle)* Lateral Variations in Geologic Structure and Tectonic Setting from Remote Sensing Data	5 TYPE OF REPORT & PERIOD COVERED Final Report March 16, 1980~Sept. 30, 1982
	6. PERFORMING ORG. REPORT NUMBER

7. AUTHOR(s) Shelton S. Alexander	8. CONTRACT OR GRANT NUMBER(s) AFOSR-77-3340

9 PERFORMING ORGANIZATION NAME AND ADDRESS The Pennsylvania State University University Park, PA 16802	10 PROGRAM ELEMENT, PROJECT, TASK AREA & WORK UNIT NUMBERS Program Code No.: 7F10 Program Element Code: A03291-14

11. CONTROLLING OFFICE NAME AND ADDRESS Air Force Office of Scientific Research Building 410, Bolling AFB, D.C. 20332	12. REPORT DATE May 1983
	13. NUMBER OF PAGES 52

14 MONITORING AGENCY NAME & ADDRESS(if different from Controlling Office) Defense Advanced Research Projects Agency Washington, D.C 20301	15. SECURITY CLASS. (of this report) UNCLASSIFIED
	15a DECLASSIFICATION/DOWNGRADING SCHEDULE

16 DISTRIBUTION STATEMENT *(of this Report)*

Approved for public release; distribution unlimited.

17. DISTRIBUTION STATEMENT *(of the abstract entered in Block 20, if different from Report)*

18 SUPPLEMENTARY NOTES

19. KEY WORDS *(Continue on reverse side if necessary and identify by block number)*

Remote sensing, digital image analysis, wave-number filtering, texture analysis, rock classification, tectonic stresses, nuclear explosions

20 ABSTRACT *(Continue on reverse side if necessary and identify by block number)*

The principal objective of this study was: (1) to assess the usefulness of remote sensing digital imagery, principally LANDSAT multispectral scanning (MSS) data, for inferring lateral variations in geologic structure and tectonic setting, and (2) to determine the extent to which these inferred variations correlate with observed variations in seismic excitation from underground nuclear explosion test sites in the Soviet Union. Soviet, French and U.S. test sites have been investigated to compare their geologic and tectonic responses as seen by LANDSAT. The characteristics of 'granite' intrusive bodies exposed at Semipalatinsk (Degelen),

DD FORM 1 JAN 73 1473 EDITION OF 1 NOV 65 IS OBSOLETE

North Africa (Hoggar), NTS (Climax stock), and an analog site in Maine (Mt. Katadin), have been studied in detail. The tectonic stress field inferred from the tectonic release portion of seismic signatures of explosions in these three areas is compared with local and regional fracture patterns discernable from imagery.

The usefulness of satellite synthetic aperature radar (SAR) to determine geologic conditions and delineate fault (fracture) patterns is demonstrated by the analysis of SEASAT data for an area in the eastern United States.

Algorithms to enhance structural boundaries and to use textures to identify rock types were developed and applied to several test sites.

Final Technical Report

LATERAL VARIATIONS IN GEOLOGIC STRUCTURE AND
TECTONIC SETTING FROM REMOTE SENSING DATA

Air Force Office of Scientific Research
Grant No. AFOSR-77-3340

Period of Performance

March 16, 1980 - September 30, 1982

Principal Investigator: Shelton S. Alexander

May 1983

Table of Contents

SUMMARY

Objectives

The principal objectives of this study were (1) to assess the usefulness of remote sensing digital imagery, principally LANDSAT multispectral scanning (MSS) data, for inferring lateral variations in geologic structure and tectonic setting, and (2) to determine the extent to which these inferred variations correlate with observed variations is seismic excitation from underground nuclear explosions test sites in the Soviet Union.

Specific objectives were to:

(1) Compare the characteristics of 'granite' intrusive bodies exposed at Semipalatinsk (Degelen), North Africa (Hoggar), NTS (Climax stock), and an analog site in Maine (Mt. Katahdin).

(2) Compare the tectonic stress field, hence fault plane orientation(s), inferred from the tectonic release portion of seismic signatures of explosions in these three areas with local and regional fracture patterns discernible from imagery.

(3) Evaluate the usefulness of satellite synthetic aperture radar (SAR) to determine geologic conditions and delineate fault (fracture) patterns.

(4) Evaluate the geologic and tectonic setting of other selected areas.

Results

The work on this project was initially focused on the Semipalatinsk and Novaya Zemlya test sites. More recently, three additional test sites have been studied: Azgir (USSR), the French test site in North Africa (Hoggar granite), and NTS (Climax stock). The Azgir site is important because its geologic setting is in an area of salt dome structures, and the French and NTS

sites because they may be good analogs of the Degelen granite at Semipalatinsk and their characteristics are well-documented. Concurrently, we assembled geologic and tectonic maps of the test sites as well as pertinent geological and geophysical publications. After a period of familiarization to correlate visually features on the imagery with salient ground features, we commenced the digital processig of these test sites with the two central objectives of (1) developing the ability to distinguish various rock types, soils, and vegetation and (2) determining the extent and characteristics of fracture and other tectonic features.

For the rock exposures (approximately 60% of the area) and soils at Semipalatinsk, we have been able to obtain a large number of spectral signatures using supervised, and unsupervised classification for approximately 60 selected training areas. By performing canonical analysis and examining class separation on the principal canonical axis, we have found that the signatures separate into two main groups, igneous plutonic rocks (mafic and acidic) and country rock complexes consisting of ligh-colored alluvium, medium grey to dark grey soils, and sedimentary rocks (e.g., limestone) plus vegetation. Characteristic signatures of each of these features are obtained such that similar geologic responses elsewhere in the region can be mapped. It is noteworthy that among the four LANDSAT bands (4,5,6,7), band 5 is the best single channel for discriminating igneous plutonic rocks from country rocks. We also have derived analogous characteristic signatures from the band ratio images (4/5, 4/6, 4/7, 5/7, 6/7) using canonical analysis and we find a comparable separation among the principal geologic features. Band ratios 4/6 and 4/7 together give the best discrimination of igneous plutonic rocks.

A similar analysis of the geologic features of southern Novaya Zemlya has been carried out using an excellent cloud-free scene (1363-07475) taken on 21 July 1973. The geologic units (folded Paleozoic sedimentary rocks) and scattered intrusive igneous bodies could be mapped and fault contacts identified. The agreement of these results with available ground-based information was confirmed in discussions with USGS scientists studying this area.

Visual analysis of imagery for the Azgir test site shows that salt dome structures can be discerned and that surface lineaments can be seen at Azgir that correspond to buried faults documented previously only through ground-based geophysical surveys.

The French test site in North Africa, specifically the Hoggar granite and surrounding structures, has been analyzed. Our initial results indicated a close correspondence in spectral signatures between the Hoggar and Degelen granite bodies, suggesting that characteristics of Degelen may be inferred from the detailed information available for Hoggar. Distinctive fracture patterns are clearly seen, including one that trends approximately N38E and corresponds to the best-fitting fault strike inferred by Harkrider for the tectonic release associated with the largest of the French explosions.

In addition to the mapping of geological units based on the training results from reflectance classification, we have investigated different texture analysis algorithms for rock type identification. One method derives textural parameters from an analysis of variability in a 3x3 or 5x5 array of pixels around each central pixel in a training area and the other compares the power in different portions of the wavenumber spectrum of the training area. In turn, these texture "images" were combined with individual LANDSAT channels

to improve rock-type discrimination. Results have been obtained for the test sites individually and comparisons were made among the Semipalatinsk, French, and NTS site granite bodies. In general, texture measures contribute significantly to rock-type discrimination. While there are discernable differences among the granite signatures for the three sites, they all are similar and distinctive with respect to surrounding lithologies. Preliminary results for an analog site in Maine Mt. Katahdin indicated signatures similar to the granites at the three test sites and distinct from surrounding rock types.

Analysis of structure features (fractures and faults) was carried out using both wavenumber spectra and strike-selective filtering algorithms developed in this study. For a given area, the dominant strike directions and dominant spatial scale of ground features can be obtained readily from the wavenumber spectrum. Enhancement and location of features having a specified strike direction and/or spatial scale is achieved by the strike-selective filtering. The software was modified to handle larger areas, because previous programs for two-dimensional Fourier transforms limited the size area that could be analyzed.

We have also merged SEASAT synthetic aperture radar (SAR) imagery with LANDSAT and ground-based geological and geophysical information for an experimental study area (Pennsylvania) in an attempt to gain additional capability to map lithologies and structural features. The SAR data provide independent information and are especially sensitive to surface texture. Analysis of NTS structures using combined SAR and LANDSAT imagery was initiated towards the end of the grant; it is clear that the SAR data are very helpful in delineating structures.

The combined use of multiple types of geophysical and remote sensing observations is highly desirable for many types of problems in geophysics and geology. An initial effort to combine LANDSAT, SEASAT (SAR), and ground-band geophysical and geological observations for a unified interpretation is discussed in the recent geophysics thesis by Ravenhurst (1980) completed under this grant. This integrated approach needs to be developed further especially with regard to making spatial registration to a common map base easy and to incorporate interactive graphic display capabilities to facilitate interpretation of these diverse data sets. Four theses have been completed under this grant. More details concerning the results of this investigation can be found in the following publications and the Appendix.

References

Baumgardt, D. and S.S. Alexander, Multispectral and Spatial Wavenumber Analysis for Pattern Recognition of Lineaments on Digital MSS Satellite Data, The Pennsylvania State University, April 1981. (Submitted to IEEE Remote Sensing.)

Parker, R.P., Application of Texture-Tone Analysis of LANDSAT Data to Geologic Exploration, B.S. Thesis, Allegheny College based on research conducted at The Pennsylvania State University, 1980, 69 pp.

Ravenhurst, C.E., Utility of Digitally Merged SEASAT-A, LANDSAT MSS, and Magnetic Field Data Sets sfor Mapping Lithology and Structure in a Vegetated Terrain, M.S. Thesis, The Pennsylvania State University, 1980, 132 pp.

Sartell, J.F., A Remote Sensing Characterization and Comparison of the Semipalatinsk Area of the Soviet Union and the Geologically Analogous Mount Katahdin Region of North-Central Maine, The Pennsylvania State University, M.S. Thesis, November 1982.

Ng, C.Y., Combined Use of Wavenumber Analysis of Landsat Digital Imagery and Seismic Data to Infer the Orientation of Tectonic Stress in the Hoggar Region in Africa, M.S. Thesis, August 1983.

APPENDIX

MULTISPECTRAL SPATIAL WAVENUMBER ANALYSIS

FOR PATTERN RECOGNITION OF LINEAMENTS ON

ON DIGITAL MSS SATELLITE DATA

Douglas Baumgardt

and

Shelton S. Alexander

The Pennsylvania State University
Geophysics Program
403 Deike
University Park, Pennsylvania 16802

April 1981

ABSTRACT

Techniques of spatial wavenumber analysis have been applied to digital MSS (Multispectral Scanner) Landsat imagery of South Mountain region in eastern Pennsylvania in order to determine the number, orientation, density, and location of lineaments. Fourier transforms of the two-dimensional digitized scenes are computed individually for each of the four Landsat bands. The Fourier power spectrum provides a coding of the density and orientation of the lineaments and the phase spectrum contains information about the relative positioning of the lineaments spatially. The two-dimensional power spectra of the different bands show that the wavenumber properties of each band differ due to variations in spatial contrasts in ground reflectance and dynamic range in the different bands. Moreover, the effects of scan line banding, ridges and known lineaments can be clearly resolved. Fourier analysis of images preprocessed by means of canonical analysis provides a means of studying the wavenumber properties of the spectral signature obtained in multispectral images. Directional or fan filtering has also been implemented to separate and enhance or subdue features in different orientations. This method, when applied to the South Mountain band 7 (0.8 - 1.1 mm) image, clearly delineates the known lineaments and reveals the existence of at least two previously undetected lineaments.

APPLICATION OF TEXTURE-TONE ANALYSIS
OF LANDSAT DATA TO GEOLOGIC EXPLORATION*

by

Raymond P. Parker

*B.S. Thesis, 1980, Allegheny College based on research conducted
at The Pennsylvania State University

ABSTRACT

Digital LANDSAT data from computer compatible tapes were applied to the problem of rock type discrimination in three nuclear test sites, in the United States, Africa, and the Soviet Union. Three preprocessing enhancements are done on all the data; contrast stretching, band ratioing, and principal components transformation. Two supervised feature extraction algorithms are analyzed; a tone extraction algorithm (STATS) and a texture extraction algorithm. The texture extraction algorithm is based upon Hsu's Texture-Tone Variables Model I. Four-band tone and seventeen-variable texture "signatures" are extracted using multiple training sites for each classification category. The tone signatures are normalized to unit vectors and combined into a mixed-image composite file. The textural signatures extracted with Hsu's measures were combined into a composite file without further modification.

The qualitative assessment of the power of the feature extraction algorithms in rock type discrimination is tested by multivariate, linear discriminant analysis (U.C.L.A's BMD07M). The texture algorithm proved more effective in discriminating the lithologies studied. The data set as transformed by the principal components technique proved most successful. Spectral reflectance characteristics of specific rock types typically show wide variation due to weathering, soil cover, and vegetation cover. This results in overlap of tone charactistics of most rocks. Principal component textural signatures successfully discriminate the differences between granitic intrusives and colluvium.

CONCLUSIONS AND SUMMARY

Two different feature extraction algorithms were applied to the problem of rock type discrimination in three nuclear test sites, in different regions on the earth. A multivariate linear discriminant analysis algorithm was applied to the extracted features to determine whether this technique can differentiate lithologic types based upon the algorithm-extracted features. The results of these assessments are summarized on a number of canonical scattergrams produced by the linear discriminant algorithm.

The feature extraction algorithm which employed spectral signatures alone does not seem to be an effective discriminator of rock types. Its inability to recognize similar features is largely a result of being based upon the spectral signatures only. This conclusion is largely supported by the linear discriminant algorithm. Moreover, texture variable number 1 is roughly the equivalent of the spectral signature extraction algorithm (STATS); it is noted that the linear discriminant algorithm never selected variable number 1 as its best discriminating variable. Therefore, it is not the perferred feature-extraction method in this study.

Texture proved to be the most powerful discriminator for rock type. Variables 8, 12, and 13 from Hsu's Model 1 texture algorithm are the most informative measures, out of the total

17 included in Model 1. On the average two of the seventeen texture variables were not chosen by the linear discriminate because they did not provide enough information.

Features extracted from the principal component images proved to be more informative than either the raw images, or the ratioed images. The reduction in the dimensionality of the data set seemed to have the effect of removing nonessential information.

Based upon the canonical scattergrams of the NTS texture signatures all three lithologic rock types were clearly discriminated. Further, based upon a composite file of textural signatures of similar rock types from different geographic regions, the canonical scattergrams illustrated that similar rock types were positively associated by their similar textural signatures, and that different rock types could be distinguished by differing, diagnostic textural signatures.

Based upon the positive conclusions of this study, the next step for further study is the development of an algorithm which can be 'trained' to recognize different lithologies on the basis of diagnostic textural signatures for each given lithology.

The Pennsylvania State University

The Graduate School

Department of Geosciences

Utility of Digitally Merged Seasat-A SAR,

Landsat MSS, and Magnetic Field Data Sets

for Mapping Lithology and Structure

in a Vegetated Terrain

A Thesis in

Geophysics

by

Casey Edward Ravenhurst

Submitted in Partial Fulfillment
of the Requirements
for the Degree of

Master of Science

November 1980

I grant the Pennsylvania State University the
nonexclusive right to use this work for the University's own
purposes and to make single copies of the work available to
the public on a not-for-profit basis if copies are not
otherwise available.

_____
Casey Edward Ravenhurst

ABSTRACT

Remotely sensed data from each part of the
electromagnetic spectrum contains potentially different and
independent information about the earth's surface and
subsurface. Interpretation of these different data sets,
together with conventional geophysical and geological
information, is greatly facilitated by merging all the data
sets such that each (spatial) resolution element has
associated with it an n-dimensional vector composed of
information from each of the n data sets. In this study,
Landsat MSS, Seasat-A Synthetic Aperture Radar (SAR), and
magnetic field data from the South Mountain area west of
Gettysburg, Pennsylvania, were registered to match each
other in spatial position, and merged. Pattern recognition
techniques were then applied to the composite data set to
determine its utility in recognizing different rock types
and structures in vegetated terrain around South Mountain.
The SAR imagery was filtered in order to reduce its
directional dependence. Principal components analysis was
used to decrease the dimensionality of the entire data set.
A texture algorithm was then applied to the first two
principal axes, and later to the third axis, in order to
enhance various geologic features. Next, the contribution
of each data set and texture measure to the separability of
rock type classes in the training area was evaluated.

A classification of the entire study area was then done using the enhanced data that contributed the most to the separability of classes.

The texture measures were found to emphasize the geologic information in the data and thus increase the separability of the rock type classes. The best classification was obtained when texture measures from each of the first three principal component axes were merged with the magnetic field data. About 40% of the area was classified as having the same rock types as the geologic map showed. The confusion of rock type classes was due to the large amount of variance within each class when compared to the between-group variance. The variance is thought to originate from three sources; registration errors, the heavy vegetation cover, and systematic noise in the SAR data.

A test of the correlation between SAR tone and texture, Landsat tone and texture, and magnetic field data, revealed no tone or texture measures linking any two of these original data sets.

The magnetic field data showed a 60% correlation with the surface geology of the area, and about 20% was correlatable with the known subsurface geology. In contrast, the satellite data was related only to the surface characteristics. Thus, the merged data set contained mainly surface information, but had a small component of subsurface information.

CHAPTER V.

DISCUSSION AND CONCLUSIONS

Discussion

Seasat SAR records information about the earth's surface that is very different from that recorded by Landsat and by other sensors (Figure 1). The SAR representation of the surface is strongly effected by layover and foreshortening, which can be corrected for with an independent data source, such as the topography of the surface. Even with topographic data, the registration of the SAR data to the true surface location must be accomplished before appropriate corrections can be made. In this study, registration of the SAR data to the Landsat data was done without applying a topographic correction to the SAR data. A relative registration accuracy of 1 kilometer or better was obtained, which is rather poor and more work needs to be done to increase the registration accuracy. An absolute measure of accuracy was not possible. The effects of layover and foreshortening contributed significantly to the registration inaccuracies (see Appendix A). In the South Mountain area, the total elevation difference is 1100 feet, resulting in a geometric error, due to foreshortening, of 1 kilometer (Appendix A, Figure 47). Because this elevation difference does not occur at one location, a registration

accuracy much better than 1 kilometer should be possible. The rubbersheet stretch of the SAR data (to fit the registration points), is the best average correction of layover and foreshortening that is possible.

The effect of the subsurface rock types on the magnetic field at the surface was found to be substantial. Filtering to remove the effect of deep sources was not attempted due to the similarity of deep strong sources and shallow wide sources. Thus, great care must be exercised in using magnetic field data to determine surface lithology. Once the surface lithology has been determined though, the magnetic field data may provide great insight into the structure of the subsurface.

A comparison of the information content of each of the data sources was made by testing the correlations among them. It was found that the SAR data is unique and cannot be derived from Landsat MSS data. The texture measures most significant in separating the rock type classes may be correlated when they are derived from the same principal component axis, but they are not correlated when derived from different axes. The magnetic field data is not strongly correlated with any of these texture measures. Each principal component and magnetic field represents a unique data set describing a different aspect of the surface and/or subsurface of the earth.

The addition of the SAR and magnetic field data sets to
the four Landsat channels, greatly increased the
separability of rock type classes in the training area.
These two extra data sets provided unique information about
the geology that was not available from the Landsat channels
alone. The Seasat SAR appears to penetrate the vegetation
canopy and interact with the surface material. However, the
vegetation affects the SAR signal to some extent. The
magnetic field data definitely contains subsurface
information. But, even the addition of these two
independent data sets could not completely solve the
difficulty inherent in identifying lithologic units in
vegetated terrain. The large variance within each class
(especially of the SAR data) due to the masking effect of
the vegetation, resulted in a within-category standard
deviation that, in the final classification, was at least of
the same order of magnitude as the separation between
categories.

Principal component transformation and then generation of
texture measures from the principal axes were used in an
attempt to increase the classification accuracy. The 5
texture measures that accounted for essentially 100% of the
variance in the data sets were written to tape and used in
the final classification. The texture measures showed
slightly more normal distributions as predicted by Hsu
(1979), in all but one of the channels and thus were more

suited to the minimum distance classifier used. Even after
all these attempts at increasing the separability of the
classes, a very poor classification accuracy was obtained
(Figures 35 and 37).

The stepwise discriminate analysis program BMD07M found a
good separability between the mean values of the training
areas, as indicated by the encouraging results obtained by
comparing the confusion matrices and scattergrams during
each step of the feature extraction. An explanation for
this must include the fact that the BMD07M program used only
the mean signatures within each training area. The large
variance must occur not between the mean values of the
training areas belonging to each class, but within each
training area itself. The main source of this variance was
probably the SAR data set due to its large "noise equivalent
difference in the scattering coefficient ($NE\Delta\sigma_0^-$)" and
coherent speckle (see Appendix A). Registration errors may
also have contributed significantly. A solution would be to
classify the average of a small area and assign a rock type
symbol to the center pixel. This would tend to decrease
both the noise within the SAR data and the effect of
registration errors.

The SAR data at 25 meter resolution has a very large
"noise equivalent $\Delta\sigma_0^-$ ($NE\Delta\sigma_0^-$)", which is the least
detectable difference in the scattering coefficient (see
Appendix A). This limits the number of gray levels that can

be resolved to about seven. Closer spaced gray scale levels are lost in the noise. Spatial averaging increases the number of resolvable gray levels as well as decreasing the $NE\Delta\sigma_0$ such that a more accurate representation of the surface is obtained.

Another major source of variance in the SAR data could be coherent speckle (see Appendix A). Speckle introduces false texture into the SAR image so that only texture coarser than this systematic component is real surface texture. Spatial averaging will decrease, but not eliminate, the effects of speckle. Because the final classification used a data set created from texture measures, coherent speckle was undoubtedly a contributor to classification inaccuracies.

The variance in a data set in which training areas have been chosen can be separated into two types; between-group variance and within-group variance. The usefulness of a data set is determined by the ratio of the two variances - the F-statistic. For the SAR data, conflicting results were obtained. In the magnetic field area, where small training areas were used, the average SAR variable within each area was less significant than the magnetic field variable and most of the Landsat variables (Table 12). In the larger survey area though, where larger training areas were used, the SAR variable was the most significant. This illustrates the effect of spatial averaging on the usefulness of the SAR data set. In this study, spatial averaging was not carried

out as one of the initial steps. Instead, every third data value was used and some information was thus lost. However, spatial averaging was achieved to some extent during the filtering process which removed the directional dependence of the SAR data.

The first attempt at classification of rock type classes did not utilize principal component axis 3 in any way. This component does nevertheless outline the linear features, as well as the structural and major geologic units of the area (Figures 15 and 17).

The striking differences between the Blue Ridge province and the Triassic Basin to the east (Figure 15) may be due to different landuse practices. Topographic maps show a transition from mainly forested land in the Blue Ridge to predominantly agricultural land in the Triassic Basin.

A comparison of the texture measures derived from axis 3 with the texture measures from the other two principal component axes, revealed that texture measure 14 would be significant in increasing the separability of the rock type classes. By using this texture measure as well as 3 texture measures from each of principal component axes 1 and 2, plus the magnetic field data, a much better classification was achieved (Figure 38).

Conclusions

This study includes an extensive amount of software development to introduce SAR data processing capabilities at the Pennsylvania State University. Computer programs were written or modified to filter the SAR data and put it in the ORSER format (used in the processing of Landsat MSS data). Programs were also written to cast the magnetic field data into this format. The SAR data could then be merged with Landsat MSS and magnetic field data. The texture measures of Hsu (1979) were tested on the merged data set and were found to contribute significantly to a reasonably good (40%) rock type classification.

By merging all the data sets, the significance of each variable to the separation of rock type classes could be easily tested and compared. The most significant variables were used in the final classification. In future analyses, other geophysical data such as gravity, resistivity, electromagnetic, and seismic velocity observations, could be included in the data set in a manner analogous to that used for the magnetic field intensity data in this study. Remote mapping of lithology and structure in heavily vegetated terrain may be improved with better registration of the SAR data to Landsat MSS data, spatial averaging of the SAR data to reduce its noise content, and inclusion of as many independent data sets as are available. By including the

surface-mapped geology of an area as one of the data sets,
an analysis of the relationship(s) between surface and
subsurface geology and structure could be undertaken.

The Pennsylvania State University

The Graduate School

Department of Geosciences

A Remote Sensing

Characterization and Comparison of the

Semipalatinsk Area of the Soviet Union

and the Geologically Analogous

Mount Katahdin Region of North-central Maine

A Paper in

Geophysics

by

Jonathan Floyd Sartell

Submitted in Partial Fulfillment
of the Reqirements
for the Degree of

Master of Science

November, 1982

Jonathan Floyd Sartell

ABSTRACT

Multispectral remote sensing data have been used to perform local and regional characterizations and comparisons of the Semipalatinsk area of the Soviet Union and the geologically analogous Mount Katahdin region of north-central Maine. A thematic mapping of local exposed lithologies and various other cover types over the Degelen and Katahdin plutons was completed as part of an effort to make a quantitative comparison of the geological and geophysical "signatures" of these two plutons. Texture transforms of data for the two study areas were calculated to 1) aid in rock type discrimination over the Degelen massif and 2) make a textural comparison of the surficial characteristics of the granite exposures. Other methods of comparing the spectral characteristics of the two plutons included means difference testing of raw, texture and band-ratio category means, and a graphical analysis of their respective spectral response distributions. Digitally enhanced color imagery was produced for the two regions to 1) offer a visual display of statistical transformations used to optimize rock type discrimination, and 2) map regional geologic variability and major tectonic features as a means of further testing the degree of geological and tectonic comparability of the two regions.

Granite and rhyolite outcrops in Maine were somewhat confused due to a persistent chlorophyll spectral influence, but various vegetative cover types mapped distinctively. Similarly, certain granite categories on the Degelen Massif mapped in a distinctive manner, but their responses were influenced to some extent by a characteristic light vegetation cover. Texture measures calculated from the first principal component axis improved the discrimination of bedrock and colluvium in

the Degelen area. A comparison of tonal and textural features showed the Degelen and Katahdin granite outcrops to be roughly similar in the infrared spectral region, while Maine rhyolite outcrops and Degelen granite detritus demonstrated a relatively high degree of textural similarity.

An analysis of enhanced imagery highlighted major similarities and differences in the geologic and tectonic regimes of the two areas. Fault patterns were denser and apparently younger in the Soviet region. Other geophysical data were also analyzed for the Katahdin region as a means for postulating possible geophysical responses of the analogous Degelen features, and to infer subsurface variability in that region.

The enhanced imagery showed the two study areas to possess similar geologic variability, but to differ in fault pattern and fracture density. Especially notable was the degree of fracturing of the Degelen Massif, and the possible implications on seismic source coupling this condition presents. A reasonable estimate of the lateral geologic and tectonic variability of the Degelen site was possible from remote sensing data alone. These results, coupled with geophysical models derived from analysis of Maine data, place some constraints on the expected variability of geophysical properties of the subsurface of the Degelen region.

CHAPTER V

DISCUSSION AND CONCLUSIONS

Discussion

Characteristics of the study areas. The usefulness of Landsat multispectral data in the spectral characterization and thematic mapping of lithologies over two study areas has been investigated. Interest in the Soviet Union study area, and in the Degelen Massif in particular, has arisen by virtue of its role as an active nuclear test site. The Mount Katahdin region of north-central Maine was chosen by other investigators as a site geologically and tectonically analogous to the Soviet area. Investigation of the Maine area is useful for the proper understanding of the tectonic setting of the Degelen region, which is necessary for improved quantitative interpretation of seismic signatures from seismic monitoring of buried nuclear explosions in that area.

The Katahdin and Degelen areas are both located in tectonic fold belts, where Paleozoic (and some Mesozoic in the USSR region) sediments and interbedded volcanics have been folded, faulted, and subsequently intruded by granites. The Katahdin and Degelen granites are themselves similar in that they are both biotite granites high in quartz and feldspar, and are broken by numerous aplitic dikes (Hon, 1980 and Kropotkin, 1945). Surrounding lithologies are similar, with sediments and volcanics of Silurian, Devonian and Cambrian age occurring (Figures 10 and 41).

However, there are differences, some of which play an important

part in lithologic discrimination and comparison of categories between these two areas. Climatic differences are readily apparent on Landsat imagery. The Degelen region (Plate 7) is a comparatively arid one, and seemingly devoid of vegetation over large areas. Signs of mechanical weathering are numerous, for example the alluvial fan on the eastern border of the Degelen massif (Plates 8 and 10). The Maine imagery (Plates 2 and 3) exhibits a much more temporate climate with fairly dense forestation prevalent. Both chemical and mechanical weathering have played a role in influencing the topography of that area. The coarse-grained granite facies of the Katahdin Batholith and others like it are relatively easily eroded and form topographic lows over the region, some now occupied by lakes. However, the fine-grained Summit facies of the Katahdin Granite has remained prominent.

Glacial process have carved the face of the mountain creating the sharp ridges and steep slopes it presently exhibits. Varying thickness of glacial till blanket the area (Caldwell, 1972). Topography of the Degelen Massif, although prominent, is much more fault-controlled as evidenced by Plates 8 and 9. There are no readily visible signs of glaciation in the latter region.

The number of lithologic exposures in the two areas differs greatly for the above reasons. Large expanses of the Degelen region (appearing blue on Plate 7) are apparently free of vegetation, and presumably fresh exposures of both bedrock and unconsolidated material are widespread. On the other hand, the only exposures of any kind in the Katahdin region are mountain peaks above treeline (Mount Katahdin, Traveler Mountain, and others) and man-made clearings. Many of the mountain slopes, moreover, possess a surficial lichen encrustation.

These climatically induced features pose a significant problem in comparing the two areas using Landsat spectral bands. However, there are several common characteristics of the responses for the granitic bodies in the two areas.

Use of Landsat MSS data. A number of ramifications for the use of Landsat multispectral data must be understood prior to its use in a project similar to this one. The four banks of sensors, each collecting data over a separate spectral region (Figure 4) average the spectral response over an area approximately one acre in size on the Earth's surface. Objects smaller than that which contrast sharply with their surroundings will influence the response for the entire picture element. Only the very surface of the Earth is observed, and these observations are a function of several factors. For soils, humus, iron, and moisture content greatly influence the reflectance (Verstappen, 1977). Vegetation over the soil obviously alters the appearance, and this in turn is influenced by the chlorophyll content of the vegetation. Rock exposures vary in spectral response with the degree of alteration by chemical and physical processes, with lichen encrustation, and with grain size (Salisbury and Hunt, 1974).

Certain problems are encountered when performing a detailed analysis of these multispectral data. The sensors aboard Landsat detect fairly wideband radiation in a spectral region which is not the most favorable for lithologic discrimination. One of the principal uses for which the satellite was originally intended is presumably the mapping of vegetation, as the sharp inflections of the chlorophyll spectral curve in the 0.5 to 1.1 micrometer region (Figure 3) coincide with the sensor bandwidths chosen for Landsat (Figure 4). The spectral responses of

many lithologies are not diagnostic in this region. Bandwidths identified as better suited for the differentiation of exposed rocks are, arranged by capability, the 1.18 to 1.30, 4.50 to 4.75, 0.46 to 0.50, and 1.52 to 1.73 micrometer regions (Siegrist and Schnetzler, 1980). Even if these more favorable bands were available, rock surfaces may be obscured by glacial till, a soil horizon, vegetation, or some material totally unrelated to the composition of the underlying lithology. With the addition of complex topographic conditions, further perturbations of the reflectances of the material in question come into play.

The scenes, as a result of these conditions, were analyzed in slightly different manners. In the Maine regions, the Landsat sensors viewed mainly the effect of chlorophyll, therefore rock outcrops and similar clearings were plainly visible, although still spectrally tainted by the photosynthetic agent. Other areas had both a covering of till and vegetation and since the forest types mapped fairly distinctively, a geobotanical analysis was useful in delineating several geologic contacts (Plates 16 to 18). Deciduous growth, apparently more sensitive to lithologic variation, appears purple on Plate 17 and light gray on Plate 18.

Over the Soviet region, chlorophyll played less important, but still noticeable, role. Although its effect on response means of the categories chosen was far less (compare Tables 7, 9 and 10), granite plutons in the region were highlighted by their reddish hue on the false color composite (Plate 7), an indication of at least light vegetation cover. Granites 1 and 2 of Table 10 demonstrate the mild chlorophyll spectral influence, which may be more properly gauged by the

"vegetation" group statistics in that same table.

Thematic mapping. The thematic mapping performed on the Maine scenes illustrated the strengths and limitations of the Landsat sensor and of the classification procedure used. Forest types, divided into deciduous and two coniferous categories, mapped in a distinctive manner, demonstrating sensitivity of the Landsat sensors to chlorophyll reflectance. Rock types, although easily distinguishable from forest and most other categories, were confused with each other and occasionally with forest clearings of uncertain surface type. One example of this was the area to the south of Mount Katahdin on Plate 5, which is perhaps the Baxter State Park headquarters location. The limit on category numbers for the classification resulted in seemingly different targets being cross-classified. Slope granite and cloud were an example of this, and the problem stemmed from the brightest group of responses being classified into the closest group, which was slope granite. An additional problem was the high population variance of the bright granite categories, which at times would have caused the population to encompass cloud picture elememts.

In the Degelen scene, classification success was gauged in a different manner due to the less prevalent vegetation cover. Granites were separable from other lithologic categories, partly on the merit of a sparse vegetation cover (see Granites 1 and 2, Table 10). Detritus distributed around the massif was linked to its probable parent material by the classificaton, and the volcanics were easily distinguishable from the granites mainly due to the volcanics' low albedoes. However, these were confused with other low-albedo deposits to the west of the massif (Plate 6). Burned areas and dark volcanics were also confused, but it

is possible that similar conditions existed at both sites.

Texture transforms. Due to limitations in the use of   .1
characteristics in the discrimination of cover types, and to the common
non-normality of pixel populations (which inhibits classification
accuracy), a number of texture measures have been devised (Hsu, 1978).
Quite often, the human eye distinguishes an object by the spatial
variability of surface point reflections from that object, and not
merely by its color. It stands to reason, therefore, that a textural
transformation should aid in the discrimination of lithologies that may
be of a similar hue, but different surface texture.

Problems encountered in enlisting texture were twofold in this
study. First, the coarse spatial resolution of the Landsat sensors
precludes a sufficiently characteristic measurement of the true textural
qualities of a target surface. Second, to maintain proper fidelity of
the textural measurements, which may differ slightly from category to
category, it was necessary to utilize transformed data in a large
integer format. This made a classification of texture data using the
ORSER software impractical.

Textural differences between lithologic types were successfully
enhanced by these transforms. Bedrock and Tertiary deposits, to a first
order distinguishable by the eye, were further separated by a textural
transformation, as demonstrated by a stepwise discriminant analysis.
The variables most useful for discriminating groups were identified on
the basis of their F-statistic and compared with those identified in a
similar manner by another researcher (Parker, 1980).

A comparison of texture variables of the Katahdin and Degelen
granites and spalls using the BMDP7M classification matrices and

scattergrams demonstrated certain similarities between these groups. The Traveler Rhyolite and Degelen granite detritus groups were found to be overlapped, as were a smaller proportion of the Katahdin and Degelen granites. Spalls were shown by the same tests to be a distinct group. It is very possible, therefore, that the rhyolite slopes, and to a lesser degree, the granite slopes of the Maine region share similar textural characteristics with the granite detritus surfaces of the Degelen Massif. That is, surface "roughness" on the scale of one acre is comparable in the two areas.

Statistical tests. The BMDP7M stepwise discriminant analysis program was a useful tool in judging category separation, whether the variables used were raw data, or texturally transformed data. From these tests, it was possible to detect an improvement in discrimination between bedrock and colluvium categories. The t-test was also useful for determing the comparability of groups based upon one variable.

Digitally enhanced imagery. The use of digitally enhanced color imagery offered an improvement over simple classification in three primary ways. One obvious advantage is the number of color tones available as opposed to distinguishable gray tones on a black and white image. Many more than just eight categories could be seen on the color imagery and gradational changes between features were visible. Overall scene contrast could be raised or lowered, depending on the analysis chosen (Plates 1 and 7). Secondly, the images incorporated a very large area, so that an understanding of the spatial distribution of identifiable features was feasible, as well as a correlation with previously mapped geology. Thirdly, the ability to combine three

preliminary images into one final composite was very useful. An example of this was the ratioed data, which was demonstrated by the DISCRIM classification matrix tests to be of little statistical help in lithologic differentiation. However, the combination of three ratioed images produced final images of both study areas that offered some of the best correlation with known geology. This was especially the case for the Mount Katahdin area.

Geophysical implications. Regional gravity data over northern Maine demonstrates a characteristic behavior over felsic intrusions, of which Mount Katahdin is an example (Figure 9). Gravity lows are located over these plutons because of the relatively low density of their constituent minerals. Mafic plutons, however, exhibit a higher density thereby producing positive anomalies. Magnetic anomalies over the intrusive bodies are more irregular and respond mainly to the magnetite content of the metamorphosed country rock adjacent to the batholiths, and to tabular volcanics interbedded with steeply dipping sediments of the region (Figure 16).

The lack of comparable geophysical data for the Soviet site prompts us to postulate theoretical responses of the similar lithologies of that area. Gravity lows would probably be found over the Degelen Massif and its counterparts, as their constituent minerals are similar to those comprising the Maine igneous bodies. Analogous magnetic anomaly patterns perhaps can be inferred, since regional lithologies are comparable with some volcanic bodies around the plutons. Linear magnetic features should follow the trend of fold axes. Specifically, at Degelen they should trend in a southeast-northwest direction. The magnetic response over the Degelen Massif itself would most likely be

dominated by the Devonian volcanics on its eastern margin (Figure 10).
A magnetite deposit, worked in the last century (Kropotkin, 1945) would,
of course, highly influence magnetic patterns near the pluton. Magnetic
and gravity profiles together likely could be used to infer the geometry
of the plutons at depth, if they become available in the future.

Analysis of enhanced imagery demonstrated some regional similarity
between the two sites, but there are important differences between the
Katahdin and Degelen granites. Fault patterns in the Degelen area are
of higher density, with at least one currently active. Fault patterns
in Maine are sparser and apparently inactive. The Degelen Massif
exhibits widespread fracturing which can affect source coupling of
nuclear detonations occurring in the granite. The Katahdin pluton, on
the other hand, shows a relative lack of faulting although jointing of
the granite is a predominant feature. The regional lithologic
variability defined by this remote sensing analysis, coupled with
gravity and magnetic data over similar features in Maine, provides some
constraints on the lateral variability of geophysical and geological
properties at depth.

Conclusions

Results of this study have shown that:

1) Remote sensing data are useful in detecting regional
   geologic variations in the Semipalatinsk region of
   the USSR and the Mount Katahdin area in Maine.

2) Enhanced imagery (e.g. density-sliced band
   combinations, band ratios, principal component
   transformations, and contrast-stretched bands)
   produced a visual contrast between surface terrains
   that aided greatly in mapping the location of Soviet
   plutons and in delineating faults and regional
   geologic contacts in both the Semipalatinsk and Maine
   area.

3) Analyses demonstrated a textural similarity between
   Katahdin and Degelen igneous rock outcrops, but also
   showed the Degelen spall to possess distinctive
   textural characteristics different from surrounding
   parent rock units.

4) Regional fault patterns are comparable for the two
   regions; however, fracturing is a feature more
   characteristic of the Degelen Massif than the
   Katahdin Pluton.

5) Geophysical, geological, and tectonic parallels
   between the Degelen and Katahdin fold belt regions,
   substantiated by remote sensing observations, provide
   some constraints upon expected geophysical and
   geological variability of the subsurface of the
   Degelen area.

The Pennsylvania State University

The Graduate School

Department of Geosciences

Combined Use of Wavenumber Analysis of

Landsat Digital Imagery and Seismic Data

to Infer the Orientation of Tectonic Stress

in the Hoggar Region in Africa

A Thesis in

Geophysics

by

Carolyn Yee-han Ng

Submitted in Partial Fulfillment
of the Requirements
for the Degree of

Master of Science

August 1983

I grant The Pennsylvania State University the nonexlcusive
right to use this work for the University's own purposes and
to make single copies of the work available to the public on
a not-for-profit basis if copies are not otherwise available.

                                            _____
                                             Carolyn Yee-han Ng

ABSTRACT

Spatial wavenumber analysis of multi-spectal scanner Landsat images has been used to study the orientation and location of structural lineaments in the region of the Hoggar massif in southern Algeria, Africa. Fourier transforms of two-dimensional digital scenes are computed for each of the four Landsat channels. The Fourier amplitude and power spectra provide information on the spatial density and orientation of the lineaments. Other image enhancement and extraction techniques such as principal components and cluster analyses have been used either individually or in combination with the wavenumber analysis to map lineaments which may be related to significant geologic and tectonic features. All results are compared to a previous photointerpretation of the imagery and to available seimic observations on the mechanism of "tectonic release" associated with nuclear explosions detonated in the Massif.

Major results are in agreement among the wavenumber analysis, photointerpretation and seismic observations. In particular, the N38 E strike-slip fault inferred by Harkrider (1976) from analysis of surface wave radiation patterns is consistent with the prominent northeastern striking features observed in both the wavenumber spectra and the original imagery. From this study and previous work relevant to the area, the maximum principal compressive

stress axis is inferred to have been in the east-west direction in the past, but at present it is oriented in the north-south direction. This orientation is consistent with the present-day direction of African-Eurasian plate motion and with focal mechanisms of recent large earthquakes to the northwest near El Asnam, Algeria.

CHAPTER V

DISCUSSION AND CONCLUSIONS

Discussion

Previous Interpretation

As discussed earlier in Chapter 2, Harkrider's (1976) interpretation of the seismic surface waves associated with the nuclear explosion, Sapphire, showed that the equivalent earthquake contribution corresponded best to a left-lateral vertical strike-slip fault striking approximately N38 E. Consequently, the maximum principal compressive stress is in the N7 W or NS direction. This result is consistent with the present NNW direction of plate movement and stress orientations associated with recent earthquakes in Northern Algeria, as discussed in the next section. Harkrider (1976) also noted that energy release from a regional compressive pre-stress in the NS direction might have caused the tectonic component observed. A N-S compressive stress is also consistent with the observed seismic velocities being higher in the NS direction than in the EW direction in the test area (Faure, 1970). However, the geologic trends of distinct lithologic units in the area are N-S and may be a better explanation of the higher velocities in the N-S direction.

The results are important for the inference of the tectonic stresses currently prevailing in this area and the

tectonic history of this part of Africa.

Present Interpretation

Suppose the northeast-trending lineament observed in the wavenumber analysis of the massif indeed corresponds to a left-lateral vertical strike-slip faulting as suggested by Harkrider (1976). There should be an observable left-lateral displacement along the fault in the granite massif and on similar trending faults in its vicinity. However, the evidence of this sense of movement is lacking on the NE trending structures observed in this study. On the contrary, the observable northeast-striking faults in the general vicinity of the massif exhibit a net right-lateral movement, offsetting even the older north-south-trending 4 30' fault (see Figures 2 and 27a).

An east-west maximum horizontal compressive stress is needed to cause right-lateral strike-slip offset on these northeast-trending faults. However, if the present maximum compressive stress is indeed oriented NS, then left-lateral movement on those pre-existing NE-trending faults would be favored, compared to movement on other available fracture orientations in the area. Therefore, if the prevailing stress has changed from EW to NS compression, then the resulting total left-lateral displacement under the present regime has not been sufficient to overcome the total right-lateral offset achieved when the earlier EW compressive stress regime was active. Before a conclusion

on the type and direction of the prevailing regional stress can be drawn, a more complete view of the present and past tectonic history needs to be considered.

It should be noted that the geographical location of the Hoggar massif is closer to the Atlas belt of northwest Africa than to the rift zone in the east (no.1 and 3 in Figure 10c). Assuming that there may be some association in the seismic and tectonic characteristics between the Hoggar massif and the Atlas belt, the latter is considered briefly in light of the inferred present general NS direction of movement of the African plate with respect to the Eurasian plate.

Tectonic release in the Atlas Belt. Focal mechanisms of the aftershocks of the 1980 El Asnam (36.2 N, 1.5 E), Algeria earthquake located in various segments of fault breaks give mostly thrust solutions with some strike-slip component (Ouyed et al., 1982). Principal compression axes are dominantly in the NNW direction, and in the eastern area, aligned even more N-S. The azimuthal trend derived from the averaged compression axes yields N34 W, with a plunge of 5 to the north-west. This value agrees well with the implied N22 W convergence direction in the El Asnam area in Minster and Jordan's (1978) study of the position of the pole of rotation between the African and Eurasian plates. Hence the stress release associated with this particular

earthquake event and its aftershocks is compatible with the compression caused by the instantaneous plate motion.

Association with the Hoggar Region.   Apart from the recent tectonic history presented above, there had been a considerable amount of right lateral strike-slip movement in the late Paleozoic to Mesozoic along the South Atlas fault zone that strikes approximately N75 E (Sykes, 1978). This fault zone was again reactivated in post-Triassic time during the opening of the North Atlantic (Mattauer et al., 1972; LePichon et al., 1977).   As mentioned earlier in Chapter 2, similar phases of fault rejuvenation have been found within the Hoggar.   During Tertiary and Quaternary times there were a number of reactivation phases of the faults, including the 4 30' system and its feathering diagonal normal and strike-slip faults, which were accompanied by volcanic activity in the form of basalt flows (Bogdanov, 1972).

Given this tectonic history of the Atlas belt, two major questions about the Taourirt Tan Afella massif remain to be answered. Does the NE strike inferred from seismic surface wave radiation patterns as well as by image analysis using Fourier transforms and photo-interpretation methods represent the reactivation of pre-existing fractures, and is it a response to the present-day plate tectonic processes that cause the near N-S opposing movement of the African and

Eurasian plates? The answer to both seems to be yes. Based on the photo-interpretation of the entire Landsat scene, right-lateral offsets on NE trending lineaments (faults) are unmistakable. Notice also that there are conjugate NW trending features on the imagery as found by wavenumber analysis. If the present prevailing stress direction is indeed NNW to NS, as is consistent with the study of the Algerian earthquake and other contemporary tectonic evidence in the Atlas belt, then the principal horizontal compressive stress axis must have been dominantly ENE to EW in the past to produce the observed right-lateral offsets on NE-trending faults.

Tectonic Implications

Based on the previous work discussed in Chapter II and the results of the study, we can reconstruct some of the key elements of the tectonic history of the Hoggar region. A dominant east-west maximum compressive initial stress field would have fit in the orogenic scene of the Hoggar in late Precambrian. This lateral compression created trends of folds at right angles (i.e., NS) to the compressive stress axis. It also led to rupture along thrust planes of pre-existing faults, including the 4 30' fault and others. Originally these NS faults were formed as high-angle thrust faults implying a very early stress regime with EW compression and least principal stress axis vertical. Then erosion, peneplanation and deposition ocurred, followed by

an epeirogenic uplift in late Paleozoic. The resulting minimum stress axis then changed to a horizontal direction, though the predominant stress distribution remained as east-west compression. Consequently, northeasterly right-lateral strike-slip faults together with conjugate northwesterly left-lateral ones developed. Then during the opening of the North Atlantic in late Triassic, the faults were rejuvenated under EW compression. More right lateral strike-slip movement occurred along the NE faults and left lateral strike-slip movement along the NW faults, under a similar stress regime as before. Subsequently, regional rifting might have started to develop as discussed in Chapter 2. Under a possible stress regime that has the minimum principal axis in the NNE direction and the maximum compressive stress axis vertical, rifting would have accounted for the existence of the WNW negative Bouguer anomaly lineament discussed earlier (Figure 8). Furthermore, rifting may explain the N70 W fractures observed by ground studies, by wavenumber analysis and by photointerpretation. Meanwhile, rift-type volcanism seemed to be active in Tertiary and Quaternary. Intrusion of uprising asthenospheric material would be facilitated by the pre-existing deep-seated strike-slip faults. Finally, a change of stress orientaion occurred that reflects the direction of present-day plate movement.

The NNW convergence of the Eurasian and African plates favors left lateral strike-slip on NE-trending faults or

right lateral strike-slip on NW trending faults. However, the duration or vigor of present tectonic stress conditions has not been sufficient to overcome earlier right-lateral offsets on the NE-trending features in the study area, thought the regional stress in North Africa may be sufficient to suppress the potential WNW rift discussed in Chapter 2.

Conclusions

The following conclusions are made from this study:

(1) Wavenumber analysis of digital Landsat data helped identify both obvious and subtle structural features in the Taourirt Tan Afella granite massif and its vicinity.

(2) Close agreement has been found among structural features identified through enhanced image analysis, ground-based geological observations, photo-interpretation and seismic studies. In particular, the existence of a previously undocumented northeasterly set of lineaments is confirmed at the test site. These results illustrate the value of the combined use of remote sensing methods and conventional geological and geophysical methods for tectonic interpretations.

(3) Based on the interpretation of surface waves observations for the nuclear test, Sapphire, Harkrider (1976) concluded that the tectonic release is best explained by a left-lateral strike-slip double-couple source striking N38 E. This implies that the maximum principal compressive

stress is oriented in a NNW-NS direction. This trend is in agreement with a dominant trend identified in the image analysis, but observed net offsets are right-lateral on the NE-trending features

(4) The implied NNW-NS compressive stress direction in the study area is in agreement with earthquake studies of North Algeria and present-day plate convergence between the African and Eurasian plates.

(5) From a reconstruction of the tectonic history of the region, the stress regime is found to have changed at least three times. East-west compressive stresses in late pre-Cambrian time caused thrust faulting along the north-south striking faults. Later the least-principal stress changed from vertical to horizontal and this led to right-lateral strike-slip movement along the NE-striking faults and left-lateral strike-slip along the conjugate NW-striking faults. In recent geologic time, a change in the compressive axis to NNW-NS has occurred that is supported by several lines of evidence. Under this stress regime the sense of the fault movement is reversed on the NE and NW-trending faults, that is, left-lateral strike-slip on the NE-trending faults.

(6) In accord with the stress history and other geological and geophysical data, rifting may have occurred in the region but has now subsided, or the rifting is still in its early stage of development. Additional information will be required before a conclusion can be drawn concerning

the role of the rift feature in the tectonic history of the Hoggar area.

Suggestions for future research

Several techniques can be refined or incorporated into the existing programs for digital processing of remotely sensed data:

(1) Part of the existing Fast Fourier Transforms program need to be modified or even rewritten. By increasing core storage memory, processing of large data sets like 256x256 pixels or more will be possible. This will improve the regional view of a study area.

(2) Two-dimensional digital filters ought to be implemented and utilized for large data sets needed for passing or rejecting desired regional-scale features.

(3) Radar imagery, wherever available, should be utilized as one of the chief sources of remote sensing data. The Seasat Synthetic Aperture Radar (SAR), for example, has high sensitivity to surface rock and soil texture, and it acts as an edge enhancer, both of which may be especially helpful in delineating faults and other structural boundaries.

(4) Various signal enhancement techniques such as band ratioing which adjusts lighting conditions (shadows) can be used in conjunction with wavenumber analysis and/or by itself just as the principal components analysis was used.

(5) Use data from different sun angles to improve

resolution of structural features.

(6) Texture analysis and discriminant analysis can be applied to the data for additional feature extraction.

The Pennsylvania State University

The Graduate School

Department of Geosciences

A Remote Sensing

Characterization and Comparison of the

Semipalatinsk Area of the Soviet Union

and the Geologically Analogous

Mount Katahdin Region of North-central Maine

A Paper in

Geophysics

by

Jonathan Floyd Sartell

Submitted in Partial Fulfillment
of the Reqirements
for the Degree of

Master of Science

November, 1982

_____
Jonathan Floyd Sartell

We approve the paper of Jonathan Floyd Sartell.

Date of signature:

September 24, 1982

Shelton S. Alexander

Shelton S. Alexander, Professor of
Geophysics, Chairman of the
Geophysics Program, Advisor

24 Sept, 1982

Carl K. Graham

Earl K. Graham, Professor of
Geophysics

Sept. 24, 1982

Peter M. Lavin

Peter M. Lavin, Associate Professor
of Geophysics

Sext. 24, 1982

J. Ronald Eyton

J. Ronald Eyton, Associate Professor
of Geography

ABSTRACT

Multispectral remote sensing data have been used to perform local

and regional characterizations and comparisons of the Semipalatinsk area

of the Soviet Union and the geologically analogous Mount Katahdin region

of north-central Maine. A thematic mapping of local exposed lithologies

and various other cover types over the Degelen and Katahdin plutons was

completed as part of an effort to make a quantitative comparison of the

geological and geophysical "signatures" of these two plutons. Texture

transforms of data for the two study areas were calculated to 1) aid in

rock type discrimination over the Degelen massif and 2) make a textural

comparison of the surficial characteristics of the granite exposures.

Other methods of comparing the spectral characteristics of the two

plutons included means difference testing of raw, texture and band-ratio

category means, and a graphical analysis of their respective spectral

response distributions. Digitally enhanced color imagery was produced

for the two regions to 1) offer a visual display of statistical

transformations used to optimize rock type discrimination, and 2) map

regional geologic variability and major tectonic features as a means of

further testing the degree of geological and tectonic comparability of

the two regions.

Granite and rhyolite outcrops in Maine were somewhat confused due

to a persistent chlorophyll spectral influence, but various vegetative

cover types mapped distinctively. Similarly, certain granite categories

on the Degelen Massif mapped in a distinctive manner, but their

responses were influenced to some extent by a characteristic light

vegetation cover. Texture measures calculated from the first principal

component axis improved the discrimination of bedrock and colluvium in

the Degelen area. A comparison of tonal and textural features showed the Degelen and Katahdin granite outcrops to be roughly similar in the infrared spectral region, while Maine rhyolite outcrops and Degelen granite detritus demonstrated a relatively high degree of textural similarity.

An analysis of enhanced imagery highlighted major similarities and differences in the geologic and tectonic regimes of the two areas. Fault patterns were denser and apparently younger in the Soviet region. Other geophysical data were also analyzed for the Katahdin region as a means for postulating possible geophysical responses of the analogous Degelen features, and to infer subsurface variability in that region.

The enhanced imagery showed the two study areas to possess similar geologic variability, but to differ in fault pattern and fracture density. Especially notable was the degree of fracturing of the Degelen Massif, and the possible implications on seismic source coupling this condition presents. A reasonable estimate of the lateral geologic and tectonic variability of the Degelen site was possible from remote sensing data alone. These results, coupled with geophysical models derived from analysis of Maine data, place some constraints on the expected variability of geophysical properties of the subsurface of the Degelen region.

TABLE OF CONTENTS

LIST OF TABLES

LIST OF FIGURES

LIST OF PLATES

ACKNOWLEDGEMENTS

CHAPTER I.

INTRODUCTION

For many years, observers using various remote platforms have attempted to characterize and map geologic structures on the Earth's surface. From the earliest of such attempts, where photography was accomplished from a balloon, to today's sophisticated aircraft and cameras, most imaging has been accomplished with photographic film utilizing visible and near-infrared wavelength radiation. However, with the advent of multispectral scanner and digital recording technology, a wealth of quantitative information for significant portions of the electromagnetic spectrum has become available to researchers. Such scanners have been put to commercial use in conventional aircraft for some time, but with the launch in 1972 of the first of three Landsat Multispectral Scanner systems, an unprecedented global imaging capability was achieved. Orbiting at a nominal altitude of 918 kilometers, the Landsat satellites can scan a ground swath 185 kilometers wide in four spectral bands and under almost constant illumination. These flight paths also permit data collection in areas that would otherwise be totally inaccessible. The Landsat data have thus been widely used by geoscientists, foresters, land use planners, and professionals in other fields as well.

The Electromagnetic Spectrum

The electromagnetic spectrum spans an extremely wide range of wavelengths. Figure 1 shows this range and illustrates the phenomenon of variable atmospheric transmission, or atmospheric absorption as it is more commonly called. Atmospheric absorption permits the recording of only certain wavelengths through a number of discrete spectral "windows". At the far left of the spectrum shown is the ultraviolet region occupying a range of 0.27 to 0.4 micrometers which, due to strong atmospheric absorption, has so far been only of limited use in studying the Earth. Next comes the visible range, which extends from 0.4 micrometers (violet light) to 0.78 micrometers (red light) and is the range of wavelengths within which most photographic films operate. The next group of wavelengths, 0.7 to 1000 micrometers, falls into the infrared group. Beyond 10 micrometers, what is recorded is mainly emitted rather than reflected radiation, and no photographic film is of much use beyond these lower infrared wavelengths. Beyond the far infrared region is the microwave range of radiation which extends in wavelength from 1000 micrometers to approximately three meters. An important application of microwave radiation is radar, which has been used extensively for imaging purposes. Two prime examples are Side-Looking Airborne Radar (SLAR) and the Seasat-A Synthetic Aperture Radar (Ravenhurst, 1980).
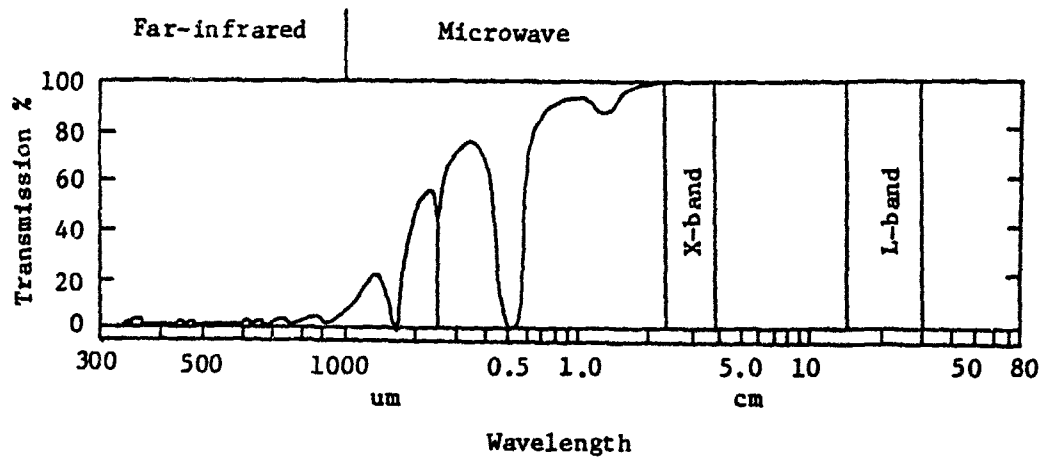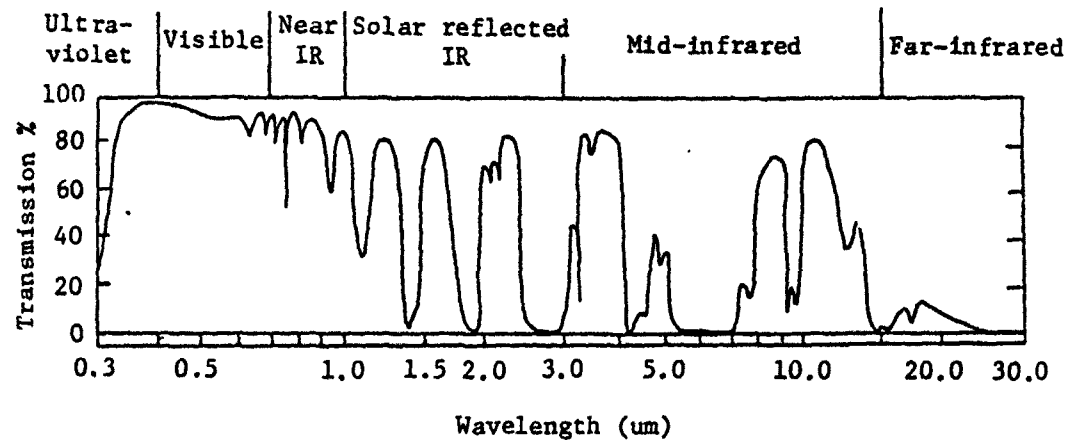
Figure 1. Generalized atmospheric transmission bands and Landsat spectral band widths (After Goetz and Rowan, 1981).

Spectral Behavior of Rocks, Minerals and Vegetation

The spectral information available in the visible and near-infrared regions is the result of variation of reflectivity caused by electronic and vibrational processes at the molecular level (Hunt et al., 1973; Salisbury and Hunt, 1974). These researchers concluded, however, that the principal contituents of the materials studied (crushed, fresh rock samples) did not show intrinsic features, because most of their characteristic absorption bands occur outside the visible to near-infrared range. Most of the discernable spectral features, or bands, detectable in the visible to near-infrared region were found to be due to the presence of iron and water. This applies to igneous and metamorphic rocks, as well as to rocks of sedimentary origin. One important exception for some sedimentary materials, however, is the strong absorption feature at a wavelength of 2.3 micrometers due to the carbonate ion.

Several difficulties are encountered when visible and near-infrared spectral responses are used to discriminate between lithologic materials (Salisbury and Hunt, 1974). Many rock-forming materials do not display a characteristic spectral response within the 0.5 to 1.5 micrometer region, and even those spectral curves that are distinctive may be dominated by the presence of a relatively minor constituent mineral or an alteration product not directly related to the the bulk composition of the parent material. The absolute reflectance of a rock depends heavily upon its particle size; furthermore, many rocks contain opaque minerals that reduce overall reflectivity. Finally, those characteristic features that do exist, for example the carbonate band, may be partly obscured by atmospheric absorption.

It is therefore advantageous to investigate other regions of the electromagnetic spectrum which would yield information more useful in the discrimination of rock types. The longer infrared wavelengths of 1.0 to 3.0 micrometers, barring the 1.4 and 1.9 micrometer atmospheric absorption bands, yield more recognizable spectral characteristics than the visible bands. The region around 1.6 micrometers demonstrates a high reflectance for most rock types, as it is midway between the iron absorption band at the ultraviolet-visible boundary and a strong OH vibrational feature at 2.74 micrometers (Cameron et al., 1981). Landsat-D, launched in July 1982, will provide data at these longer spectral wavelengths. In addition to four sensors similar to those aboard Landsats 1 through 3, three more units have been added which will collect data in the regions of 1.55-1.75 micrometers, 2.08-2.35 micrometers, and 10.40-12.50 micrometers (EROS Data Center, 1982). Data from these bands will certainly add to the geoscientist's capabiltity of inferring geological relationships from space.

Despite the difficulties inherent to the visible and near-infrared spectral regions, many positive conclusions may be drawn concerning geological discrimination utilizing those wavelengths. Although the mineral components of felsic granites are themselves spectrally indistinct, curves for laboratory granites display a characteristic pattern as shown in Figure 2. This is typified by a slow but steady rise in reflectivity through the range of 0.4 to 1.4 micrometers. Other felsic rocks, rhyolite being an example, demonstrate similar behavior (Hunt and Salisbury, 1973). Intermediate and mafic igneous rocks display a lower overall reflectivity due to increased opaque minerals relative to quartz and similar transparent minerals. Phonolite is
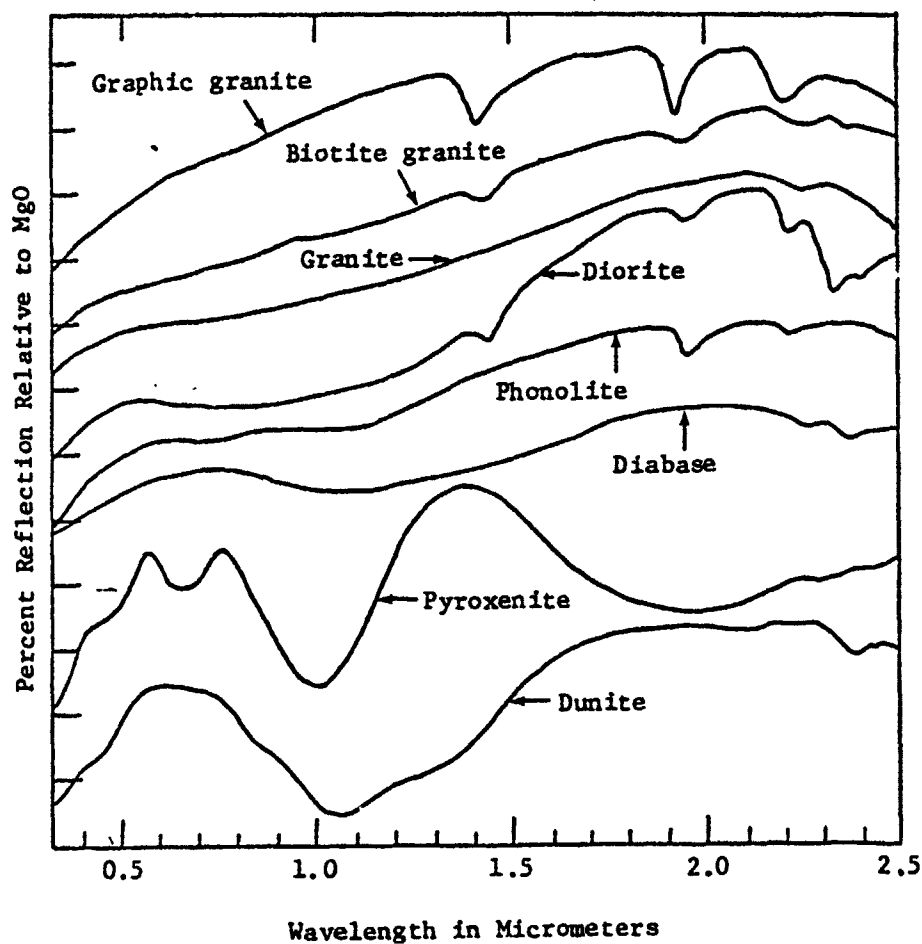
Figure 2. Igneous rock reflectance spectra, separated vertically for clarity (After Salisbury and Hunt, 1974).

characteristic of intermediate rocks, and its minor pyroxene and olivine components produce, respectively, the weak ferric and ferrous bands near 0.7 and 1.1 micrometers. Diabase is an example of the coarser-grained intrusives and all its bands are subdued due to a high magnetite content; also there is a broad absorption band near 1.05 micrometers caused by ferrous iron in the hornblende and olivine components of the rock. The ultramafics, pyroxenite and dunite, contain fewer opaques and therefore show the strongest ferrous iron bands. Pyroxenite shows two such bands at 1.0 and 2.0 micrometers and dunite displays one at 1.1 micrometers. Sedimentary rocks also commonly show iron bands, the usual cause being the ferric oxide stain on sandstone grains.

Vegetation commonly has a marked effect on the spectral response of the underlying geologic material, sometimes obscuring it altogether (Siegal and Goetz, 1977; Ravenhurst, 1980). This masking is most severe with rocks of low albedo. On the other hand, dead or dry vegetation has relatively little effect, since its spectral curve is similar to that of rocks (Siegal and Goetz, 1977). Shown in Figure 3 is the spectral response curve for a green leaf which demonstrates the chlorophyll absorption and reflectance bands at .6 and .7 micrometers that correspond to Landsat Band 5 and Band 6, respectively.

To combat the obscuring effects of clouds and vegetation, longer radar wavelengths have recently been brought into use. The SEASAT-A Synthetic Aperture Radar (SAR) is an active imaging system (providing its own source of illumination) that uses microwave radiation at a wavelength of 23 centimeters. Such a wavelength is little affected by clouds or by a vegetative canopy in viewing the Earth's surface, and it samples from a few centimeters to a few tens of centimeters of the
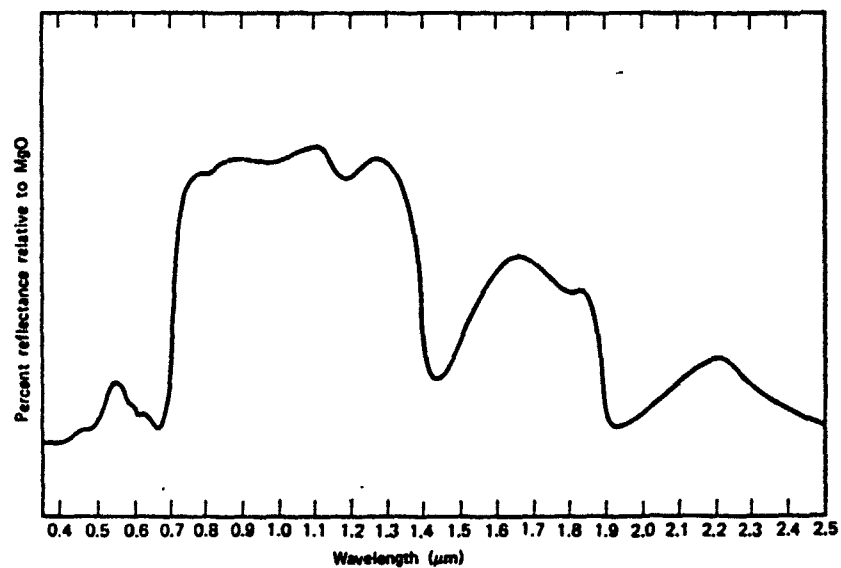
Figure 3. Typical response curve for a green leaf (after Raines and Canney, 1980).

surface materials. SEASAT digital data were enlisted by Ravenhurst (1980) in conjunction with other data to infer geological structure of southeastern Pennsylvania. Unfortunately these data do not yet exist for most of the Earth´s surface.

Capabilities and Limitations of the Landsat MSS

Geometrical configuration of the satellite. The Multispectral Scanner System (MSS) incorporated by the Landsat satellite is made up of several components (Slater, 1979). A scanning mirror projects a portion of the ground scene through a Richey-Chretien telescope, which in turn focuses the image onto an array of 24 optic fibers. These fibers then transfer square instantaneous fields of view (IFOV´S) onto a bank of 24 detectors. The detectors are arranged into four groups of six sensors, each group sensing a different portion of the visible and near-infrared spectrum as shown in Figure 1. As the satellite moves along its polar orbit, six lines of data are thus collected in four spectral bands with a single mirror sweep. The same orbital path is repeated every 18 days (more frequently toward the Earth´s poles), thus making it possible to image the same scene on a regular basis.

Although slight differences exist among the three Landsat missions, the overall geometric configuration of the data collection system is generally constant (Slater, 1979). Using a nominal altitude of 918 kilometers for the satellite and focal lengths of 82.09, 82.30 and 82.46 centimeters for MSS 1 through 3, respectively, the IFOV or picture element (pixel) size for each satellite is 76.05, 76.27 and 76.23 meters square, plus or minus 0.5 meter. With a gap of approximately 5.5 meters

between ground-projected IFOV's in the in-track direction, a single
mirror sweep thus collects data in a swath 484 meters in width, measured
along track. The average across scan sampling interval is approximately
58.0 meters for each satellite. This is calculated from the preflight-
determined sampling rate, and from a count of picture elements across
actual scenes collected by the three satellites. Data users should
remember, however, that even though the across track sampling interval
was decreased to 58.0 meters in order to improve resolution in that
direction, the Landsat IFOV is nonetheless 76 meters by 76 meters. Thus
the spatial resolution is of this order, although features much smaller
than this can be detected if they contrast sufficently with their
surroundings. Furthermore, each pixel represents an average reflectance
over the IFOV.

Spectral resolution. The average spectral curves of the Landsat
MSS sensors are shown in Figure 4. Although the nominal sensing ranges
usually cited for the four spectral detectors are 0.5 - 0.6 micrometers
for Band 4, 0.6 - 0.7 micrometers for Band 5, 0.7 - 0.8 micrometers for
Band 6 and 0.8 - 1.1 micrometers for Band 7, it is obvious that each
sensor has a peaked sensitivity at certain wavelengths. This is
especially true in the case of Band 7, where the response falls off
sharply to a small value at 1.0 micrometers.

Atmospheric interference and solar illumination considerations.
Much has been written regarding the atmosphere's effect on light
traveling through it. Fraser (1969) discusses the role of the
troposphere and stratosphere in atmospheric absorption and scattering.
The troposphere, ranging in height from 8 kilometers at the poles to 18
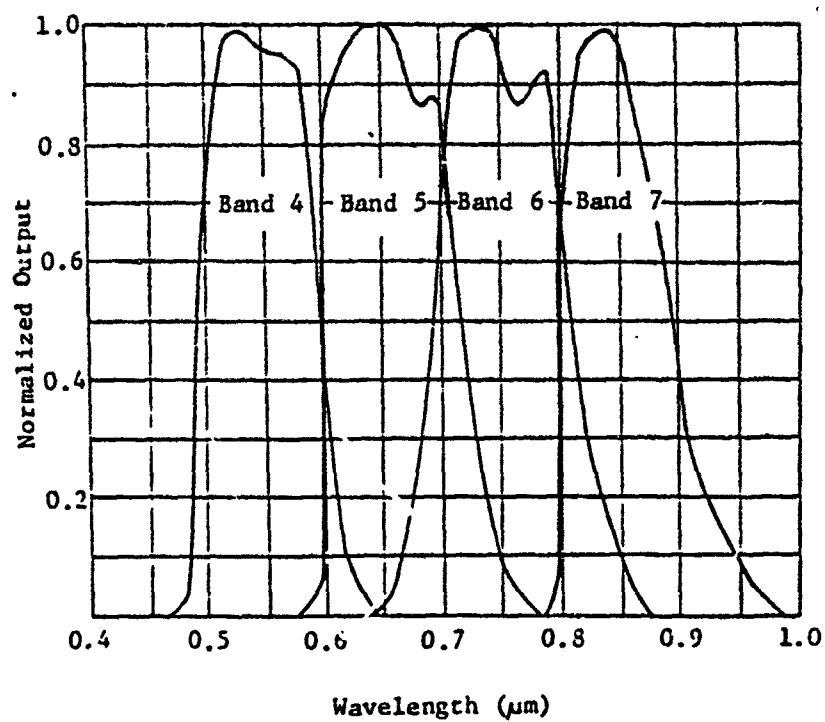
Figure 4. Average relative spectral responses of the four Landsat MSS sensors (After Slater, 1979).

kilometers at the equator, contains most weather phenomena. The associated water vapor and various other particulates present the most serious obstacles to transmission of electromagnetic radiation. The overlying stratosphere contains ozone, mostly concentrated around 30 kilometers in height, which strongly absorbs ultraviolet radiation.

Atmospheric scattering presents additional problems. This is because scattered radiation from up to 30 meters outside of a sensor's IFOV tends to affect an individual pixel's reflectance value. This situation worsens in areas of high contrast (Turner, 1975). The effect of the reflectivity of surrounding pixels is superimposed on the actual target area. A hazy atmosphere compounds the problem, and even the relatively sharp boundaries of a field or pond can be blurred (Dave, 1980).

Fortunately, the effects of sun illumination angle on overall scene reflectance is not as critical. As illustrated in Figure 5, clouds play an important role in scene illumination, but there is little change in brightness as the sun moves from 90 degrees to 30 degrees overhead. Below 30 degrees, however, there is a rapid falloff in solar intensity. From this we can conclude that differences in sun angle on the mean brightness level of a scene are not critical, provided the illumination angle is over 30 degrees.

Topographic effects. Another phenomenon having a large effect on intrascene mapping of pixel reflectances and interscene comparison of spectral responses is the dependency of reflectivity on the slope angle of the target area. Holben and Justice (1980) attempted to quantify this effect using hand-held radiometers, and simulated Landsat sensor response to various topographic regimes. They also tested the
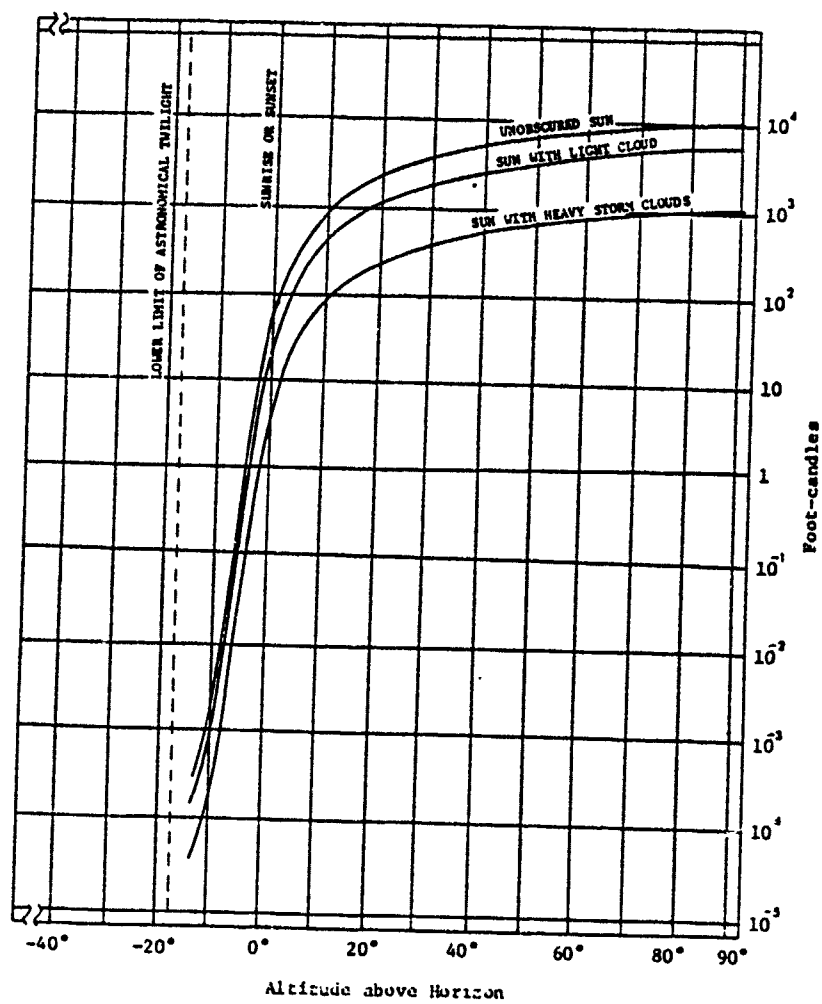
Figure 5. Effect of sun elevation on scene illumination (After Fraser, 1969).

appropriateness of simple incidence models for modelling the radiance from a surface. One such incidence model is the Lambertian assumption, which essentially holds that direct radiance is a function of the illumination inciJence angle, and not the viewing angle. They concluded that the magnitude of the topographic effect varied as a function of sun angle, azimuthal orientation of the slope, and the slope inclination (Figure 6). Their evidence also seems to suggest that the Lambertian assumption may prove valid only over a restricted range of slope angles, and may not be appropriate for certain types of ground cover. Smith and others (1980) rejected the Lambertian assumption for a cover type composed of Ponderosa pine and suggested that it would be more valid for slopes of less than 25 degrees. Joyce (1978) recommended that slope categories be established for 0 - 10% slopes, 10 - 30% slopes, 30 - 50% slopes, and slopes greater than 50%.

Other researchers (Rowan et al., 1974; Taranik, 1974; Merifield et al., 1975; Gillespie, 1980) utilized a ratio technique in minimizing the topographic effect. This method stems from the assumption that the decrease or increase in radiance brought about topographically is linear for all four spectral bands. Therefore, ratioing two bands pixel by pixel would produce a more constant distribution of reflectance values, provided the material being imaged remains constant. A more thorough review of the ratio technique can be found in the discussion of methods in chapter three.
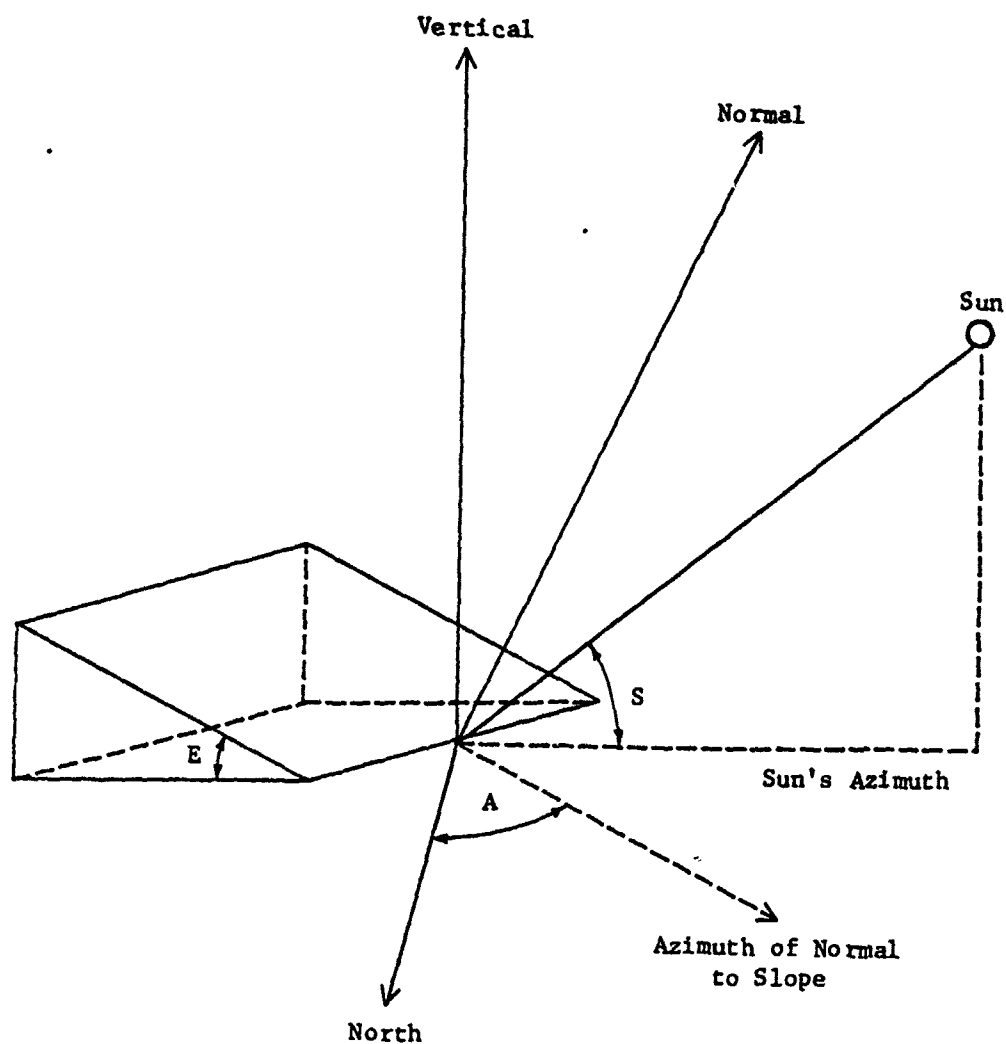
Figure 6. Topographic parameters affecting local scene radiance.
Topographic parameters are:
E = Slope inclination
S = Sun elevation
A = Azimuthal orientation of slope
(After Holben and Justice, 1980).

Software Systems Utilized

Software systems used in the various stages of data anaylsis in this study were from several sources. The most important ones are listed here.

The Office of Remote Sensing of Earth Resources (ORSER). The ORSER software system, central to this research, is a package developed over the years at Penn State by individuals involved in many different fields. Designed to operate in a batch processing mode, the ORSER programs can accommodate several types of digital data, including aircraft and terrain data. They are also highly capable of handling large data sets and of performing various statistical transformations and classifications. A more complete description of the ORSER system can be found in the ORSER User's Manual (Turner et al., 1982).

The Pennsylvania State University Department of Geography. A series of programs written by Dr. Ronald Eyton of the Penn State Department of Geography was of great assistance to this study. Originally developed, in part, for the detailed analysis of cultural features on digital imagery, this package incorporated a more "pixel-by-pixel" approach in the processes of feature identification, selection, and classification.

The Statistical Analysis System (SAS). The SAS system is a versatile and powerful series of statistical analysis and graphics routines developed by the SAS Institute, a consortium of statisticians

from a wide variety of fields. A description of the SAS programs may be found in the SAS User's Guide (Helwig and Council, 1979).

BMDP Statistical Software. The BMDP software package was developed under the auspices of the Department of Biomathematics of the University of California at Los Angeles. The BMDP program used here was BMDP7M, a stepwise discriminant analysis routine. BMDP7M program characteristics are summarized in the BMDP user manual (Dixon et al., 1981).

Display Media

Several devices are available at Penn State for the display of digital imagery. Simple character maps can be produced on the IBM high speed line printer (Figure). Color capability is provided by a Ramtek color CRT system interfaced to the IBM 3081 mainframe computer. The display medium used most often in this study, however, was the Versatec 8222A Electrostatic Plotter. Although it plots in gray tones only, it is extremely versatile in that it produces images at almost any scale (up to a maximum width of 21 inches with 200 pixels per inch) over a possible 32 gray levels. Versatec images were used in the color compositing method described in Chapter III.

Statement of Problem

The usefulness of remote sensing data for inferring lateral geologic variability, tectonic setting, and lithologic comparability in areas of partly exposed plutonic intrusions is tested in this paper. If remote sensing can be used for such inferences, it will be possible to

Figure 7.   Gray level of the Mount Katahdin area, Band 5, 20 August 1976.
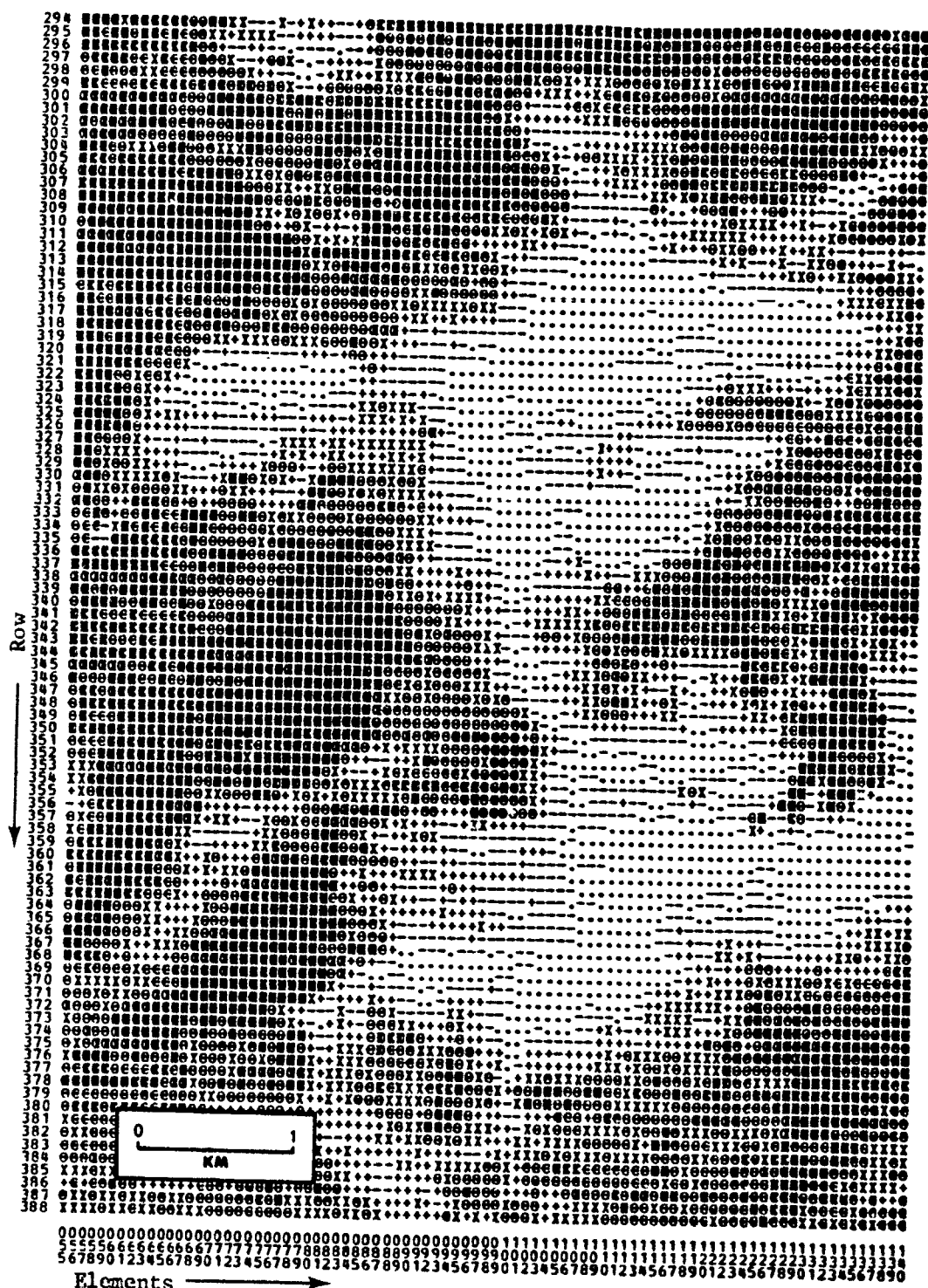
place important constraints on the expected variability in associated geophysical properties of the sub-surface. Two geographically remote regions are investigated, one located in the Soviet Union and the other in the northeastern United States. Interest in the former is a result of its use as an active nuclear test site; the latter is important because of its geologic and tectonic resemblance to the Soviet test region. An understanding of the local geologic and tectonic structure of the Soviet site is important to the accurate assessment of the size of explosions from seismic monitoring of this testing activity. Due to the impracticality of conducting on-site studies at the proving ground, it is useful to investigate a geologic analog (the northeastern United States area) that is more accessible for ground-based studies. We would thus improve our understanding of the seismic response (source coupling) in the inaccessible region. Determining this coupling requires a knowledge of the regional as well as local geology and fracturing of the test site and how this geological "filter" affects and responds to a buried explosion in a given location.

The Semipalatinsk Nuclear Proving Grounds, located 160 kilometers southwest of Semipalatinsk, Kazahkstan, USSR, is a principal Soviet test site (Figure 8). A good candidate for its geologic analog is the Mount Katahdin area of northern Maine (Figure 9). The purpose of this study is to compare these areas using primarily remote sensing observations. The approach is 1) to discriminate between surface spectral classes in the Katahdin and Semipalatinsk areas by means of both spectral and textural feature extraction subsequent spectral thematic classification, and by the production of computer enhanced color composite imagery of the areas, and 2) to compare their signatures statistically to test the

Blank

Figure 8. Location of study area, Kazahkstan, Soviet Union.

Birnk

EXPLANATION

STRATIFIED ROCKS

Tertiory and Cretaceous
Atlantic Coastal Plain. Includes Qua-
ternary in southeastern Massachusetts

Jurassic and Triassic

Permian and Carboniferous
Includes post-Acadian Devonian east of Hudson River

Devonian (pre-Acadian) and Silurian
May include older rocks in parts of Maine,
New Hampshire, and southern New England

(a)   (b)
Ordovician and Cambrian
(a) foreland, (b) folded. In Maine and New
Brunswick, includes rocks mapped as
Siluro-Ordovician. May include some older
or younger rocks, particularly in southern
New England. Dash pattern of (b) is not
intended to represent structural trend
lines

STRATIFIED AND PLUTONIC ROCKS

Precambrian
May include Paleozoic rocks, particularly
in eastern Massachusetts and Rhode
Island

PLUTONIC ROCKS
Paleozoic and Mesozoic

Alkalic

(a)   (b)
Calc-alkalic, including mafic
(a) Ordovician and Ordovician (?)
(b) post-Ordovician

Ultramafic

STRUCTURE SYMBOL

Logan's Line and inferred boundary of
Taconic allocthon

Figure 9.   Generalized geology of the northern Appalachian Orogeny
(after White, 1968).

Location of study area –

GENERALIZED GEOLOGIC MAP
OF THE
NORTHERN APPALACHIAN REGION
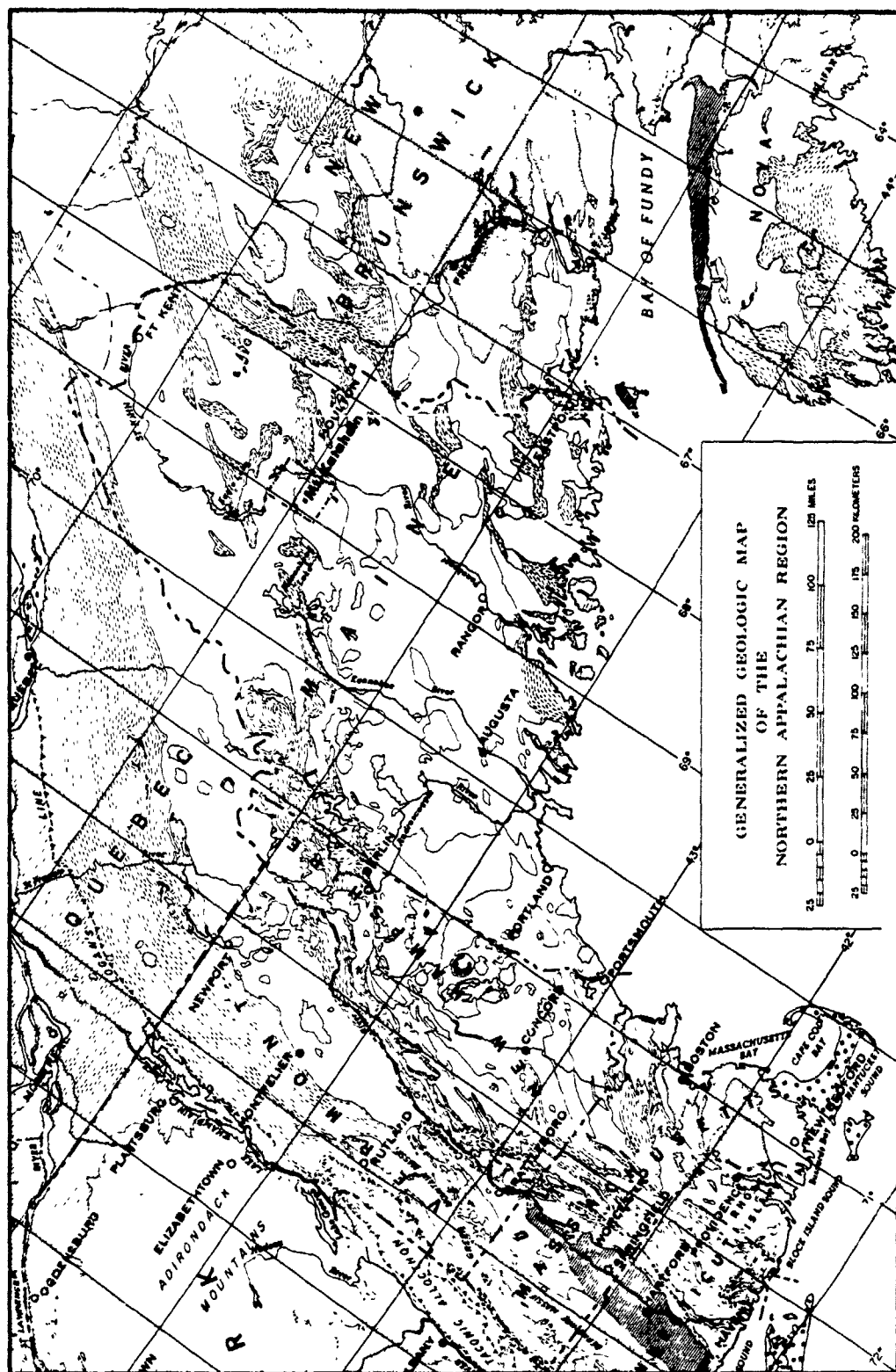
extent to which these postulated geologic analogs give similar
responses. In addition, the scale and degree of lateral variability in
inferred properties will provide an indication of the probable scale of
heterogeneity in other geophysical characteristics; this approach can
help to define "geophysically distinct" areas within the test site.

CHAPTER II.

STUDY AREAS

The Semipalatinsk Area

Regional structure and stratigraphy. The Semipalatinsk area of
Kazahkstan, USSR is a geologically complex region. Structurally, it can
be classified as a fold belt similar to the Appalachian Fold Belt of the
eastern United States. Lower Paleozoic sedimentary and volcanic rocks
have been deposited, folded, and faulted; and subsequent granitic
intrusion and other forms of metamorphism are also observed (Figure 10).
There are shear zones of numerous parallel-trending faults, and moderate
to highly folded younger Paleozoic rocks are also intruded by granites.
Unconsolidated Tertiary deposits vary in thickness, but generally
speaking, lake deposits are the most notable of these.

The Degelen Granite. The Degelen Granite Massif is one of the
region's more obvious geologic structures. It has been described in the
literature (Kropotkin, 1945) as a normal and leucocratic coarse-grained
or porphyry-like biotite granite. Pink or pink-gray in color, it
consists mainly of orthoclase-perthite (up to 60% of the rock), quartz
and albite or albite-oligoclase. It is cut by dikes of microgranites,
granite porphyries and by thin veins of aplite. Breaking through
Devonian and Lower Carboniferous deposits, the Degelen Massif is easily
recognized by virtue of its subcircular shape and relatively high,
rugged topography.
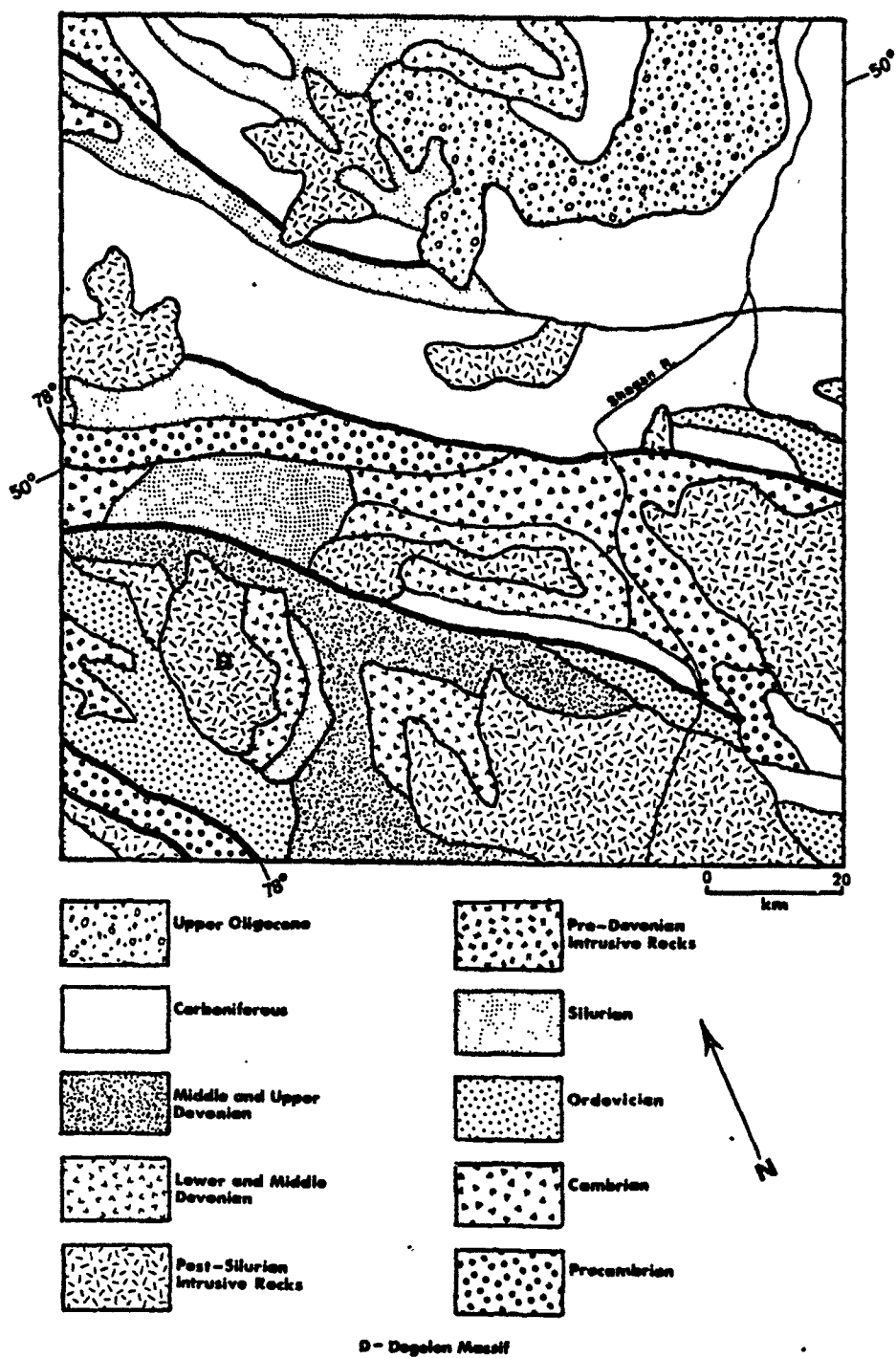
Figure 10. Geology of the Degelen Massif area, USSR. (Ministry of Geology, USSR, 1968).

Two areas in the region will be considered. The larger area surrounding the massif (Plate 1) will be the subject of enhanced image analysis and the immediate vicinity of the body (Plate 8) will be the site of the feature extraction and statistical analysis procedures.

The Mount Katahdin Area

Regional structure and stratigraphy. The Mount Katahdin area of northern Maine lies, like its Soviet counterpart, in a highly faulted and variably metamorphosed fold belt. This is a northern extension of the Appalachian Orogenic Belt, and can be most simply described structurally as a parallel series of anticlinoriums and synclinoriums. Figure 11 illustrates the primary tectonic features of the northern Appalachian Orogeny.

Descriptions of the regional stratigraphic relationships found in Boucot (1959), Larrabee et al. (1965), Pavlides et al. (1956), Espenshade and Boudette (1967), and Roy (1980), are summarized here. Late Precambrian to Middle Ordovician quartzites, slates, graywackes, and cherts are interlayered with tuffaceous rhyolites. The Upper Ordovician is represented by three major lithofacies. The mafic volcanic lithofacies forms a broad tract in northwestern Maine and perhaps continues into Quebec. East of this is a more or less contemporaneous belt of slates and graywackes, and still eastward of this is a thick limestone formation which makes up much of the Aroostook-Metapedia Belt (Figure 11). Middle and late Silurian lithofacies are respectively characterized by fine-grained deepwater sediments and flysch deposits. There is an important belt of Early
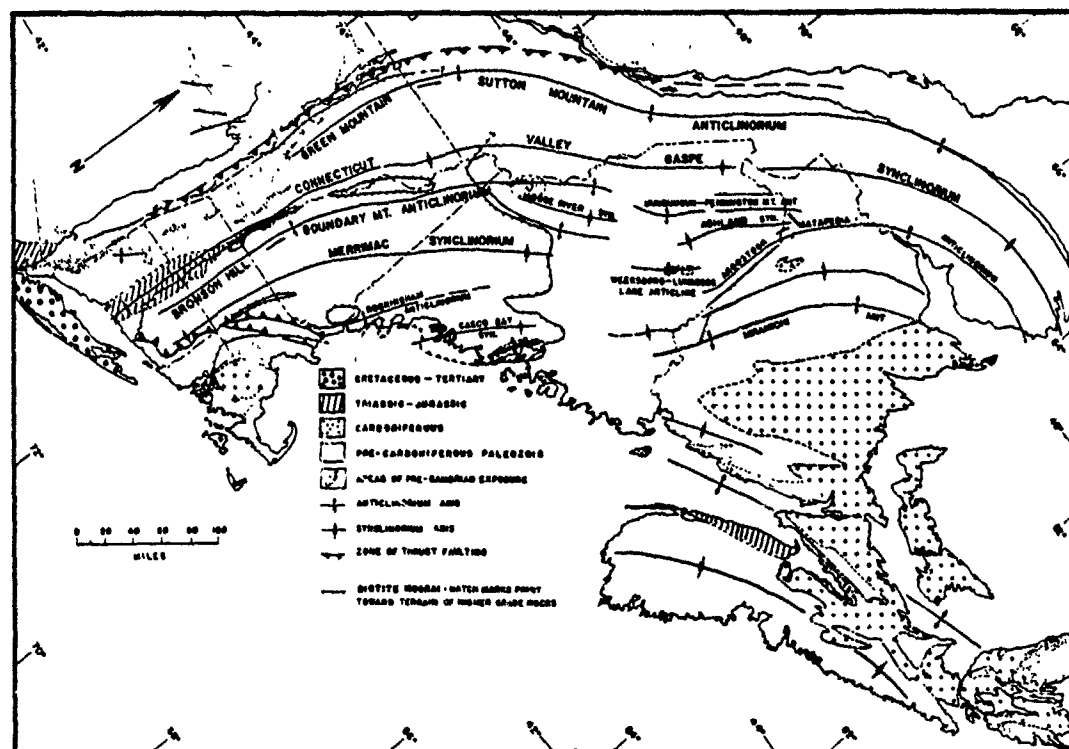
Figure 11. Principal tectonic features of the northern Appalachian
Orogeny (After Roy, 1980).

Devonian interlayered sedimentary and volcanic rocks in the northeastern part of the area, while much of Late Devonian time is represented there by a widespread gray slate and graywacke sequence. The Devonian differs, however, in areas of northwestern Maine. In that region, the lower section is a lithologically variable collection of sandstones, conglomerates and limestones interleaved with slates; and the upper part is made up of generally fine-grained and well-cleaved slate.

Volcanism. The Middle to Late Devonian Acadian Orogeny, while marking the end of most Paleozoic sedimentation, marked the beginning of a widespread episode of volcanism in northern Maine. Rankin (1968) describes an important belt of nearly contemporaneous and lithologically similar volcanics and shallow intrusives he calls the Piscataquis Volcanic Belt. He goes on to postulate the existence of an ancient island arc system of which these rocks were a part.

The most noteworthy member of this belt is the voluminous Traveler Rhyolite, which lies in a large, structurally depressed area on the northwest limb of the Weeksboro-Lunksoos Lake Anticline (Figure 11). Typically a greenish-gray or bluish-gray to almost black aphanitic rock, it commonly weathers to a whitish rind (Rankin, 1980). The rhyolite can be divided into a basal Pogy Member and an overlying Black Cat Member, both of which are differentially-compacted welded ash flow tuffs. Though once a submerged caldera, the rock is now exposed as bright outcroppings atop Traveler Mountain and other hills directly north of Mount Katahdin in Baxter State Park.

Plutonism. Subsequent to the emplacement of the volcanic extrusives of the Piscataquis Volcanic Belt, a series of both mafic and

felsic post-orogenic plutons was intruded a short distance to the southeast. These were named the Greenville Plutonic Belt by Hon (1980), and two important members are the mafic Moxie Pluton, a long, irregularly shaped body that extends roughly northeastward-southwestward, and the felsic Katahdin Pluton, which intrudes the Moxie at its northeastern termination (Figure 12). Although the Katahdin is younger, both plutons exhibit contact metamorphic aureoles; there is also a marked lack of foliation, indicating their post-orogenic emplacement.

The Katahdin Pluton is one of the most unique and important Devonian intrusives in northern Maine (Hon, 1980). It marks the sudden end of a belt of igneous activity (Figure 12), parallels the acidic Piscataquis Volcanic Belt, and abuts ultramafic bodies (the Moxie Pluton) which points to a coupling of mantle-crust igneous activity during the Acadian Orogeny. Hon (1980) also estimates post-orogenic regional uplift of the pluton to be approximately 5%, grading linearly from northeast to southwest. Thus the geometry is that of a flat laccolith not fully unroofed where it is in contact with the Traveler Rhyolite to the north.

The unique character of the Katahdin Pluton, especially its topographic prominence, can be explained in part by the zoned nature of the granite. The Katahdin Granite, constituting 95% of the pluton, has been divided into several facies. The core is comprised of a massive, structureless medium-grained biotite granite, the Doubletop Facies. This grades upward into the Chimney Facies, and toward the summit of Mount Katahdin, the granite takes on the miarolitic nature of the Summit Facies (Figure 13). Other textural varieties, located toward the
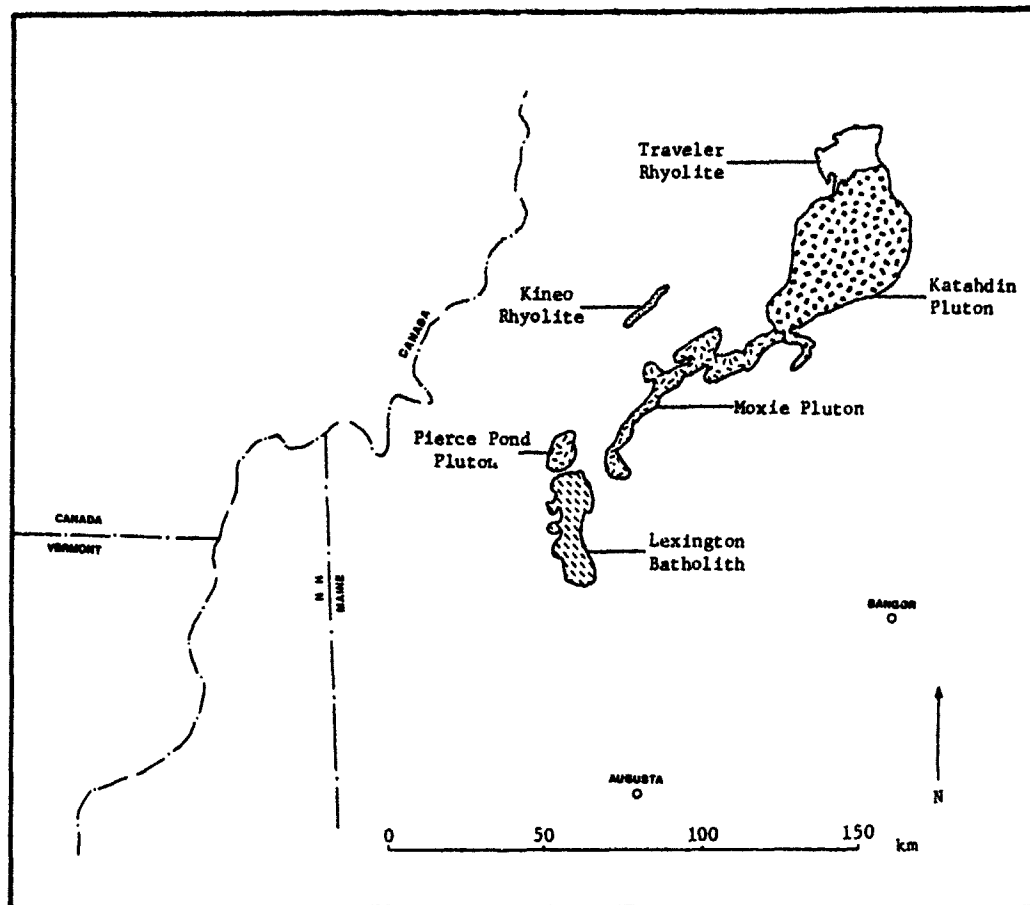
Figure 12. Major intrusives of northern Maine (After Hon, 1980).

Summit Facies

Chimney Facies

South Brother Facies

Wassatoquoic Facies

Doubletop Facies
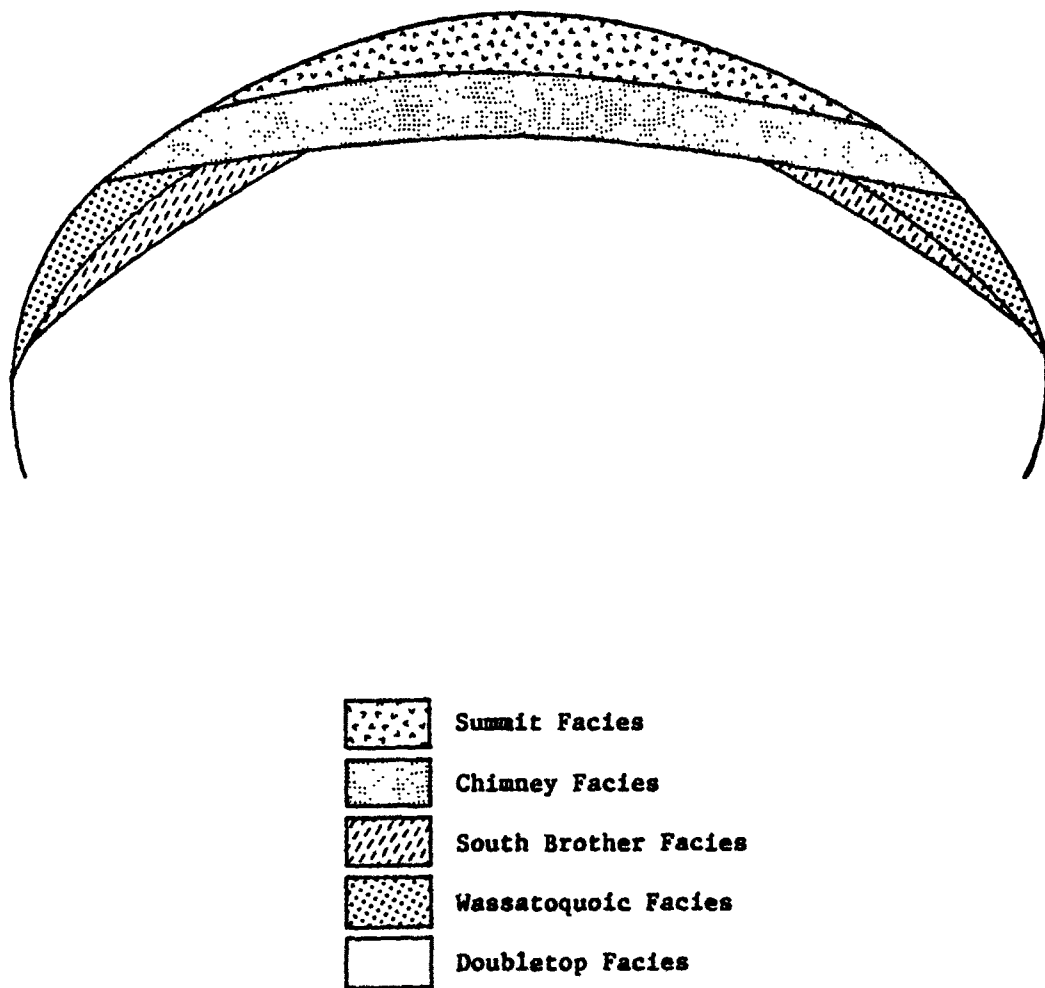
Figure 13. Schematic diagram of facies locations within the Katahdin
Pluton (After Hon, 1980).

perimeter of the pluton where the granite comes into contact with the country rock, are the Wassataquoik and South Brother Facies. The most notable characteristic of the "outer zone" facies, the Chimney, Summit and South Brother, is their relative resistance to erosion. The Summit Facies, due to this high degree of erosional resistance, forms a "capping" against weathering at higher elevations, and is primarily responsible for Mount Katahdin's 1708 meter (5267 foot) elevation at Baxter Peak. Figure 14 shows the distribution over the pluton of these textural variations, which are probably due to differential cooling rates as the magma solidified beneath the Traveler Caldera (Hon, 1980). Other members of the pluton shown on Figure 14 include the Debsconeag Granodiorite and the Horserace Quartz Diorite.

Pleistocene glaciation. Much of the present-day morphology of Mount Katahdin and the distribution of surrounding surficial deposits can be related to Wisconsinan-aged glacial episodes (Genes, 1980). Cirques have been carved into resistant peaks underlain by Katahdin Granite, and especially noteworthy is the remarkable freshness of the arretes that have resulted (Caldwell, 1980).

Regional structural and geophysical evidence. The gravity data collected for northern Maine yield some some clues concerning the subsurface geologic structures. Kane and Bromery (1966, 1968), using gravity data, conclude that: 1) regional gravity anomalies have their source, at least in part, in the upper part of the crust, 2) large local gravity anomalies are due to igneous bodies, and 3) some felsic plutons probably extend much further laterally than their surface exposure indicates. Negative anomalies occur commonly over felsic plutons, while
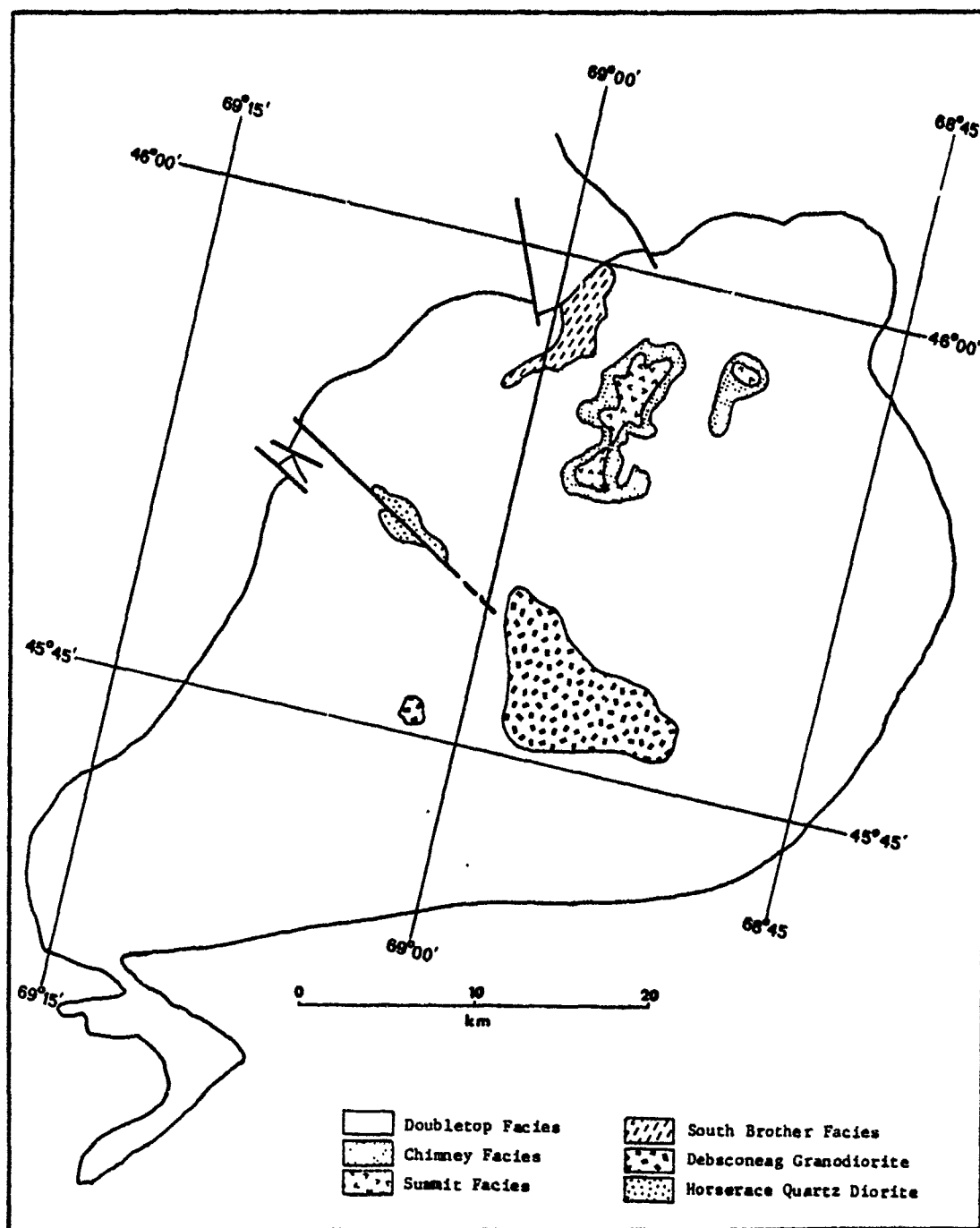
Figure 14. Geologic map of the Katahdin Pluton (After Hon, 1980).

positive anomalies are located over their mafic counterparts. This is primarily due to density differences between the constituent minerals of felsic and mafic rocks. Shown in Figure 15 is a summary of Kane and Bromery's work; also indicated are three primary zones into which they divide the state on the basis of regional gravity trends. The correlation of a large negative anomaly with the Katahdin Batholith is typical of the gravitational response of these bodies.

Magnetic anomalies, on the other hand, are sporadically distributed over the felsic plutons of the area. This is principally due to the concentration of magnetite in the contact metamorphosed country rock abutting the plutons. Mafic igneous intrusions with a large magnetite content, for example the Horserace Quartz Diorite (Figure 14), also add to the local magnetic variability. Aeromagnetic data in the vicinity of the Katahdin Pluton (Figure 16) show the effects of the bordering metamorphics (A on Figure 16) and of the diorite intrusion (B on Figure 16). In contrast to this, tabular volcanics interlayered with steeply dipping sediments tend to display a distinctively linear pattern, denoted by the letter C on Figure 16 (Allingham, 1960).

Figure 15. Bouguer gravity map of Maine (After Kane and Bromery, 1968).

Figure 16. Aeromagnetic anomalies of the Mount Katahdin region of
            northern Maine (After Williams et al., 1978). Relative
            magnetic highs indicated by shaded areas.

            A - Magnetic response of contact metamorphic country rocks;

            B - Magnetic response of Horserace Quartz Diorite;

            C - Magnetic response of dipping interbedded volcanics and
                sediments.

CHAPTER III.

METHODS

Data Collection

Landsat scenes. Several criteria were used in the search for
Landsat scenes to be used in this study. Since multiscene data were
important to the quantitative characterization and comparison of the
Maine and Russian granites, two scenes were chosen for each site. In
the Katahdin area, it was necessary to select summer scenes due to the
partial or total snow cover at the top of Mount Katahdin inherent to
every other season. Scenes with little or no cloud cover and haze were
also sought. Table 1 lists the identification information for the
scenes chosen. The Semipalatinsk region is shown in the color composite
of Plate 1, and in Plate 2 and 3 are the color composites of the 23 July
1973 and 20 August 1976 scenes, respectively.

Maps. Many different types of information in map form were
available for the Mount Katahdin area. Topographic maps of the Presque
Isle and Millinocket, Maine 1° X 2° quadrangles (1/250,000 scale) were
used for regional orientation. More local topographic information was
provided by 1/62,500 scale Katahdin and Traveler Mountain 15-minute
series quadrangle maps, and by more recent 7.5-minute series
orthophotoquads (1/24,000 scale) of the area. General ground cover
information was obtained from Land Use and Land Cover maps of the
Millinocket and Presque Isle 1° X 2° quadrangles (U. S. Geological

Table 1. Characteristics of Landsat scenes used in this study.

Scene I.D. No.	Scene Date	Location	Center Point
251976-14344	20 August 1976	N. Central Maine	N46°34′ W68°34′
1365-14595	23 July 1973	N. Central Maine	N45°59′ W70°10′
1658-05015	12 May 1974	Kazahkstan, USSR	N50°15′ E78°10′
2946-50456	11 May 1976	Kazahkstan, USSR	N50°15′ E79°23′

Survey, 1980). Regional geological information used in analyzing

enhanced imagery (see the section in this chapter entitled "Production

of Digitally Enhanced Imagery") was provided by the Preliminary Geologic

Map of Maine (Doyle, 1967), and geophysical data over the Katahdin

pluton discussed in Chapter I was furnished by Boucot et al. (1964) in

their Geological and Aeromagnetic Map of Northern Maine.

Data sources for the USSR site were fewer in number, but still

helpful. Operational navigation charts produced by the Defense Mapping

Agency were useful in orientation, and regional geologic information was

available on 1/2,500,000 and 1/7,500,000 scale geologic maps produced by

the Ministry of Geology of the USSR (1964 and 1957, respectively). The

study area on the 1/2,500,000 map is reproduced in Figure 10.

Aerial photography. Aerial photographs of the Mount Katahdin

region proved to be indispensable in topographic orientation and

training field selection. Adjacent photographs from the same flightline

were used in stereo to portray topographic features of the mountain

accurately, and to correlate individual pixels with specific topographic

regimes.

Preprocessing

Scene subsetting. Before the actual data analysis could commence,

various preprocessing steps had to be taken. One of these was the

subsetting of the area of interest from the NASA tape to a smaller, more

easily managed data set. Since the computer compatible data tapes

obtained through the EROS Data Center divided the Landsat scene into

four quarters, each contained in a separate tape file, two of these

files had to be spliced together if the area of interest lay across the boundary between them. This was accomplished by obtaining the scene row and column limits for each file from the tape file header, subsetting the files to two separate tapes, and using the ORSER program SPAN to join the two files at the appropriate column numbers so that a continuous array of pixel values was formed. Once this was completed, a gray tone map of each study area was produced using the ORSER program NMAP to locate the line and element specifications with which to subset the final data set containing the study regions. These were then written either to tape or disk files.

Recalibration. One raw data problem that must be corrected if its effects are severe is a phenomenon known as "sixth line banding". This is caused by sensitivity differences in the six sensors comprising the instrument bank for each channel. If one of these sensors has a response slightly different from the other five, a noticeable banding effect occurs (Figure 17A). To counteract this, Merembeck et al. (1974) developed an algorithm, now implemented on the ORSER system, which calculates the mean and standard deviation for each sixth line (six means and standard deviations in all). After locating the offending sensor or sensors in this manner, the user makes the appropriate correction by specifying the desired mean and standard deviation that each channel is to acquire. Since, of course, the same values are specified for all the channels, a first-order standardization of sensors is performed by this operation. The correction is of the following form:

$$\hat{x}_{ijk} = \frac{(x_{ijk} - \bar{\bar{x}}_{kl})}{s_{kl}} * s_{kl}' + \bar{\bar{x}}_{kl}'$$
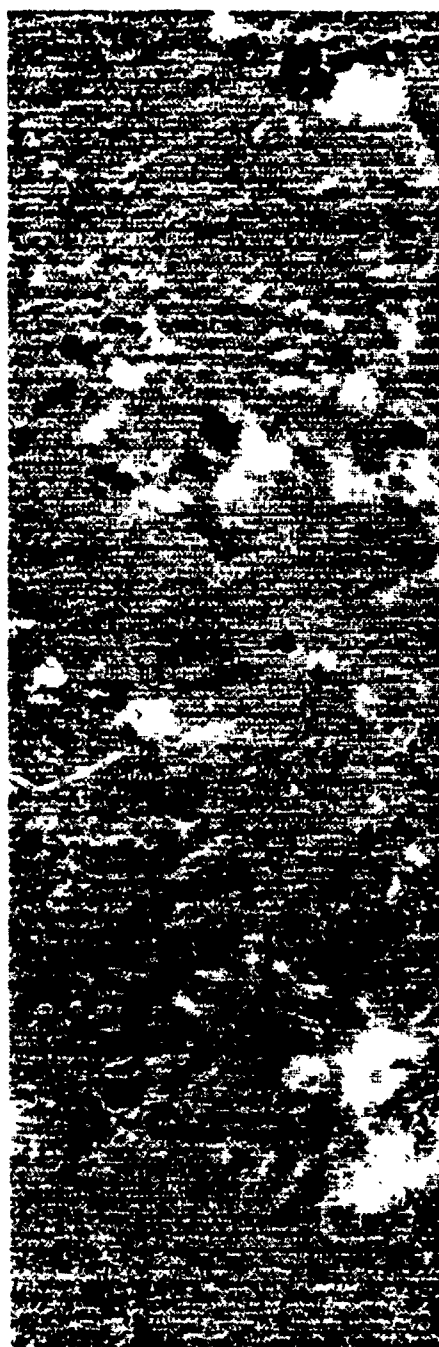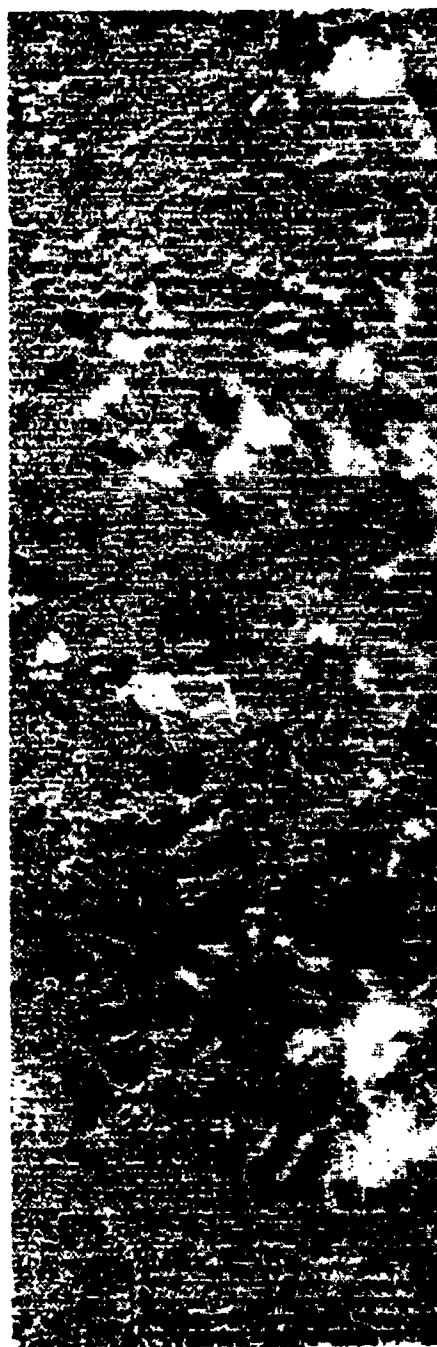
A   B

Figure 17.   Landsat subscene, 23 July 1973.   (A) Unrecalibrated.
(B) Recalibrated for 6th line banding.

where

$\hat{x}_{ijk}$ = recalibrated value for scan line i, element j, and channel k;

x_{ijk} = corresponding original value;

$\bar{x}_{kl}$ = computed mean for channel k and for line = modulo(j,6) + 1;

s_{kl} = corresponding standard deviation;

s_{kl}' = recalibrated standard deviation computed as the average of unaffected standard deviations for channel k;

$\bar{x}_{kl}'$ = corresponding recalibration mean.

Figure 17B illustrates the partial clearing of the banding accomplished by this algorithm. The correction of sixth line banding was useful not only in increasing image quality, but also in minimizing channel response perturbation due to sensor variability. The latter aspect of this procedure is important in the quantitative section of this study.

Principal component transformations. A useful step in the analysis of a large data set, in this case a Landsat scene in digital form, is a reduction of the dimensionality of that data set. Principal components analysis is a linear transformation of the data whereby all original variance is concentrated on fewer axes while maintaining all of the original information. If the pixels describing the features of a scene are thought of as point swarms in n-dimensional space, n being the number channels in which the data were collected, the principal component transformation essentially rotates the n axes so that the first axis in the transformed space is aligned in the direction of highest variability of the data. This would be the longest axis of the ellipse containing the point swarm. Succeeding transformed axes, each

orthogonal to and uncorrelated with the others, account for less and less of the total scene variability. A more rigorous discussion of principal components analysis can be found in Merembeck and Borden (1978) and in Morrison (1968).

The ORSER programs STATS, HISTRAN, and SUBTRAN were utilized in performing the principal components transformation. The subscene of interest was input to STATS, which calculated the covariance matrix for the scene along with the corresponding characteristic roots and vectors. The rescaled matrix of characteristic vectors (modal matrix) was then used as input to the HISTRAN program, which produced a histogram of each axis describing the transformed space. Linear rescaling and translation factors used to fit the data distribution along each axis to a 0 to 255 dynamic range (the ORSER data format) were calculated from these histograms. Finally, the modal matrix and rescaling and translation factors were specified to the SUBTRAN program, which wrote the transformed data to disk or tape files.

In this study, the principal component transformation was performed for two reasons. First, it was desirable to compress the information content of a scene along fewer axes to facilitate certain aspects of later data analysis. In particular, the texture transformation, to be discussed later in this chapter, operated only on one channel of data at a time. It was therefore expedient to use it on the most meaningful channels. Secondly, only three of the component images could be combined in the three-color compositing method used in this study (see section in this chapter entitled "Production of Digitally Enhanced Imagery"), and selection of channels to be imaged was simplified due to the fact that the first three principal component axes contained nearly

all of the scene variance. At the same time, these axes were more
likely to contain unique information, since they were uncorrelated.

The Discrimination of Rock Types: Thematic Classification

General methods. The discrimination and mapping of rock types over
the Maine and Kazahkstan study areas using Landsat multispectral data
was central to this investigation and was accomplished through a number
of steps. Initially, the Landsat scene over the target areas was
compared to available ground truth, and tentative lithologic
identification made of potential training areas. These training areas
were, in effect, sample populations for which multivariate statistics
were to be calculated for use in later classification and lithologic
charecterization.

Next, the most objective and efficient methods of selecting
training areas were chosen, the decision based mainly upon the volume of
ground truth information available for each study area. Joyce (1978)
suggested that the minimum size for a training field be approximately 16
hectares (40 acres) or about 30 pixels in size. He also recommended the
choice of at least three training sites per ground cover category in the
event one was to be discarded due to an inconsistent mean or standard
deviation. Once these training areas were chosen, the response values
for the four spectral bands were extracted and written, pixel by pixel,
to a disk file using the program ITRAIN (Eyton, 1978a). The
distinctiveness or redundancy of the training fields chosen was tested
by inputting this list to the Statistical Analysis System (SAS) DISCRIM
discriminant analysis program. Redundant training fields were either

dropped from the analysis or combined with others to better define a cover type category which both groups were postulated to represent. Through repeated iterations of this process, the number of categories over each study area was reduced to eight or less. This was the maximum number of classes that could be displayed on the final classification map. This limitation to eight classes was not considered problematic because a number greater than that would most likely tend to confuse the final map, which was produced using the program VCOLOR (Eyton, 1978a). VCOLOR's classifier utilized a canonical transformation which was calculated using the linear discriminant functions output by the DISCRIM program.

The Mount Katahdin Area. The availability of ground truth and relative homogeneity of land cover simplified the selection of training areas over the Mount Katahdin region (Plates 2 and 3). The first step in correlating the Landsat scene with the ground truth was the production of gray-tone maps of the target areas. One such map of the immediate Mount Katahdin area is reproduced in Figure 6. Since the outcrops exposed above treeline on Mount Katahdin were brightest in the visible bands relative to their surroundings, a gray-tone image of Band 5 was compared to stereo photographs of the region. A raw data dump of Band 5 pixel values was then performed using the program IREAD (Eyton, 1978a), and actual pixel values were correlated with corresponding regions on the aerial photography. In this manner, two categories of granite, "slope" and "plateau", were chosen as the granite classes for both the 20 August 1976 and 23 July 1973 scenes.

In order to further test rock type discrimination in the area, training sites were also chosen over outcrops of the Traveler Rhyolite

located atop Traveler Mountain and other peaks north of Mount Katahdin.
These sites were identified with the aid of the land use maps, Band 5
gray-tone maps, and raw data dumps. Areas of bright spectral response
similar in outline to the "bare exposed rock" category of the land use
map (rhyolite in this instance) were located, and pixels of uniform,
consistently bright response were chosen as training fields for the
rhyolite.

Training sites for forest cover were selected in a slightly
different manner. The infrared channels, Band 6 and Band 7, were most
sensitive to vegetational variation; therefore, gray-tone images of Band
6 were compared to the land use maps to choose vegetation categories.
Two main categories, deciduous and coniferous forest, were selected, and
the coniferous cover was subdivided into shadowed (on mountain slopes
away from direct sun illumination) and sunlit coniferous. Deciduous
forest was not subdivided for either Maine scene. Water (lakes and
streams) was chosen as a seventh category, and since there were a small
number of cumulus clouds appearing on the 23 July 1973 scene, an eighth
"cloud" category was established for that scene.

The list of response values, arranged by categories, was then input
to the DISCRIM program. DISCRIM utilized a classification criterion
that was determined by a measure of generalized squared (Mahalanobis)
distance between groups, calculated using the pooled covariance matrix.
Once this classification criterion was determined, each case was then
assigned to the group to which it was closest in this transformed
canonical space.

This canonical transformation played a significant role in
subsequent classification. The axes describing the data point swarms

were, on the basis of the statistics of training fields specified, rotated and rescaled so as to maximize the between-group covariance relative to the within-group covariance. Categories in this new space were thus more distinct and less likely to be confused.

Not all cases were, of course, correctly assigned to their originally specified category during the initial analysis of training fields. Table 2 is a classification matrix produced by DISCRIM as an aid in measuring the separability of input populations. Misclassified cases were identified and deleted from the more distinct classes, but if two categories were highly confused, they were combined or one was dropped as being redundant. For example, the rhyolite and plateau granite categories of the 23 July 1973 scene were strongly overlapped, as indicated in Table 2. They were therefore combined with the idea that they would then form a more easily classified "plateau rock" category. Table 3 illustrates the inter-relationships of the new categories after the rhyolite and plateau granite groups were combined, and misclassified pixels from other categories were dropped. If the diagonal members of the final classification matrix were as close as possible to 100%, the resulting discriminant functions would promote a more accurate classification of the scene, since the training fields generating them were "cleaned" by this method.

The categories shown in Table 4 were later utilized in classifying the entire subscenes. The linear discriminant functions based on the improved training field statistics were used in the program VCOLOR, which produced three "color-component" maps on the Versatec plotter. These were later made into color positive photographs which were, in turn, overlaid to form a seven-category color classification map of each

Table 2. Classification matrix of 23 July 1973 training field
          categories. Categories are:

          1 - Rhyolite
          2 - Slope granite
          3 - Plateau granite
          4 - Shadowed coniferous trees
          5 - Sunlit coniferous trees
          6 - Deciduous trees
          7 - Water
          8 - Clouds

From Class:	Percent of observations classified into class:							
	1	2	3	4	5	6	7	8
1	46	29	23	0	3	0	0	0
2	12	82	6	0	0	1	0	0
3	33	25	41	0	0	0	0	0
4	0	0	0	100	0	0	0	0
5	.7	10	.7	.7	87	.7	0	0
6	0	0	0	0	0	100	0	0
7	0	0	0	1	0	0	99	0
8	0	0	0	0	0	0	0	100

Table 3. Classification matrix of cleaned categories, 23 July 1973
scene. Categories are:

1 - Plateau rocks
2 - Slope granite
3 - Shadowed coniferous trees
4 - Sunlit coniferous trees
5 - Deciduous trees
6 - Water
7 - Clouds

From Class:	Percent of observations classified into class:						
	1	2	3	4	5	6	7
1	99	1	0	0	0	0	0
2	4	96	0	0	0	0	0
3	0	0	100	0	0	0	0
4	0	0	0	100	0	0	0
5	0	0	0	0	100	0	0
6	0	0	0	0	0	100	0
7	0	C	0	0	0	0	100

Table 4. Names and map colors of final categories chosen over 23 July 1973 and 20 August 1976 scenes.

Scene Date	Category No.	Category Name	Color, Final Classification
23 July 73	1	Plateau rocks	Red
	2	Slope granite	Yellow
	3	Shadowed coniferous trees	Blue
	4	Sunlit coniferous trees	Cyan
	5	Deciduous trees	Green
	6	Water	Black
	7	Clouds	White
20 August 76	1	Rhyolite	Red
	2	Slope granite	White
	3	Plateau granite	Yellow
	4	Shadowed coniferous trees	Blue
	5	Sunlit coniferous trees	Cyan
	6	Deciduous trees	Green
	7	Water	Black

area in Maine as s, own in Plates 4 and 5. The image production process
is discussed in more detail in the section in this chapter entitled
"Production of Digitally Enhanced Imagery." Table 4 lists the final
classes and the colors assigned to them on the classification maps.

The Degelen Massif Area. Because ground truth of the quality of
that used in the northern Maine area was not available for the
Semipalatinsk area, changes in the method of training field selection
were necessary. Hoffer et al. (1974) and Khorram and Katibah (1981)
used a "supervised" cluster analysis method in mapping mountainous
terrain and other irregular cover types. These researchers selected
this approach because neither a totally supervised nor unsupervised
classification produced suitable results. Such a method was deemed
appropriate here due to the irregular topography of the Degelen Granite
Massif itself and also to the scarcity of ground truth information.
Figure 18 is a Band 6 gray level Versatec image of the massif showing
the distribution of cluster analysis blocks over it. Each of these
blocks was situated over what was tentatively identified as uniform
lithology.

The cluster analysis algorithm used was the ORSER program CLUS,
which operated in the following fashion. The block of interest was
specified along with the number of pixels to be sampled from the block.
These sample cases were arranged in an array, and a series of trial
group centroids were established. Each sample was then assigned to the
group whose centroid was the smallest Euclidean distance away. The
centroids of the resulting groups were then calculated, and the process
repeated until there was no change in allocation. The entire block of
data was then classified, with each pixel being assigned to the category

Figure 18. Location of cluster analysis blocks on Degelen Massif, 12
            May 1974.

G = Granite
S = Spall
T = Tertiary sediment
B = Burned area
V = Volcanics
P = Paleozoic sediments

whose centroid was the closest in Euclidean space. All categories were then given a symbol, and a map was produced of the data block. A more detailed discussion of the CLUS algorithm can be found in the ORSER user manual (Turner et al., 1982).

The actual training areas were then selected from the cluster blocks. These were chosen from sufficiently large areas mapped as one category by CLUS. Two to three categories of training fields were then extracted from each cluster block, resulting in a large number of training fields over each lithology. For the 12 May 1974 scene, 10 classes of granites, 7 of volcanics, 7 of Paleozoic sediments, 3 of Tertiary sediments, 11 of nuclear blast spall, and 5 of probable burned areas were set up.

At this point, training fields had to be selected upon whose statistics the final classification mapping was to be based. First, training field classes representing individual lithologies were input to the DISCRIM program. This step was important because it helped to point out which training fields were the best ones in describing the lithology in question, and which ones should be discarded. In other words, it was necessary to find the fewest number of training fields for a given lithology which could best explain the spectral characteristics of that lithology. The ORSER program STATS was also used in this process. For each training field, STATS produced the basic statistics plus a histogram of the training field data. If the pixel population of the training field deviated severely from a normal distribution, that site was dropped. Thus, for the 12 May 1974 scene, the 10 granite sites were reduced in number to 5, the 7 volcanics to 5, the 7 Paleozoic sediments to 3, and the 11 spalls to 3. The Tertiary sediment groups were kept

without change, and the training fields over the burned areas were combined. In this manner, 43 training field groups, representing 5 different lithologies or categories, were reduced in number to 19.

The next step of the analysis involved the reduction of these 19 groups to a maximum of eight to be used in the final classification. At this point, the list of response values for each category were pooled and compared for the first time in the analysis using the discrimination program. Those lithologies that appeared similar were immediately evident. The next task was to combine or delete indistinct groups, using the available ground truth information, to achieve the eight-category limit. Initially, the three spall groups were distinct enough from the other lithologies to be combined into one group. The remaining categories were more a ficult, however. Assuming that supposedly different lithologies could be spectrally similar as parent-daughter materials, for example the granite and nearby Tertiary sediments,, some groups of different lithologic categories were combined. Other groups were dropped if a majority of their member pixels were placed into other lithologic categories by DISCRIM's classification model. The eight categories were eventually formed, and their classification matrix is given in Table 5.

The classification of the Degelen Massif was then performed utilizing the linear discriminant functions obtained from the final DISCRIM run which produced the classification matrix of Table 5. These functions were input to the VCOLOR program, which produced the classification map (Plate 6). The category names and corresponding colors are listed in Table 6.

Table 5. Classification matrix of final 8 categories used in thematic
classification of Degelen Granite Massif. Categories are:

1, 2 - Granite
3 - Burned areas
4 - Granite detritus
5 - Other detritus
6, 7 - Volcanics
8 - Nuclear blast spall

From Class:	Percent of observations classified into class:							
	1	2	3	4	5	6	7	8
1	96	0	0	0	0	4	0	0
2	0	100	0	0	0	0	0	0
3	0	0	97	0	0	0	3	0
4	0	0	0	96	4	0	0	0
5	0	1	0	0	99	0	0	0
6	0	0	0	0	0	100	0	0
7	6	0	27	0	0	0	67	0
8	0	0	0	1	0	0	0	99

Table 6. Category names, numbers and colors, final classification map of Degelen Massif, 12 May 1974.

Scene Date	Category No.	Category Name	Color, Final Classification
12 May 1974	1	Granite 1	Magenta
	2	Granite 2	Red
	3	Burned areas	Black
	4	Granite detritus	Yellow
	5	Other detritus	Cyan
	6	Volcanics	Green
	7	Dark volcanics	Blue
	8	Spall	White

Discrimination of Rock Type: Landsat Band Ratios

After the training fields over the Maine and Russian study areas were collected and the classification maps produced, other tests of discrimination were performed. The first of these combined a simple ratioing of band pairs with the original data values of the two bands. Taranik (1978) suggested this procedure to combat the confusion of two categories of the same color (similar spectral response slopes) but different albedoes. The resulting values for the training field populations were tested for separability with DISCRIM. For the 12 May 1974 USSR scene, five different combinations of band ratios and raw data values were tested in this manner with only limited success. Generally, the classification matrices showed an increase in overlap between the groups, and an accompanying loss of separability. For the 20 August 1976 Maine scene, four combinations of band ratios and raw data values were used. Although the combinations utilizing Bands 5 and 7 maintained almost the same degree of discrimination as the raw bands, the overall results of these tests indicated that ratioing was of no significant help in rock type discrimination.

Discrimination of Rock Type: Graphical Representation

A graphical representation of training field populations was another means by which to investigate the discrimination of lithologies over the study areas, and to access the ability of two-band combinations to perform that differentiation. The program BVSTD (Bivariate Standard Deviation -- Eyton, 1982a) was utilized to plot training field

population distributions on the Versatec 8222A plotter. These plots illustrated the category ellipse shapes, and any overlap that occurred between categories.

Discrimination of Rock Type: Texture Transform

There are several limitations resulting from having spectral data only in the four Landsat bands. First, the bands chosen for Landsat are not the most diagnostic ones for rock type discrimination (Siegrist, 1980). Second, a non-normal distribution of responses over traiuing areas commonly results, making ensuing characterization and clssification difficult since most classifiers assume normal population distributions. Finally, surface tonal features themselves commonly are not uniquely characteristic of a material, and, therefore much interest has arisen in the use of texture transforms to achieve more dependable classification of Landsat and other remotely sensed data (Hsu, 1978).

Previous use of texture. In an effort to solve these problems, Hsu (1978) devised 17 statistical measures which are listed in Table 7. He then used these measures in a classification of digitized aerial photographs to achieve a high classificaton success rate, utilizing a Mahalanobis distance classifier. Calculation of the texture measures incorporated a traveling 3 X 3 or 5 X 5 pixel window within which the texture parameters were calculated and then assigned to the center pixel. Therefore, this procedure takes the spatial variation of tone into account.

Using 11 of these texture variables, Irons and Peterson (1981) applied Hsu's technique to Landsat data over central Pennsylvania. They

Table 7. The texture-tone variables of Hsu´s algorithm (after Hsu, 1978).

	Code	Description or computational formula
1.	MEAN	Average
2.	STD	Standard deviation
3.	SKEW	Skewness
4.	KURT	Kurtosis

the four central moments

5.	MDEVN	$(x_i - \bar{x})/n$, where x_i = response value of individual pixel, $\bar{x}$ = mean
6.	MPTCON	$(x_i - x_c)/n$, where x_c = response value of center point
7.	MPTREL	$(x_c - x_i)/n$
8.	MINCON	$(x_i - x_j)/n$, i and j are adjacent pixels
9.	MINSQR	$(x_i - x_j)/n$
10.	M2NCON	$(x_i - x_k)/n$, i and k are second neighbors
11.	M2NSQR	$(x_i - x_k)/n$
12.	MADAT1	Mean area above datum 1 (100)
13.	MADAT2	Mean area above datum 2 (127)
14.	MADAT3	Mean area above datum 3 (154)
15.	MBDAT1	Mean area below datum 1 (100)
16.	MBDAT2	Mean area below datum 2 (127)
17.	MBDAT3	Mean area below datum 3 (154)

enlisted more than one (n) channel at a time to describe a pixel as a vector in n-dimensional space, and identified the mean normal vector length in the 3 X 3 window (Hsu's MEAN), skewness (SKEW), and the mean Euclidean distance between vector endpoints as the three best variables in discriminating local ground cover classes. All other variables were highly correlated with the mean Euclidean distance. However, classification of the transformed data did not prove highly successful, although an image produced with the MEUC (mean Euclidean distance) variable acted as an effective edge enhancer. They attributed the difficulty in classification to their use of a minimum distance, rather than a Mahalanobis distance, classifier. Hsu, of course, had used the latter classifier. The major problem, however, seemed to be the relatively coarse spatial resolution afforded by Landsat when compared to the panchromatic black and white photographs originally used by Hsu.

Parker (1980) in a study of Landsat data over three different geographical locations, found that Hsu's textural transforms offered an improvement over raw data in the discrimination of certain rock types. When comparing the mean responses for training areas of different lithologies, he found that the raw data did not sufficiently differentiate between granite, quartzite and colluvium. When the average textural characteristics of these training fields were compared, Parker found that the degree of separability of group centroids was enhanced. Ravenhurst (1980) incorporated Hsu's texture variables as new channels in a study where he combined raw Landsat data, Seasat-A Synthetic Aperture Radar data and magnetic data in an attempt to map geology in a forested terrain in south-central Pennsylvania. He found that texture measures calculated from the first three component axes of

this composite data set provided the best discriminatory power for use in a subsequent classification.

Therefore, texture measures were used in this investigation in an attempt to further discriminate rock types over the two study areas. Algorithms to generate Hsu's 17 texture variables were developed by Baumgardt and Pavlin (1979), and their routine was modified to write to disk the texture measures for each pixel included in the training areas, arranged according to training field numbers. This was done with the assumption that inclusion of all pixel values would provide a more adequate indication of category distinctiveness or overlap. Whereas Parker (1980) compared population means to infer category separability, here, the entire population of pixel responses was used in tests to determine discriminatory power of all variables used throughout the study. The training fields over which to sample response values for input to the texture algorithm were chosen over areas identical to the sites used for the raw band thematic mapping. The list of texture measures, 17 for each pixel, was then submitted for analysis to the BMDP7M discriminant analysis program (Dixon, 1981). At the same time, a list of raw data values, Bands 4 through 7, was submitted to the BMDP7M program in a similar fashion and the resulting classification matrices and scattergrams were compared to test which of the data sets was more adept at rock type discrimination.

Comparison of Katahdin and Degelen Granites

A major emphasis in this study was the comparison of the Katahdin and Degelen granites. Reasoning behind this included the assumption

that finding the Katahdin Granite a spectral or textural analog to the Degelen granite would lend support to its role as a geologic analog. On the other hand, since the granites are somewhat similar mineralogically, one would expect them to give similar responses. If this were not the case, the next question would be why they were dissimilar. Since a precursory problem to this comparison was a correct identification of sampling locations for which to calculate representative statistics, the complete thematic classification of both sites was accomplished first. Information available for the comparison now included sample means, standard deviations and a map of pixels classified into these sample groups.

Means difference testing (t-test). A straightforward population comparison test that was well-suited to the problem of gauging similarity of the two test granites was the means difference or t-test (Eyton, 1982b). The form of the test is as follows:

$$t = \frac{x_1 - x_2}{\hat{\sigma}d}$$

with

$$\hat{\sigma}d = \left[\frac{s_1^2}{n_1} + \frac{s_2^2}{n_2} \right]^{1/2}$$

where

x_1 = sample mean, first group;

x_2 = sample mean, second group;

$\hat{\sigma}d$ = standard deviation of the difference between two means;

s_1 = standard deviation, first group;

s_2 = standard deviation, second group;

n_1 = sample size, first group;

n_2 = sample size, second group;

The threshold value for t in all of the tests was chosen to be 2.58, corresponding to a 99% confidence limit. If t wa⁻ ˑ ːween a positive or negative 2.58, the populations were considᵤred similar. This would indicate that a sample drawn from one group would be likely to fall closer than three standard deviations to the opposing group mean, where 99% of truly similar observations would probably fall. Population similarity was then judged on the basis of the 2.58 threshold value; divergent values of t indicated population dissimilarity.

The t-test was first performed on the raw data. Means and standard deviations for Bands 4 through 7 of the granite categories for the two Maine scenes were compared to test the repeatability of Landsat´s spectral measurements. The Russian granite categories were then tested in a similar manner.

Next, ratioed bands were utilized in the means difference test. This was done with the hope that ratioing response values would rᵤmove differences caused by overall sun illumination at different sun angleᵤ, and atmospheric interferences. Also, a gross filtering of topographic variability would be accomᵤplished. Texture means for the granites of the two study areas were then tested in a similar manner. It was assumed here that texture variables would remove first-order illumination and atmospheric differences between the scenes, since the variables depended on the interrelationships of neighbᵤring pixel values, and not the values themselves. Those variables with which the other variables were most highly correlated were used in the t-testing. Figures from the granite training areas of Maine and the Soviet site

were used, and also the test site spall was incorporated into this procedure. This was done because the spall represents a fresh surface, which might be more similar to the rough, fractured glaciated surface of Mount Katahdin, barring color differences. The spall was also of interest, because of its lack of vegetative cover.

Graphical representation: raw data and ratios. Another means of comparison helpful in gauging similarity of the groups was the plotting of raw pixel values and band ratios of the granite responses of the two sites. Two bands were used with each raw data plot, and the granite categories of the two Maine scenes (Table 4) were represented on each plot. Next, the ratio combination of the raw bands were plotted in a bar graph form to afford a more easily interpreted representation of the band ratio comparison of the two sites. Again, this was done because albedo differences are removed by ratioing, whereas color differences are not.

Production of Digitally Enhanced Imagery

Photographic Methods. The color photographic methods developed for use at Penn State by Department of Geography professor Ronald Eyton and his assistant Maxcy Dickson were employed in this study. These methods are well-adapted to Versatec output. After production on the dot-matrix (200 per inch) Versatec plotter, the gray-tone images were photographed onto a 10 X 12 inch photographic negative at a reduction of about one-half. The individual images were then assigned a color that they would contribute to the final three-color composite. The three secondary colors, yellow, magenta and cyan, were used; the noisiest image (the one

with the most random information content) was assigned yellow, and the
sharpest image, cyan. This scheme was chosen because the cyan color
dominates the final color combination. The image between the two
extremes was assigned magenta. The negatives were then laid on the
appropriate color of negative-acting color key and the two films were
exposed to ultraviolet light. The exposed color key plates were then
developed, overlaid and registered to form the color composite. Plates
included in this paper were reproduced from 35 mm slide photographs
taken of these composites. These second exposures were made while the
original composites were illuminated from underneath. Since the
transference was from film to film, higher fidelity of contrast and
color was maint ined.

False color composites. A simple procedure, but one that produced
some of the most useful imagery, was the contrast-enhanced false color
composite. Images of Bands 4, 5, and 7 were produced using a 10%
density slice of all brightness levels. Chosing a subscene of the size
used here permitted more contrast to be introduced into the images.
Band 4 was assigned yellow, Band 5 was assigned magenta, and cyan was
chosen for Band 7, as the commonly accepted method for production of
imagery of this type. Plates 7, 8 and 10 were produced in this manner,
and Plates 2, 3 and 15 are images of this type produced by the EROS Data
Center, a branch of the U. S. Geological Survey responsible for the
distribution of remote sensing materials.

Band ratioing. A new technique made possible by multispectral data
collection, band ratioing has received much attention in the last 8 to
10 years. Rowan and his co-workers (1974) developed the method for use

in rock-type discrimination and detection of hydrothermally altered areas in Nevada. One observation they made was that band ratioing emphasized the differences in slope of the spectral response curves of target surfaces. Merifield and others (1975) were better able to detect differences over alluvial fan deposits utilizing a ratioed image of an area near Mohave, California. Blodget et al. (1978) found and easily mapped peralkalic granitic intrusions over an area in Saudi Arabia.

The band ratioing technique has certain advantages, but also demonstrated shortcomings. Objects of different color are frequently easier to differentiate, because their different spectral response curves are accentuated by the ratioing of two bands. However, similarly colored objects of different albedo will appear the same on a ratioed image (Gillespie, 1980). Topographic effects, to first order, are removed from a surface if the surface is of uniform color, but atmospheric effects, which are due to scattered diffuse light, are enhanced. Automatic classification is likely to be more difficult on a ratioed image due to the increased noise inherent to the process. Nevertheless, the technique has been used with success by researchers to glean information from ratioed images not visible or normal Landsat imagery (Rowan, 1974).

Ratioed images in this study were produced in the following manner. Longer wavelength bands were divided by shorter wavelengths (Band 7/Band 6, etc.) using the ORSER program SUBTRAN, and the results were linearly stretched to fit a 0 to 255 dynamic range. This was accomplished by choosing a minimum and maximum value, and then selecting a multiplication factor that would perform the scalar expansion to the desired 255 gray levels. The entire range of responses was then shifted

so that the minimum resided at 0. For the final Versatec gray tone
image, the pixel responses were divided into 10 equal classes and these
classes were assigned a Versatec gray level. Plate 11 is a ratioed
image of the Semipalatinsk region and Plate 16 is a ratioed image
depicting the Mount Katahdin area. The Semipalatinsk image was produced
assigning cyan to Bands 5/7, magenta to Bands 4/7 and yellow to Bands
4/5. The Katahdin scene used cyan for Bands 4/7, magenta for Bands 5/7
and yellow for Bands 4/5.

Principal components transformations. Another technique useful in
image processing is the principal components analysis discussed earlier.
One of this procedure's greatest advantages is that it compacts nearly
all of a scene's variance into the first three axes, which is the number
most frequently used for the color compositing process. The method
enlisted here for image production involved assigning yellow to
principal components axis 3, magenta to axis 2, and cyan to axis one.
This was the case since axis one contained the most information, which
would then be emphasized on the image by the dominant cyan color. Axis
2 contained somewhat less, and so was assigned the more moderate magenta
color. Finally, yellow was chosen for axis 3 as this axis illustrated
only the gross features of the scene, which would be mildly highlighted
by this subdued color. Plate 12 is the principal components composite
of the Semipalatinsk study region, and Plate 18 is its counterpart for
the 20 August 1976 scene over the Katahdin region.

An alternate form of principal components analysis used was the
principal component "2-2-2" method. Blodget et al. (1978), in enhancing
imagery over Saudi Arabia, transformed two bands of Landsat MSS data at
a time utilizing the principal components analysis. They combined

images of the first and second axes in various manners, and were thus more successful in discriminating different classes of bedrock lithologies. This technique was used on the 12 May 1974 Semipalatinsk scene, and several images were produced. Plate 1 and 13 are examples of this type of processing. Plate 1 was produced using the first principal component axis of Bands 4 and 5 (magenta), 5 and 6 (yellow), and 6 and 7 (cyan). Plate 13 was made using yellow for Bands 6 and 7, axis 2; magenta for Bands 4 and 5, axis 2; and cyan for Bands 6 and 7, axis 1.

Principal components and ratio combinations. Another variety of image enhancement used involved a combination of principal component images with ratioed images. Combinations found to be useful in this study were the first principal component axis of Band 6 and Band 7 composited with various arrangements of ratioed bands. Plates 14 is an example of one of the images produced in this manner. For this particular image, Band 4/5 was assigned yellow, the 5/7 ratio, magenta, and the first principal components axis of Bands 6 and 7, cyan.

CHAPTER IV

RESULTS

Feature Extraction and Thematic Classification

Training field statistics, Maine. After all thematic
classification maps were produced, an analysis of the category
"signatures" (means and standard deviations) was done. These statistics
for the 1973 and 1976 Maine scenes are shown in Tables 8 and 9,
respectively. The rock outcrops, as evidenced by the rhyolite, slope
granite, plateau granite and plateau rock categories of the two scenes
were brighter than the surrounding forest in the visible bands.
Comparing the chlorophyll spectral response (Figure 3) in the .5 to 1.1
micrometer region with the corresponding lithologic responses (Bands 4
through 7, Tables 8 and 9), it is obvious that chlorophyll absorption at
.6 - .7 micrometers is expressed in the 1973 outcrop responses, but not
in the 1976 responses. The reason for this is unclear, but it perhaps
is related to the annual life cycle of the lichens coating the rocks.
However, the sharp increase in Band 6 response for the Mount Katahdin
rocks is comparably prominent in the curve for the corresponding .7 - .8
micrometer region of Figure 3. Therefore, it is likely that the lichen
covering of the rocks at least partially alters the spectral response of
the underlying surface. When one examines the figures for the forest
categories in Tables 8 and 9, the increase of the Band 6 and Band 7
infrared responses is most striking. Deciduous forest, especially, is
bright in the infrared even though it appears dark in the visible

Table 8. Simple statistics, training area categories of 23 July 1973 Maine scene.

Category	Band	Sample Size	Mean	Standard Deviation
Plateau rocks	4	143	30.6	1.83
	5	143	25.0	1.60
	6	143	36.3	5.19
	7	143	15.8	6.09
Slope granite	4	100	34.3	2.15
	5	100	28.5	2.14
	6	100	46.6	4.39
	7	100	24.8	2.98
Shadowed coniferous	4	138	20.1	1.04
	5	138	11.7	1.21
	6	138	28.3	2.10
	7	138	16.1	1.10
Sunlit coniferous	4	116	22.4	1.65
	5	116	13.5	1.79
	6	116	42.1	4.69
	7	116	24.6	2.78
Deciduous	4	148	22.7	1.20
	5	148	12.9	0.88
	6	148	61.5	2.77
	7	148	38.8	1.58
Water	4	114	21.9	1.61
	5	114	13.1	1.52
	6	114	10.8	1.66
	7	114	3.3	1.05
Cloud	4	44	83.8	8.11
	5	44	78.4	8.81
	6	44	99.0	6.91
	7	44	47.8	2.31

Table 9. Simple statistics, training area categories of 20 August 1976 Maine scene.

Category	Band	Sample Size	Mean	Standard Deviation
Rhyolite	4	314	19.2	1.66
	5	314	19.9	1.54
	6	314	43.4	6.93
	7	314	20.2	4.39
Slope granite	4	207	25.2	2.78
	5	207	29.0	3.86
	6	207	48.1	6.52
	7	207	22.1	3.71
Plateau granite	4	156	19.6	1.57
	5	156	22.8	1.64
	6	156	35.4	4.91
	7	156	16.4	3.10
Shadowed coniferous	4	295	12.2	0.93
	5	295	11.0	1.24
	6	295	22.5	1.65
	7	295	10.2	0.90
Sunlit coniferous	4	253	12.4	0.84
	5	253	11.3	0.95
	6	253	28.5	1.21
	7	253	13.7	0.84
Deciduous	4	425	15.7	1.06
	5	425	13.0	0.98
	6	425	57.1	5.28
	7	425	30.7	3.16
Water	4	127	11.9	0.87
	5	127	8.7	0.69
	6	127	9.0	0.91
	7	127	1.7	0.68

region. The increase of Band 6 over Band 5 is consistently over 300%. Training field statistics for water in both scenes show a steady drop in Band 4 through Band 7. To summarize these effects, it can be concluded that a chlorophyll response, which is prevalent over the scene, dominates the deciduous and coniferous forest responses. Although the chlorophyll alteration is weaker over the granite, it is persistent, as illustrated by the 60% and 100% rise in Band 6 exhibited by the granites and rhyolites, respectively. This effect is due to a thin covering of lichens over the rock surfaces, a condition which was verified by an on-site investigation by the author.

Training field statistics, USSR. Results of training field extraction for the Soviet site are listed in Table 10. Readily apparent is the relative stability of most of the categories across Bands 5 and 6 with a further drop in Band 7 (considering a doubled value for that channel, as NASA normally scales it by 1/2 during processing). This points to an extremely light or immature vegetation cover. Granite classes 1 and 2, however, exhibit an effect similar to that of chlorophyll, and on the false color composites of Plates 7, 8 and 10, the reddish tint (normally due to vegetation) of the central massif is plainly visible. To verify this as likely being a chlorophyll-caused phenomenon, additional training sites were chosen over the narrow, valley-like features assumed to be partially vegetated drainage patterns in the topographically low valleys. A typical set of values for the valley vegetation is the "vegetation" class of Table 10. This category showed responses more typical of chlorophyll as illustrated in Figure 3. From this, it could be argued that the third "Granite detritus" category represents a granite relatively undisturbed by a vegetation canopy.

Table 10. Simple statistics, training field categories, 12 May 1974
Soviet scene.

Category	Band	Sample Size	Mean	Standard Deviation
Granite 1	4	111	34.4	1.45
	5	111	30.8	1.49
	6	111	34.4	1.57
	7	111	16.5	0.81
Granite 2	4	115	37.5	0.92
	5	115	37.9	1.53
	6	115	42.7	1.58
	7	115	20.1	0.66
Granite detritus	4	180	42.3	2.00
	5	180	46.2	1.49
	6	180	47.5	1.58
	7	180	41.6	0.83
Burned areas	4	131	29.8	1.31
	5	131	25.6	1.89
	6	131	23.6	1.99
	7	131	10.3	1.06
Other detritus	4	152	41.5	1.52
	5	152	41.1	1.48
	6	152	42.9	1.42
	7	152	18.8	0.60
Light volcanics	4	161	37.9	1.37
	5	161	35.3	1.24
	6	151	36.0	1.37
	7	161	15.8	0.71
Dark volcanics	4	54	32.4	1.81
	5	54	28.1	2.08
	6	54	28.8	2.20
	7	54	11.9	1.65
Spall	4	188	56.7	5.56
	5	188	66.7	5.47
	6	188	64.2	5.00
	7	188	27.1	2.17
Vegetation	4	24	36.0	1.55
	5	24	33.8	2.18
	6	24	42.7	2.12
	7	24	20.5	0.93

This group, along with the Granite 1 and Granite 2 groups (representing a light vegetation cover) were then used in the comparison of the Degelen and Katahdin granites. Other categories that appeared relatively free of a chlorophyll-tinted cover were the "Other detritus", "Light volcanics", "Dark volcanics", "Burned areas" and "Spall". Categories which may be regarded as vegetation-free granites, spall and granite detritus, show a fairly consistent pattern of high responses on Bands 5 and 6, and low responses on Bands 4 and 7 (with Band 7 doubled as previously described).

To verify this postulated pattern of responses for bare granites, a cluster analysis was performed over the Hogar granite massif, located in the Sahara Desert of north Africa. It was assumed that a vegetation canopy would be negligible over such a region, and that the Hogar granite outcrop "signatures" would act as somewhat of a standard against which to compare other "bare granite" responses. Results of this test showed that the response curves for the Degelen spalls and Hogar outcrops were, in fact, quite similar in shape, although the granites were of slightly different albedo.

Thematic classification, Maine sites. The thematic classification maps produced for the two Maine scenes were next evaluated for accuracy. This was done with the aid of ground truth information in the form of aerial photographs, land use and cover maps, and topographic maps of various scales. Personal logs and recollections of on-site investigations were also consulted.

Classification accuracy for the 20 August 1976 scene (Plate 5) was satisfactory. There was general agreement between the thematic map and the land use maps concerning forest type and distribution. The

deciduous-coniferous forest boundaries matched quite well. Not all areas classified as "shadowed coniferous" were located on slopes facing away from the sun; therefore, an evergreen forest type of lower reflectivity likely exists on sunlit slopes as well.

There were some discrepancies found on the map, however. Some of the peripheral areas of Mount Katahdin were incorrectly classified as rhyolite, and some of the rhyolite areas to the north were partly classified as plateau granite. The cleared area to the south of Mount Katahdin is presumably the Baxter State Park headquarters and surrounding camping areas, and the cleared areas are similar to the rhyolite category.

These problems stem from two causes. First, there were an insufficient number of categories to accommodate all of the spectral groups included in the scene. For instance, the cleared area south of the mountain should have been in a category of its own. Secondly, and more importantly, many of these features were simply too similar for Landsat's sensors to distinguish. For example, the same ground cover, lichen, was probably covering the slopes of both the granite and the rhyolite peaks to the north, so that there was confusion between the two. Also, the basic mineralogical composition of the two lithologies is somewhat similar, so the spectral responses of the weathered surfaces in the absence of lichens would be similar.

One item of interest is Mount Katahdin's high slope reflectivity. This was partly due to high slope angles facing into the sun, but also to the highly fractured surface of the rock. Such a surface texture would be a more efficient reflector of sunlight. The lichen covering, as well, would increase the infrared reflectance.

On the 23 July 1973 classification map (Plate 4, compare with Plate 5), several things were immediately apparent. First, the cleared area south of the mountain was missing, indicating that the area remained forested until 1974 or 1975. More area on this classification was assigned to the "shadowed coniferous" category than on the 20 August 1976 scene. This could have been due, perhaps, to more stressful conditions in 1973 lowering the chlorophyll reflectivity of the conifers, or perhaps wet conditions on that day were responsible for lower infrared reflectance. In any case, the deciduous-coniferous boundaries remained fairly constant, demonstrating the ability of Landsat's visible and near-infrared sensors to distinguish forest types. The cloud covering was, on occasion, misclassified into the next brightest category, slope granite. The odd appearance of the righthand edge of the 23 July 1973 classification map is due to erratic pixel values at the scene boundary.

Thematic classification, Degelen Massif. After a comparison of the classification map of the Degelen Massif (Plate 6) with the corresponding multidate color composites of the massif (Plates 8 and 10) and the Soviet geologic map (Figure 10), the reasonableness of the classification can be gauged. The red and magenta colors (see Table 6) of Granites 1 and 2 stayed fairly well within the boundary of the granite as indicated by the geologic map. Granite 2 apparently included most of the vegetation located in the stream channels. Stringers of Granite 2 extend out from the massif as vegetated stream channels would. The magenta Granite 1 category was almost exclusively limited to the shadowed regions, that is, the slopes of the hills facing away from the sun's direct illumination. The "Light volcanic" rock category on the

eastern border of the massif (assigned the color green) was overlapped with the "Other detritus" category to the west, denoted Ordovician sediments on the geologic map (Figure 10). It is unlikely that sediments with the volcanics as a source material could be transported over the massif to be deposited at that site. There was also an overlap of the "Dark volcanics" with the "Burned areas". The spall mapped distinctly, due to its very high response in all four channels. The granite detritus likewise plotted in a fairly consistent manner. In addition to being localized around the northwestern part of the massif, it followed outwash patterns away from the massif and was also located around the periphery of the spall. Its location here is further evidence that the granite detritus and spall groups together represent vegetation-free granite responses, albeit of different albedoes. The spall's higher reflectivity was doubtless due to its very rough surface texture acting to enhance its reflectance. As an indication of the roughness of the spall, the standard deviation of that category (Table 10) is very high.

To summarize these findings, it can be stated that 1) the Granite 2 and possibly the Granite 1 categories were intermixed with light vegetation, 2) the Granite detritus and Spall categories represent granite surfaces relatively free of vegetation, 3) volcanics and Paleozoic sediments surrounding the massif were difficult to separate, and 4) dark volcanics and burned areas were also difficult to separate.

Discrimination of Rock Types: Graphical Representation

Raw data plots. A form of analysis helpful to the evaluation of

cover type separability and Landsat sensor performance in discrimination was the two-dimensional plotting of training field population distributions. This was done using the program BVSTD (Eyton, 1982a) which plotted the distributions on the Versatec electrostatic plotter. A discussion of these plots and their significance follows.

A Band 7 versus a Band 6 plot for the 23 July 1973 scene is shown in Figure 19. The large variance of the plateau rock category is evident, as is the uncustomary lack of strong correlation between these two infrared channels in describing this category. The shadowed conifer category is entirely contained within the plateau rock category. This is because both of these groups have a high infrared response. The visible bands are more adept at differentiating these two groups. Water has a characteristically low infrared response, and at the other extreme are the very bright cloud responses. Finally, the deciduous trees form a very distinct group in the infrared spectral region. Figure 20 illustrates a slightly negative correlation of Band 7 with Band 5 for all categories but cloud. That is, as Band 7 responses increase, Band 5 values decrease. Also notable is the relatively uniform responses on Band 5 for the coniferous, deciduous and water categories, which are well separated on Band 7. These two channels apparently are good discriminators of the categories chosen here. Figure 21 shows that Bands 6 and 5 also afford good category separation. The Band 6-Band 4 plot was similar and is not included. A plot of Band 5 vs. Band 4 (Figure 22) illustrates the high correlation and poor category separation that exists on these two bands. For this scene, then, it is evident that Bands 7 and 5 together offer the best discriminatory power using raw band pairs.
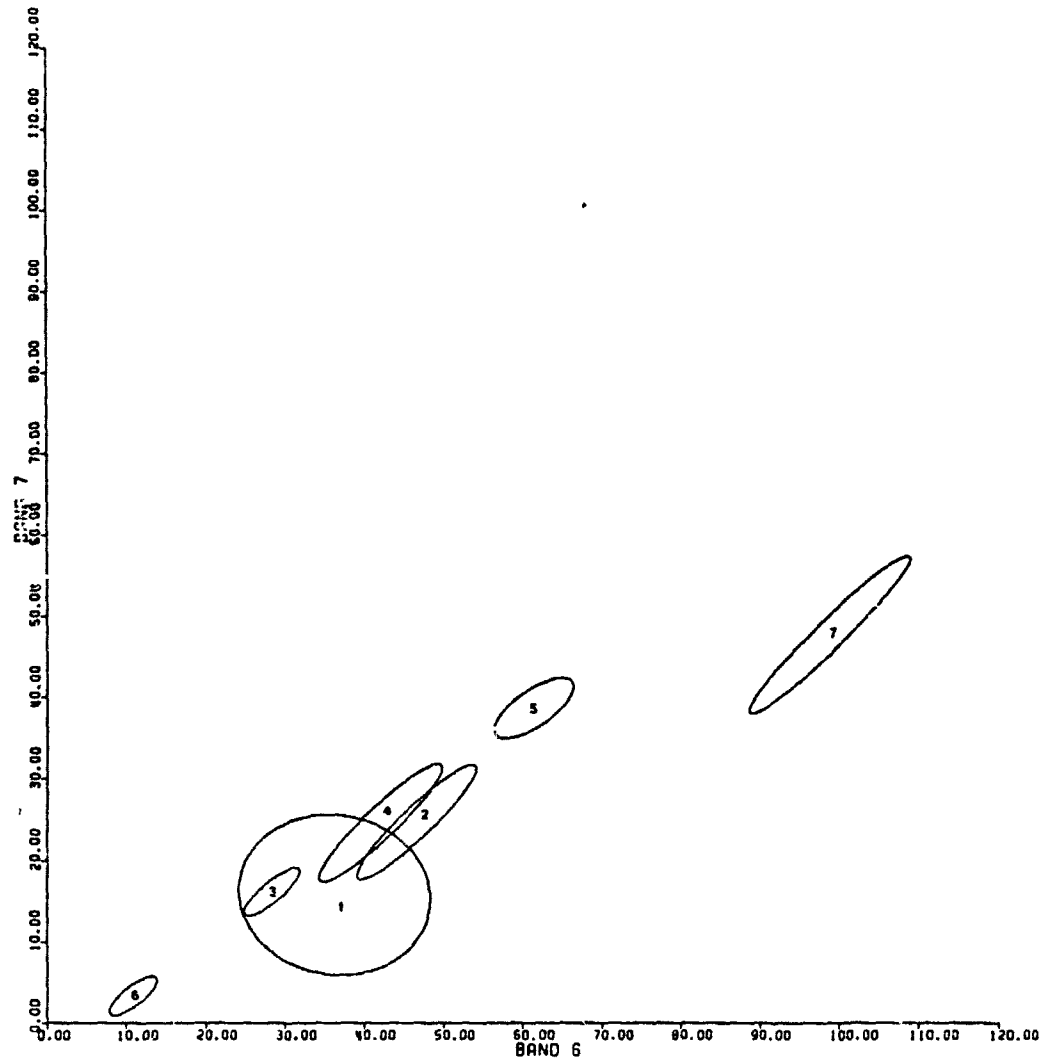
Figure 19. Training area population distributions, Band 7 vs. Band 6, 23 July 1973. Categories are listed in Table 4, p. 52.
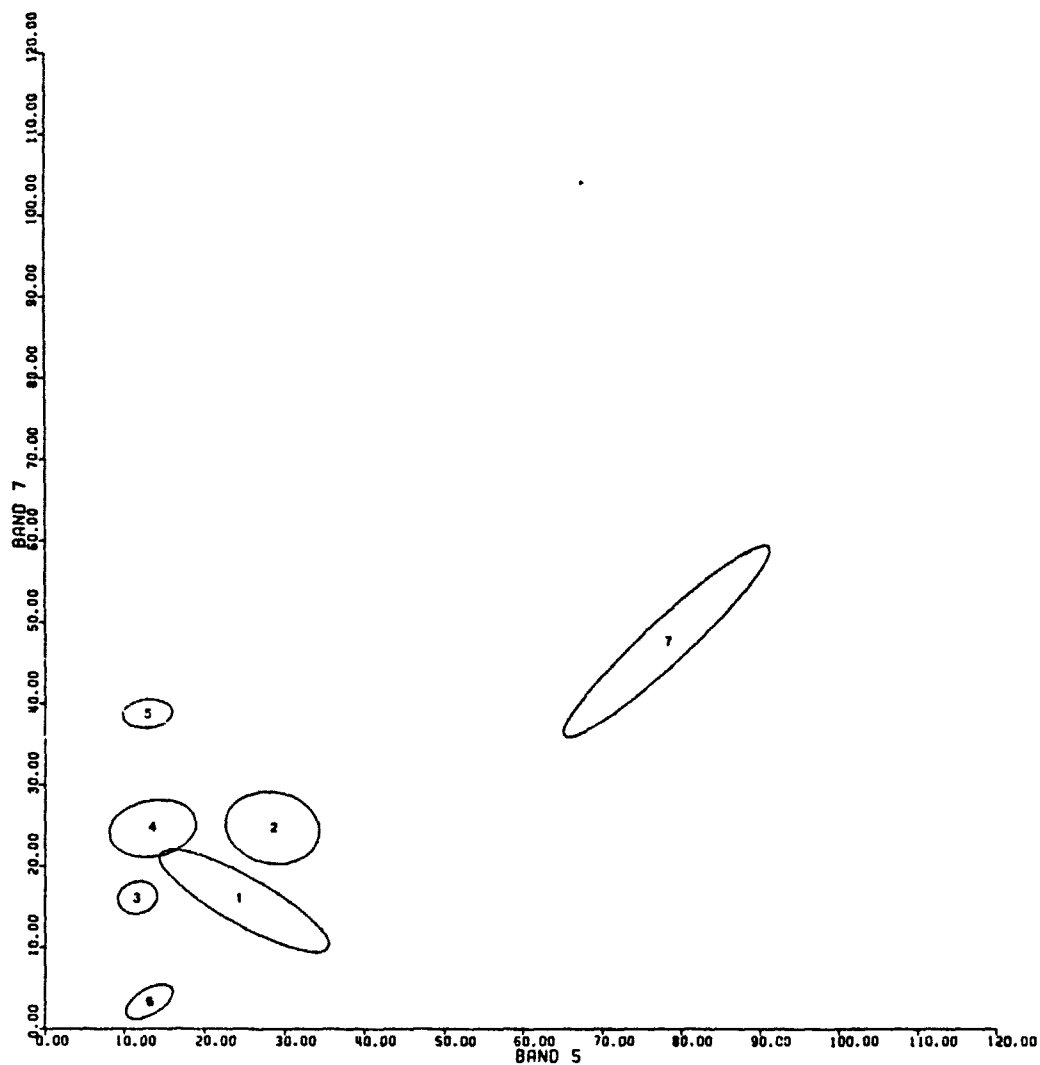
Figure 20. Training area population distributions, Band 7 vs. Band 5, 23 July 1973. Category numbers in Table 4, p. 52.
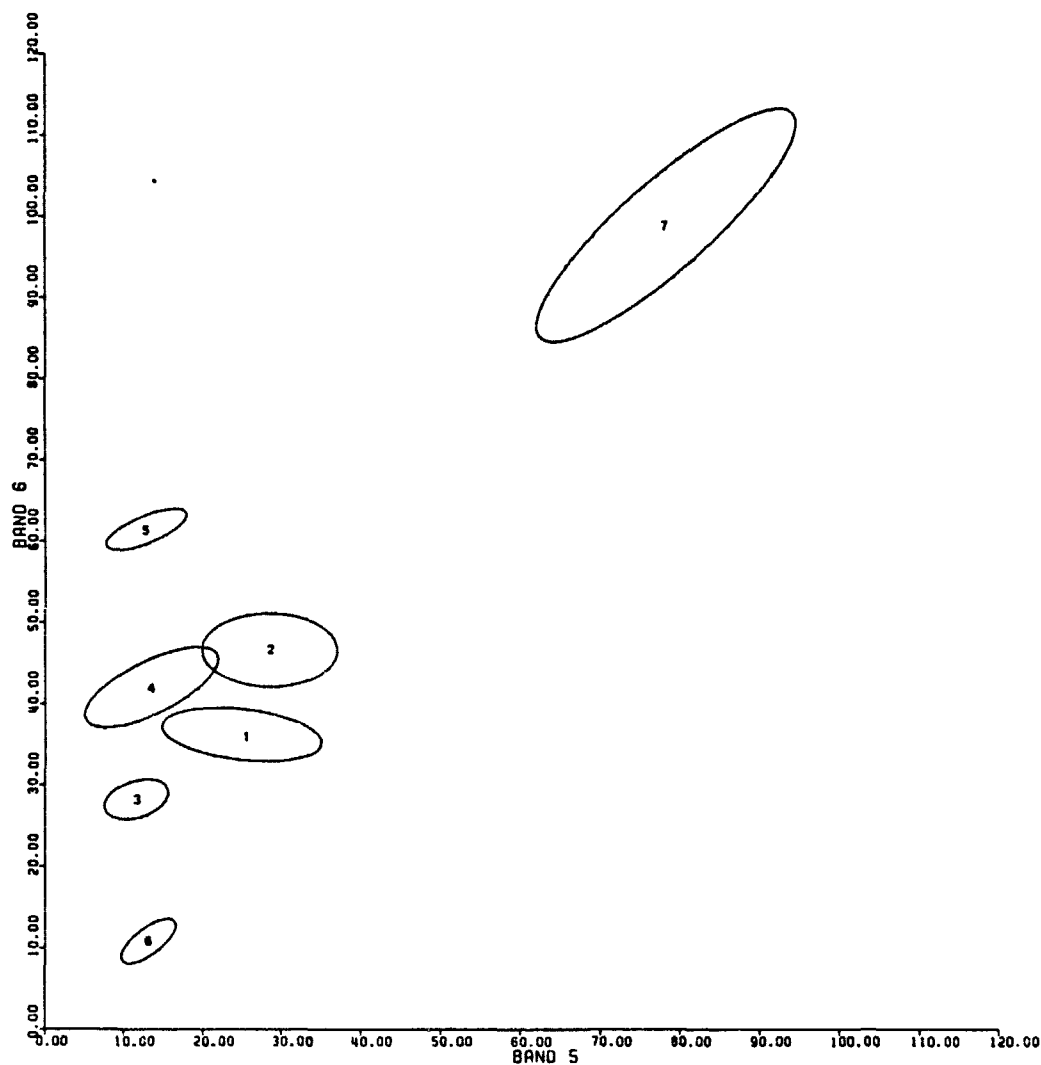
Figure 21. Training area population distributions, Band 6 vs. Band 5, 23 July 1973. Category numbers in Table 4, p. 52.
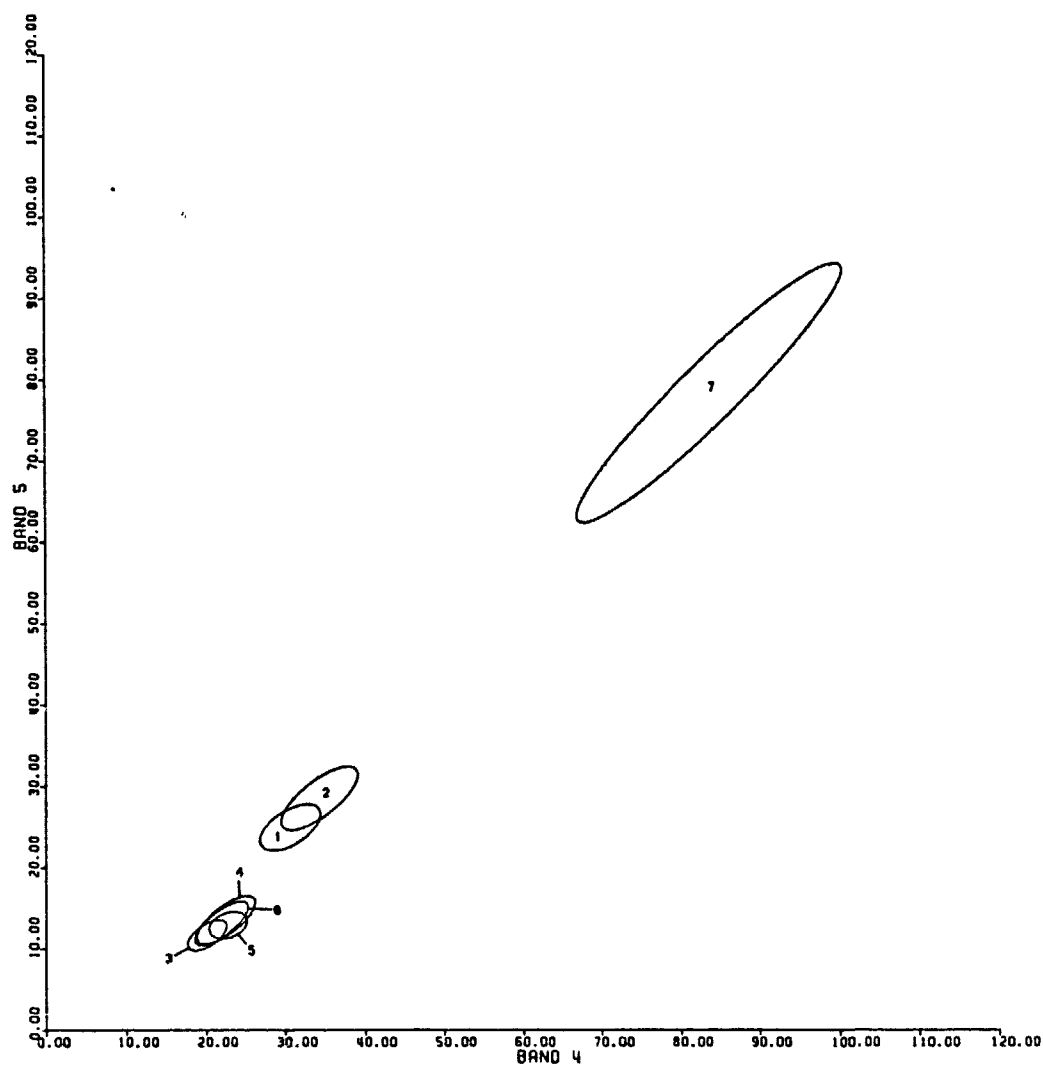
Figure 22. Training area population distribution, Band 5 vs. Band 4, 23 July 1973. Category numbers in Table 4, p. 52.

Plots for the 20 August 1976 scene exhibit somewhat similar behavior. In the plot of Figure 23A, bands 6 and 7 demonstrate strong correlation, and only the water, shadowed coniferous, sunlit coniferous and, marginally, the plateau granite categories are distinguishable. Also of interest is the elongated cloud shapes, indicating a large population variance, and the similar slopes of the categories point to the similar spectral influence of chlorophyll. The rocks and forest are further apart on the Band 7-Band 5 plot of Figure 23B. In Figure 24, Bands 5 and 4 again show a high degree of correlation, and the two coniferous groups are totally overlapped. This is an indication that the chlorophyll effect only becomes evident in the infrared region of the spectrum.

For the comparatively arid Degelen region, the plots are much more uniform, and only a few are included here. Figure 25A is a plot of Band 7 vs. Band 6 which again shows a high degree of correlation between the bands and a large amount of category overlap. Category 8, spall, demonstrates its rough surface texture by virtue of its large variance, or cloud shape. The plot of Figure 25B is of Band 7 versus Band 4 which depicts the categories as being slightly further apart, but there is still some overlap of the "burned area" and "dark volcanic" categories. A plot of Band 5 versus Band 4 (Figure 26) shows a confusion of Granite 1, dark volcanics and burned areas.

Band ratio plots. Band ratios, plotted in a bar graph style, were useful in interpreting the results of the ratioing process. Plots for the 23 July 1973 scene, a portion of which are included in Figures 27 and 28, are indicative of the spectral effects of chlorophyll on the responses of the ground cover classes. The Band 7/Band 6 plot (Figure
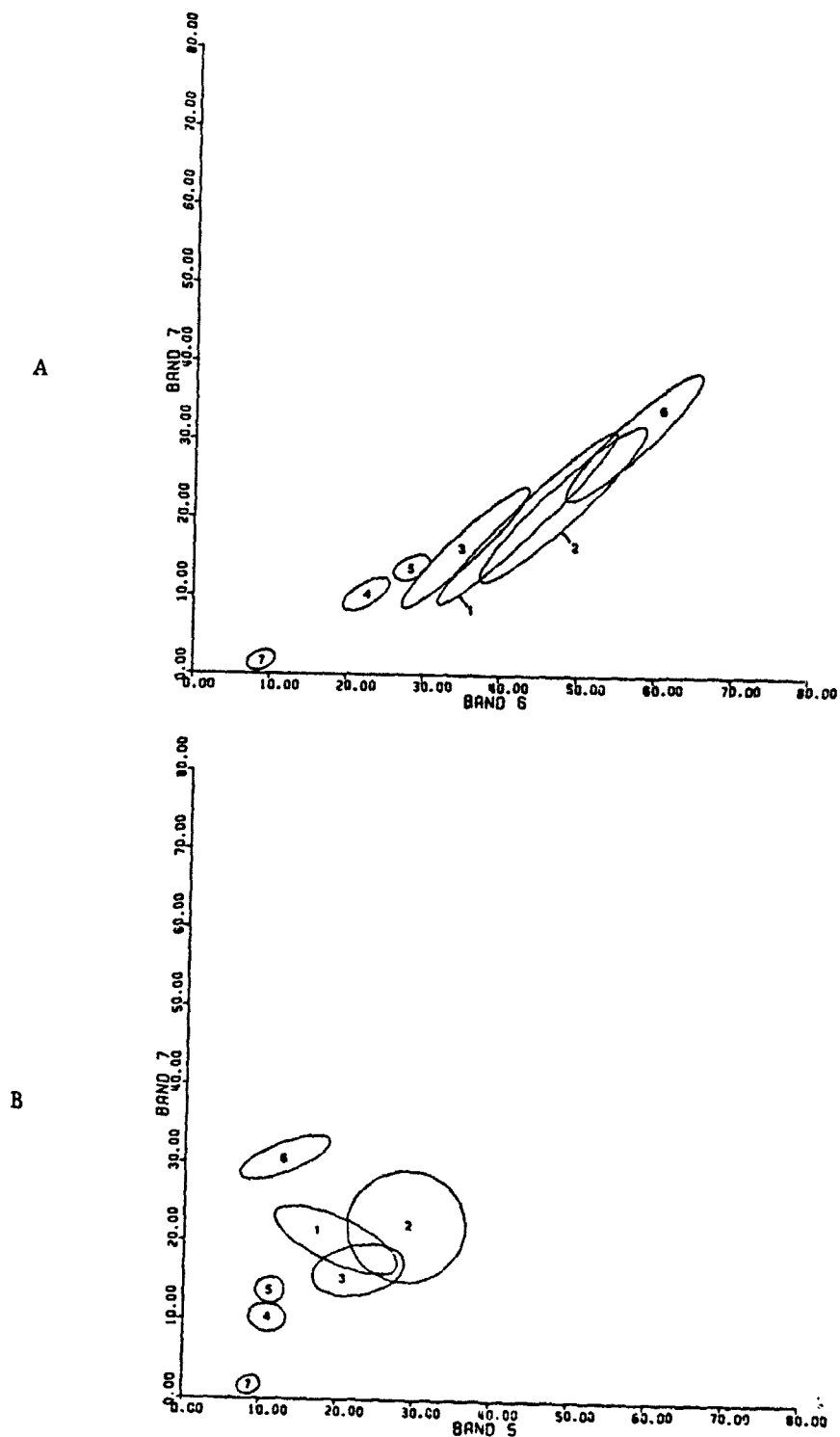
Figure 23. Training area population distributions: (A) Band 7 vs. Band 6; (B) Band 7 vs. Band 5. 20 August 1976 Katahdin area. Category numbers in Table 4, p. 52.
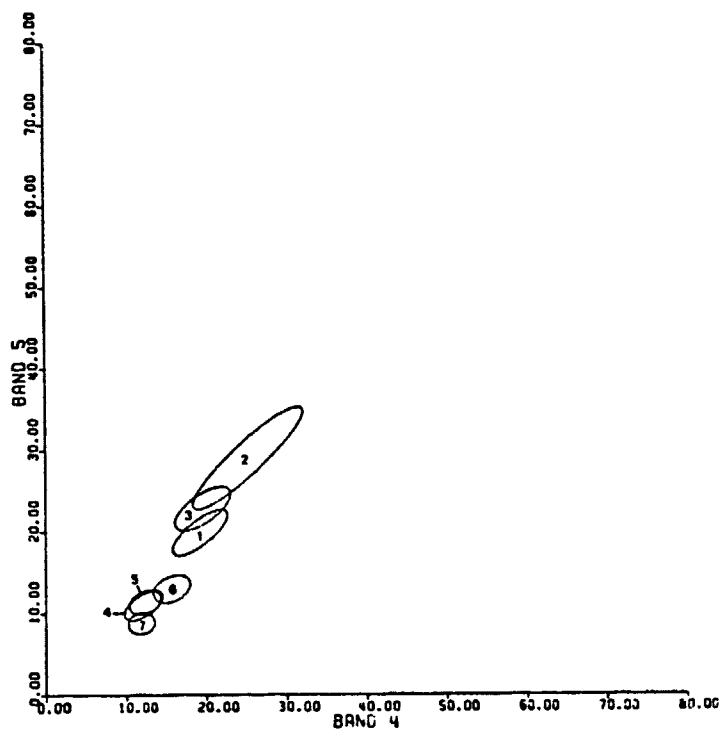
Figure 24. Training field population distributions: Band 5 vs. Band 4, 20 August 1976 Katahdin area. Category numbers in Table 4, p. 52.
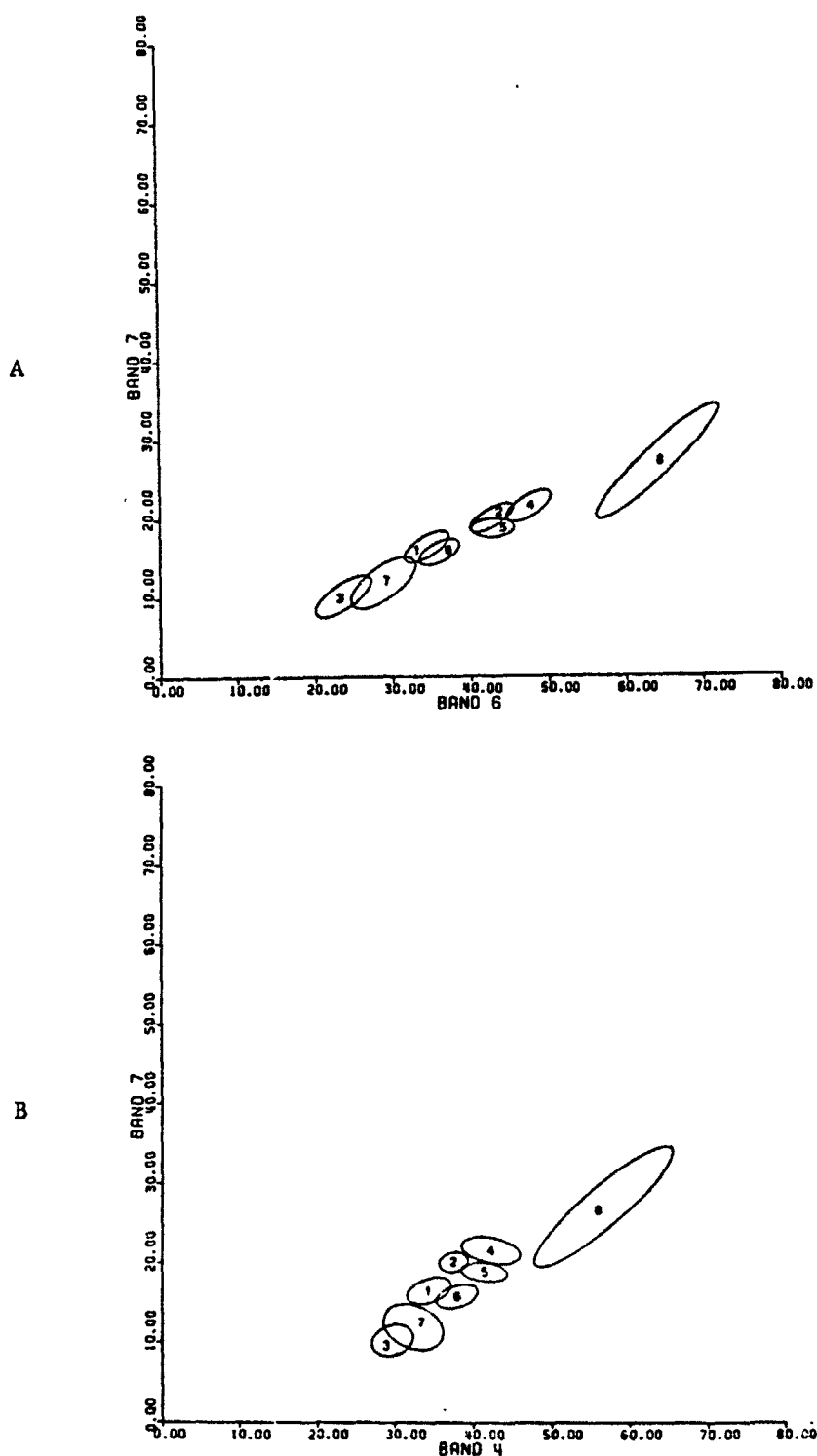
Figure 25. Training area population distributions: (A) Band 7 vs. Band 6; (B) Band 7 vs. Band 4. 12 May 1974 Degelen area. Category numbers in Table 6, p. 58.
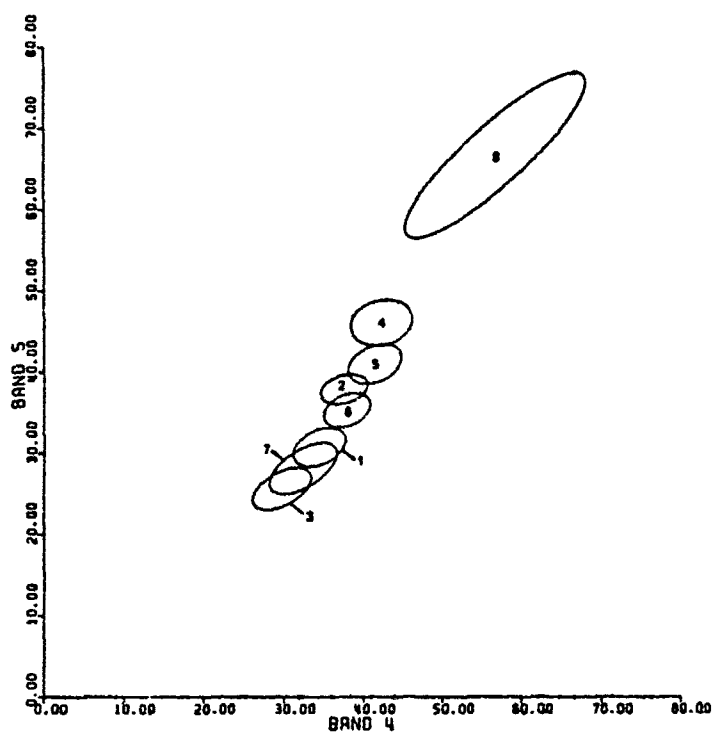
Figure 26. Band 5 vs. Band 4, 12 May 1974 training areas. Category
numbers in Table 6, p. 58.

27A) shows the higher Band 7 responses for the "greener" categories, the forests, while the cloud category shows a more equal response of Bands 6 and 7. The Band 7/Band 5 plot (Figure 27B) illustrates the high infrared-visible ratio effect due to chlorophyll, which, of course, lessens over the water and cloud categories. In Figure 28, the effect continues on a plot of Band 6/Band 4, and the Band 5/Band 4 plot demonstrates the slight chlorophyll absorption band at .6 - .7 micrometers. The absorption band is more accentuated over the forest categories, and water also has a lower Band 5 response. The cloud category again shows a flat spectral slope over Bands 4 and 5, as evidenced by its ratio being equal to 1.

In the 20 August 1976 scene ratio plots, similar conditions exist, but to different degrees. In Figure 29A, Band 7/Band 6 illustrates the more flat-topped chlorophyll curve of Figure 3 in the .7 to 1.1 micrometer spectral region (categories 1 through 5). Again the water category is distinctive. The Band 7/Band 5 plot of Figure 29B accentuates the infrared - visible region difference in the forest categories, numbers 4 through 6. The Band 6/Band 5 chart of Figure 30A shows similar behavior, and the ratio of Bands 5 and 4 (Figure 30B) demonstrates the outcrops to be very distinguishable from the forest in the visible bands.

Plots of the Degelen band ratios indicate a much weaker chlorophyll effect. Categories 1, 2, and 9 (Granite 1, Granite 2 and Vegetation) are categories with some vegetative cover, and the Band 7/Band 6 plot (Figure 31A) supports this conclusion, as does the Band 6/Band 5 graph (Figure 31B). According to the Band 7/Band 6 ratio, the spall category appears devoid of vegetation when it is compared to the larger ratio of

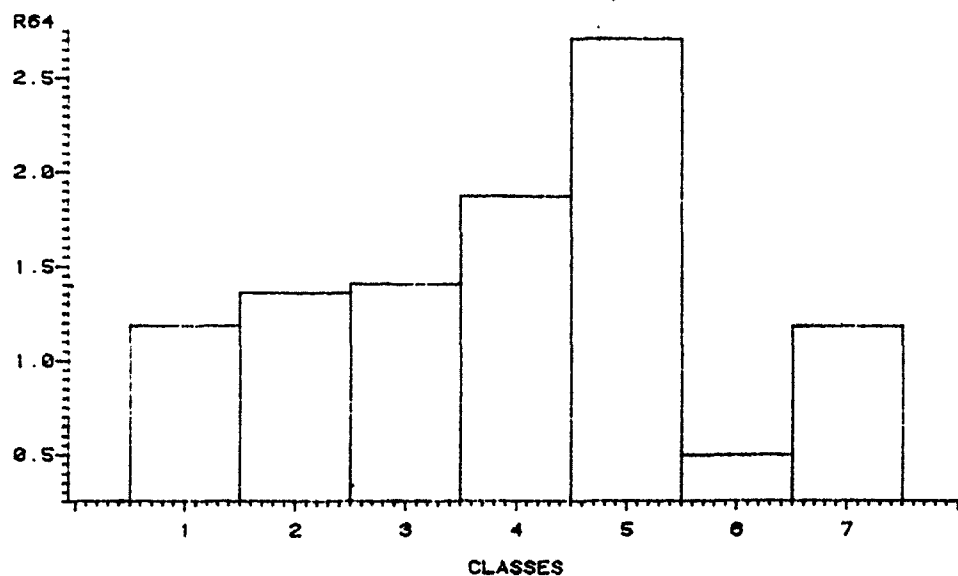# KATAHDIN LAND COVER CLASSES
23 JUL 73 BAND7/BAND6

A
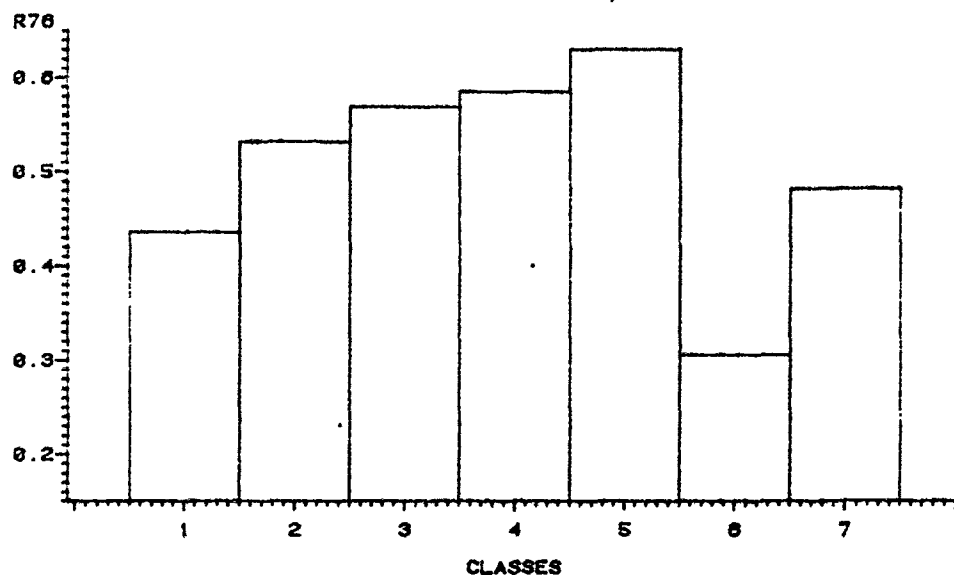
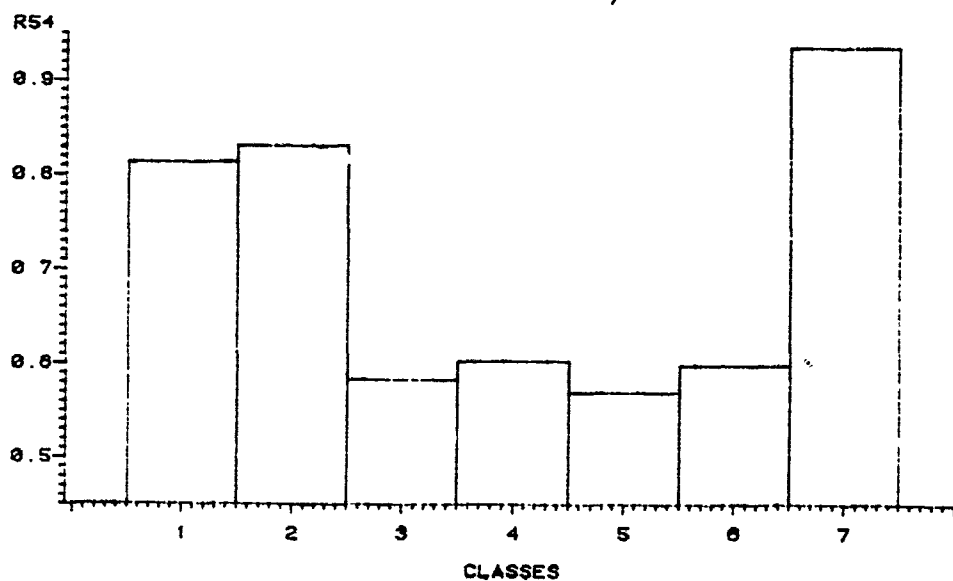# KATAHDIN LAND COVER CLASSES
23 JUL 73 BAND7/BAND5
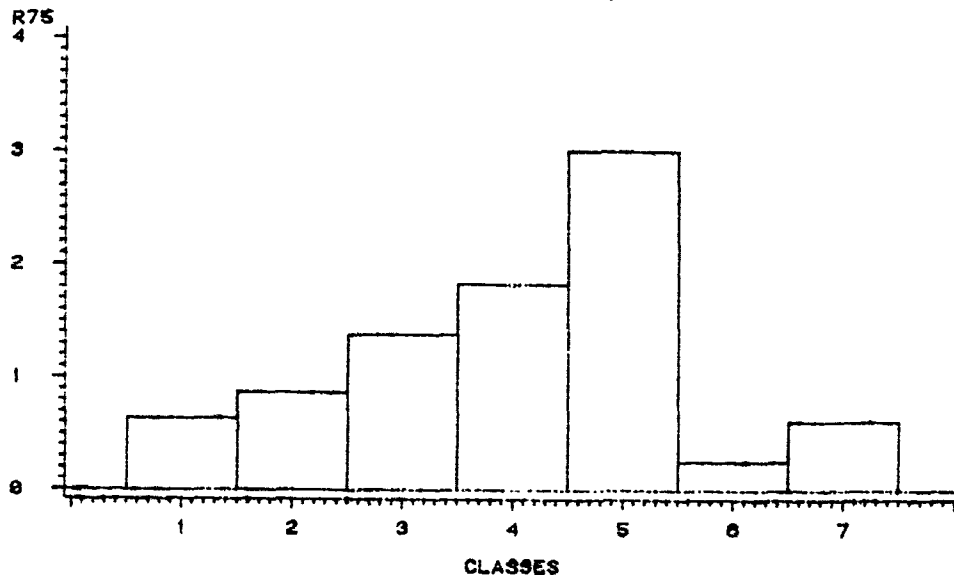
B

Figure 27. Ratioed bands of 23 July 1973 training areas.
(A) Band 7/Band 6 and (B) Band 7/Band 5. Category numbers
in Table 4, p. 52.

KATAHDIN LAND COVER CLASSES
23 JUL 73 BAND6/BAND4

CLASSES

A

KATAHDIN LAND COVER CLASSES
23 JUL 73 BAND5/BAND4

CLASSES

B

Figure 28. Ratioed bands, 23 July 1973 training areas. Category
numbers in Table 4, p. 52.
(A) Band 6/Band 4, (B) Band 5/Band 4.

KATAHDIN LAND COVER CLASSES
20 AUG 76 BAND7/BAND6

A

KATAHDIN LAND COVER CLASSES
20 AUG 76 BAND7/BAND5

B

Figure 29. Ratioed bands, 20 August 1976 training areas.
(A) Bands 7/Band 6, and (B) Band 7/Band 5. Category numbers
in Table 4, p. 52.

KATAHDIN LAND COVER CLASSES
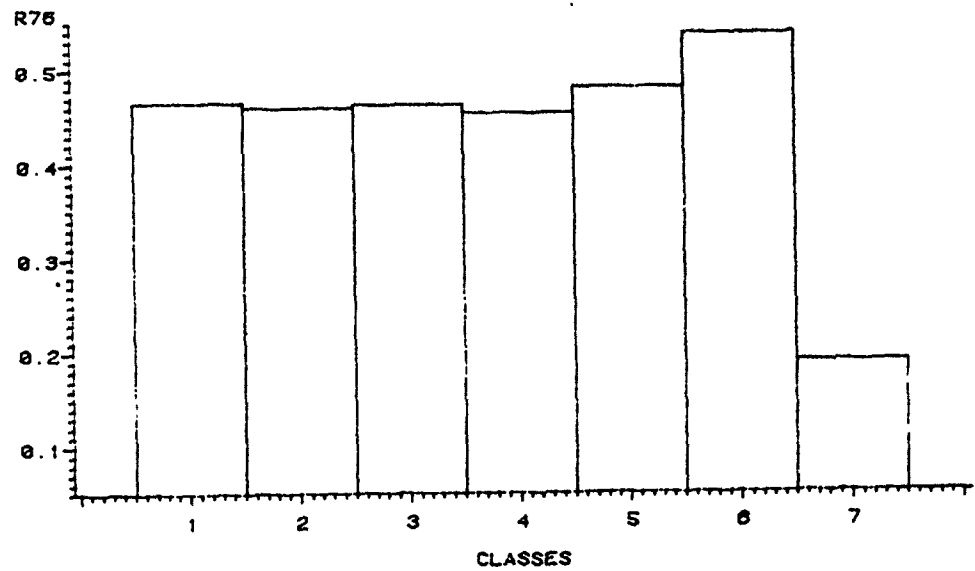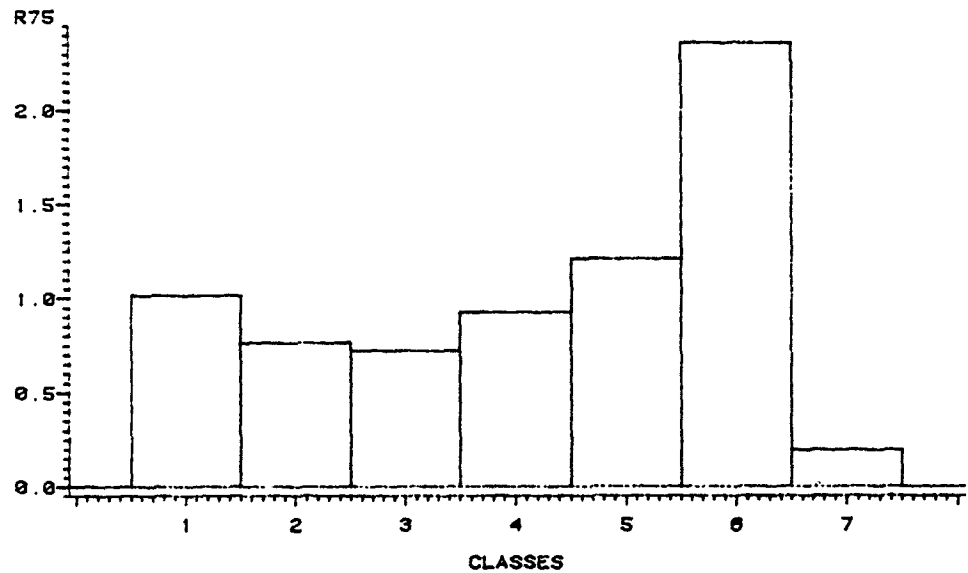### 20 AUG 76 BAND6/BAND5

A
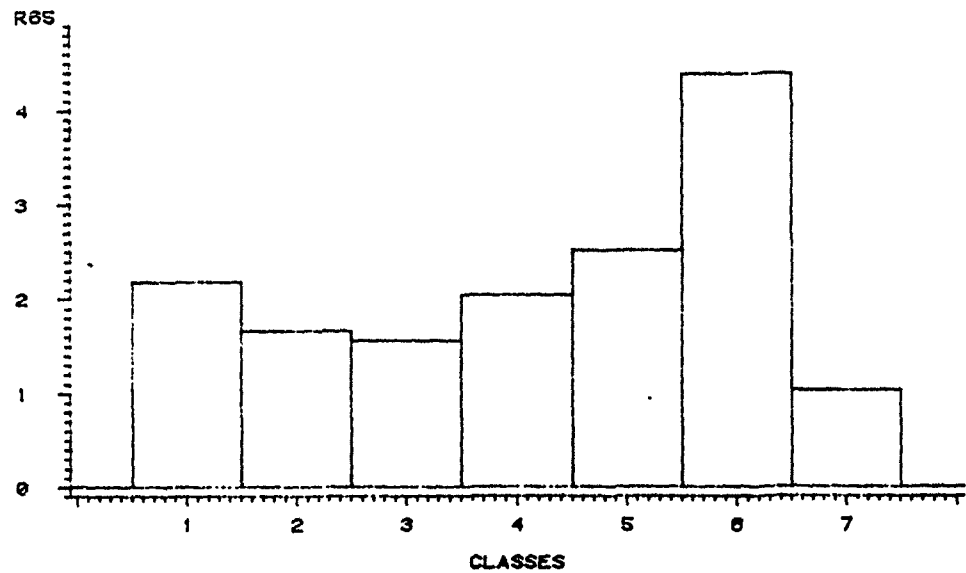
KATAHDIN LAND COVER CLASSES
20 AUG 76 BAND5/BAND4
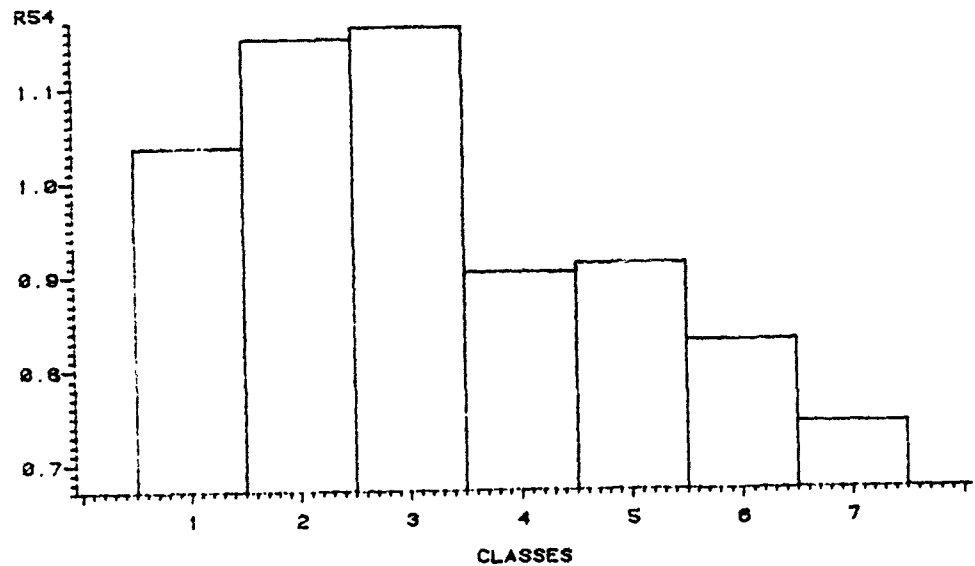
B

Figure 30. Ratioed bands of 20 August 1976 training areas.
(A) Band 6/Band 5, and (B) Band 5/Band 4. Category numbers
in Table 4, p. 52.

DEGELEN LAND COVER CLASSES
12 MAY 74 BAND7/BAND6

A

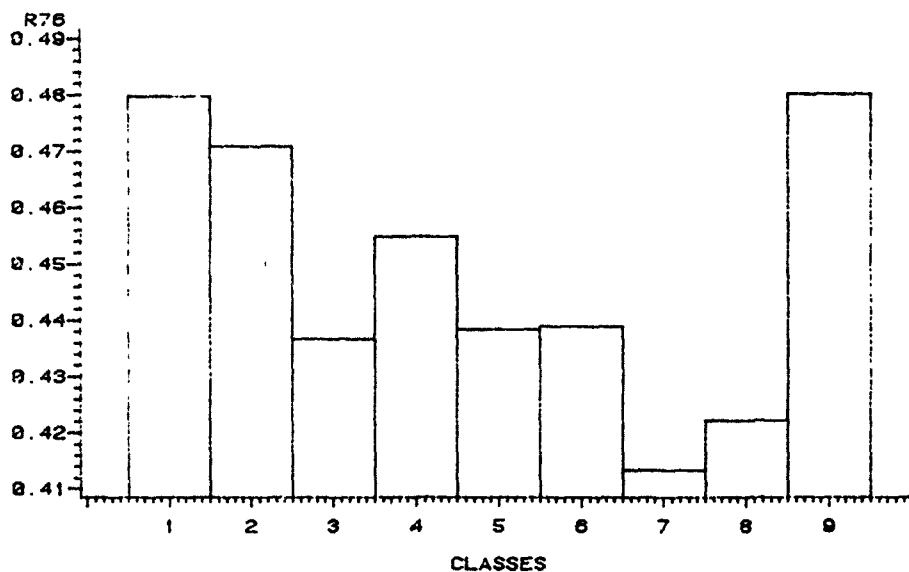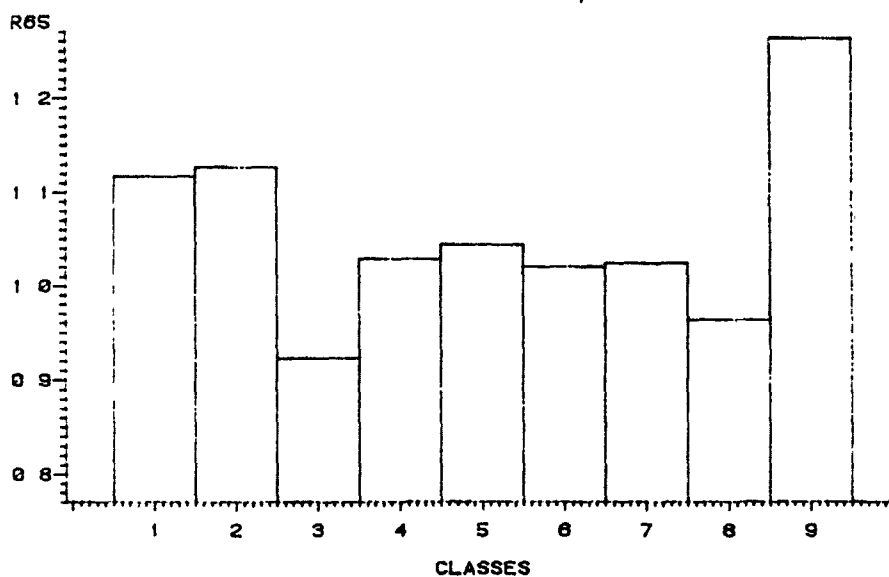## DEGELEN LAND COVER CLASSES
12 MAY 74 BAND6/BAND5

B

Figure 31. Ratioed bands, 12 May 1974 Soviet training areas.
(A) Band 7/Band 6, and (B) Band 6/Band 5. Category 9 –
vegetation, other categories in Table 6, p. 58.

category nine, vegetation. The values for the Band 6/Band 5 ratios of

Figure 31B seem to fall into three relatively distinct groups. That is,

Granite 1 and Granite 2 (numbers 1 and 2) have a higher infrared-visible

ratio as does the vegetation category. There is then a lower plateau of

responses comprised of categories 4 through 7, which are lower albedo,

unvegetated rock outcrops. Finally, the burned areas (category 3) and

spall (category 8) have even lower ratio values, pointing to a very

slight, perhaps nonexistent vegetation cover. On a plot of Band 6/Band

4 (Figure 32A), the scarcity of the vegetation over the scene is made

evident, as all of the ratios have values that are close to 1.0. If

this graph is compared with the Band 6/Band 4 graph of Figure 21, the

difference in vegetative cover of the two areas is striking because of

the difference in the ratios. More specifically, the Katahdin ratios

range from 1.5 to 2.5 and the ratios here all range from .8 to 1.2.

Finally the Band 5/Band 4 ratios (Figure 32B) seem to indicate

brightness on the scene. Categories 4 and 8 (Granite detritus and

spall) had the highest reflectivity on the scene, and categories 1, 3

and 7 (Granite 1, located on slopes away from the sun, burned areas, and

dark volcanics) had low reflectivities.

Discrimination of Rock Types: Texture Transform

The 12 May 1974 Degelen scene was chosen for the rock type texture

discrimination tests; the analysis was not performed on the Maine scenes

for several reasons. First, the arid Soviet region offered a far

greater variety of rock types to differentiate and it seemed that more

than two rock types would be helpful in properly gauging the usefulness

DEGELEN LAND COVER CLASSES
12 MAY 74   BAND6/BAND4

A

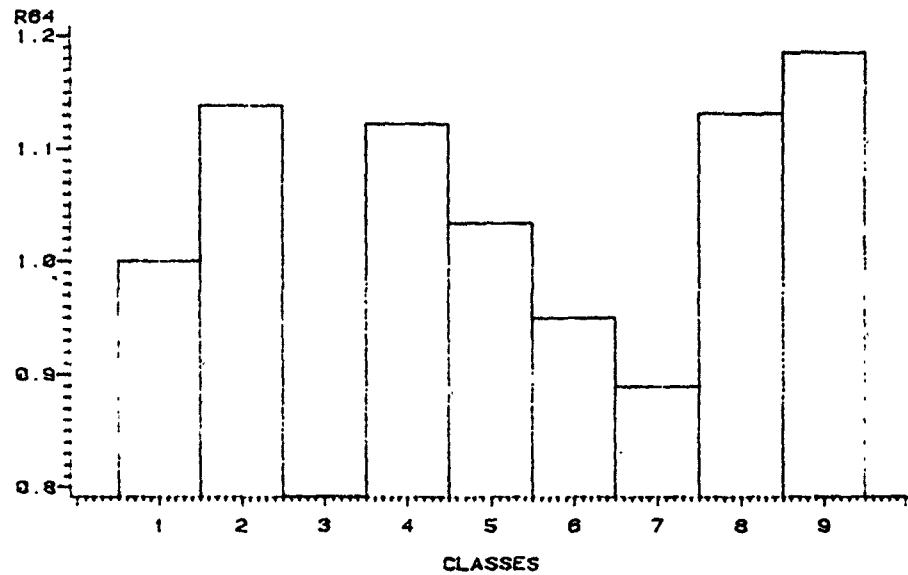# DEGELEN LAND COVER CLASSES
12 MAY 74   BAND5/BAND4
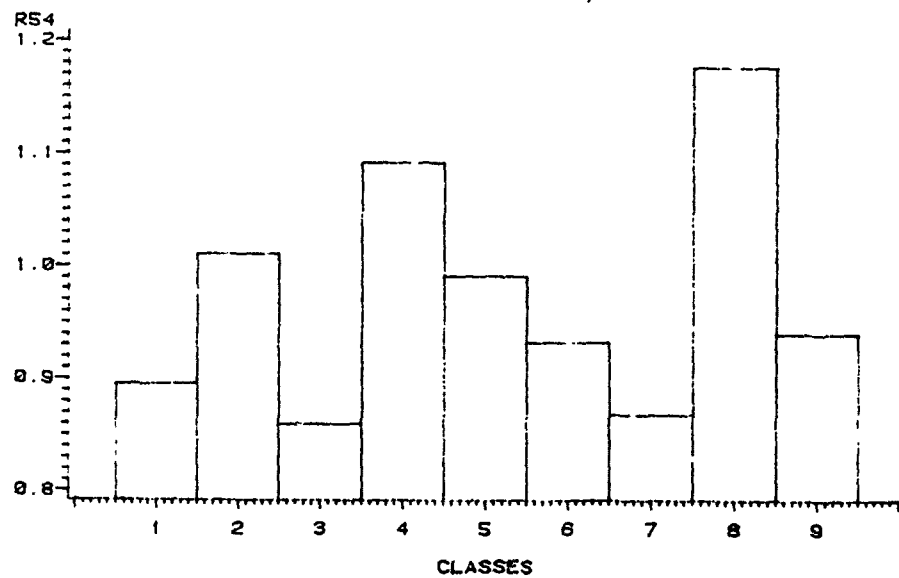
B

Figure 32.   Ratioed bands, 12 May 1974 Soviet training areas.
(A) Band 6/Band 5, and (B) Band 5/Band 4.   Category 9 —
vegetation, other categories in Table 6, p. 58.

of the texture transform in performing rock discrimination.

Analysis of raw bands. A pixel list of raw data responses for 17
training areas was input to the BMDP7M program which performed a
stepwise discriminate analysis on the data. The resulting
classification matrix is shown in Table 11. The 17 categories used in
this analysis were chosen from an intermediate list of categories,
reduced in number from the original 43 training field catorgories.
Classification was not extremely accurate, as attested by Table 11.
Volcanic numbers 2 and 4 appear somewhat distinct, but the spalls that
were distinct in the earlier classification are intermingled with other
categories. Figure 33 is a "scattergram" of the category means, plotted
on the first two canonical axes. These, of course, are the axes which
best differentiate the groups. The groups are aligned in a very simple
manner, from brightest on the left to darkest on the right. This is to
be expected, since the Landsat sensors merely detect albedo differences
of categories.

Comparison of raw bands and texture measures. The next step was to
input Hsu's 17 texture measurements, pixel by pixel, for these same
training fields and then to compare the two results. These texture
measures were calculated from principal components axis one, and datum
planes used with this data set (see Table 7) were 100, 127, and 154, due
to the 0-255 scaling of the data set.

Table 12 is the classification matrix of this analysis, which shows
some interesting results. Accuracy percentages indicate that, compared
to the raw data test, some groups are slightly more confused, while
others are much more distinct. Examples of the latter are the Granite

Table 11. Classification matrix of lithologic categories using raw data, 12 May 1974 Degelen area.

Categories are:

G1, G2, G4 – Granite

V1, V2, V3, V4, V5 – Volcanics

P1, P2, P3 – Paleozoic sediments

T1, T2, T3 – Tertiary sediments

S1, S2, S3 – Spalls

Blank

Figure 33. Scattergram of category means, lithologies of 12 May 1974
Degelen area, raw data. Symbols are:

1, 2, 3 - Granite

4, 5, 6, 7, 8 - Volcanics

9, A, B - Paleozoic sediments

C, D, E - Tertiary sediments

F, G, H - Spalls

OVERLAP OF DIFFERENT GROUPS IS INDICATED BY *

8.75

7.00

5.25

3.50

1.75

0.00

-1.75

-3.50

-5.25

-7.00

-8.75

C A N O N I C A L   V A R I A B L E   2

-12 -11 -10 -9. -8. -7. -6. -5. -4. -3. -2. -1. 0. 1. 2. 3. 4. 5. 6. 7. 8. 9. 10

CANONICAL VARIABLE 1

Table 12. Classification matrix of lithologic categories using texture variables calculated from principal components axis one.

NUMBER OF CASES CLASSIFIED INTO GROUP —

GROUP	PERCENT CORRECT	G1	G2	G4	V1	V2	V3	V4	V5	P1	P2	P3
G1	96.0	48	0	0	0	2	0	0	0	0	0	1
G2	70.8	0	34	0	0	0	0	0	1	0	0	0
G4	62.5	0	0	40	0	0	0	0	0	0	0	0
V1	25.4	2	5	0	16	0	0	0	0	1	2	0
V2	88.3	0	0	0	0	53	0	0	0	0	0	0
V3	80.8	5	0	0	0	0	42	10	0	1	0	0
V4	64.2	0	10	0	1	0	14	34	25	2	0	0
V5	51.0	0	6	7	0	0	0	0	23	32	0	0
P1	50.0	0	7	23	2	0	0	0	0	0	2	0
P2	33.9	0	0	0	0	0	0	0	0	0	19	0
P3	55.0	0	0	0	0	0	0	0	0	0	0	0
T1	52.5	0	0	0	0	0	0	0	0	0	0	3
T2	82.7	0	0	0	0	0	0	0	0	0	0	1
T3	97.2	0	0	0	0	0	0	0	0	0	0	0
S1	43.4	0	0	0	0	0	0	0	0	0	0	0
S2	70.0	0	0	0	0	0	0	0	0	0	0	0
S3	44.6	0	0	0	0	0	0	0	0	0	0	2
TOTAL	62.5	60	62	70	29	55	56	84	59	47	49	33

GROUP	PERCENT CORRECT	G1	G2	G4	V1	V2
G1	96.0	72	73	51	52	53
G2	70.8	0	0	0	0	0
G4	62.5	0	4	0	0	0
V1	25.4	6	15	0	0	0
V2	88.3	0	0	0	0	0
V3	80.8	0	0	0	0	0
V4	64.2	0	0	0	0	0
V5	51.0	0	0	3	0	7
P1	50.0	10	7	0	0	0
P2	33.9	0	5	0	0	0
P3	55.0	4	5	0	0	0
T1	52.5	1	70	36	31	10
T2	82.7	0	0	15	49	6
T3	97.2	0	0	19	5	24
S1	43.4					
S2	70.0					
S3	44.6					
TOTAL	67.5	60	106	73	85	48

Categories are:

G1, G2, G4 — Granite

V1, V2, V3, V4, V5 — Volcanics

P1, P2, P3 — Paleozoic sediments

T1, T2, T3 — Tertiary sediments

S1, S2, S3 — Spalls

1, Volcanics 3 and 5, and Tertiary sediments 2 and 3. Furthermore, the spall groups are, between themselves, much more uniform and distinct. Figure 34 is the corresponding scattergram which shows the relative polarity of the spalls, and the alignment of many of the other groups. This indicates that the categories are now well-defined and arranged according to surface texture in addition to albedo. The darkest categories, Granite 1 and three other volcanic categories, are neatly separated from the others. These groups represent shadowed areas, which presumbaly would have a more spatially uniform arrangement of pixel responses. In a subsequent analysis these dark groups were deleted to test separability of the remaining classes. The resulting classification matrix showed no significant improvement, which indicated that a stepwise discrimination of one set of groups was not highly dependent on the presence or absence of another, very different group.

The next test of the texture transform involved principal component axis 2. The 17 measures were calculated for this axis, and the data values submitted to BMDP7M for analysis. Table 13 is the classification matrix of the groups, which indicates an overall increase in confusion. However, Figure 35 illustrates an interesting feature of this particular analysis. The three granite categories, mean numbers 1, 2, and 3 on this plot, appear on one side of the scattergram, evidence that principal components axis 2 emphasizes edge enhanced features. Similar tests of principal components axis three demonstrated poor separability of categories.

A useful feature of the stepwise discriminant analysis performed by BMDP7M is an evaluaton of the performance of variables incorporated into each step of the analysis. Each variable's discrimination performance

Figure 34. Scattergram of category means, lithologies of 12 May 1974
            Degelen area. Texture variables calculated from PC axis 1.
            Symbols are:

                        1, 2, 3 - Granite

                      4, 5, 6, 7, 8 - Volcanics

                    9, A, B - Paleozoic sediments

                    C, D, E - Tertiary sediments

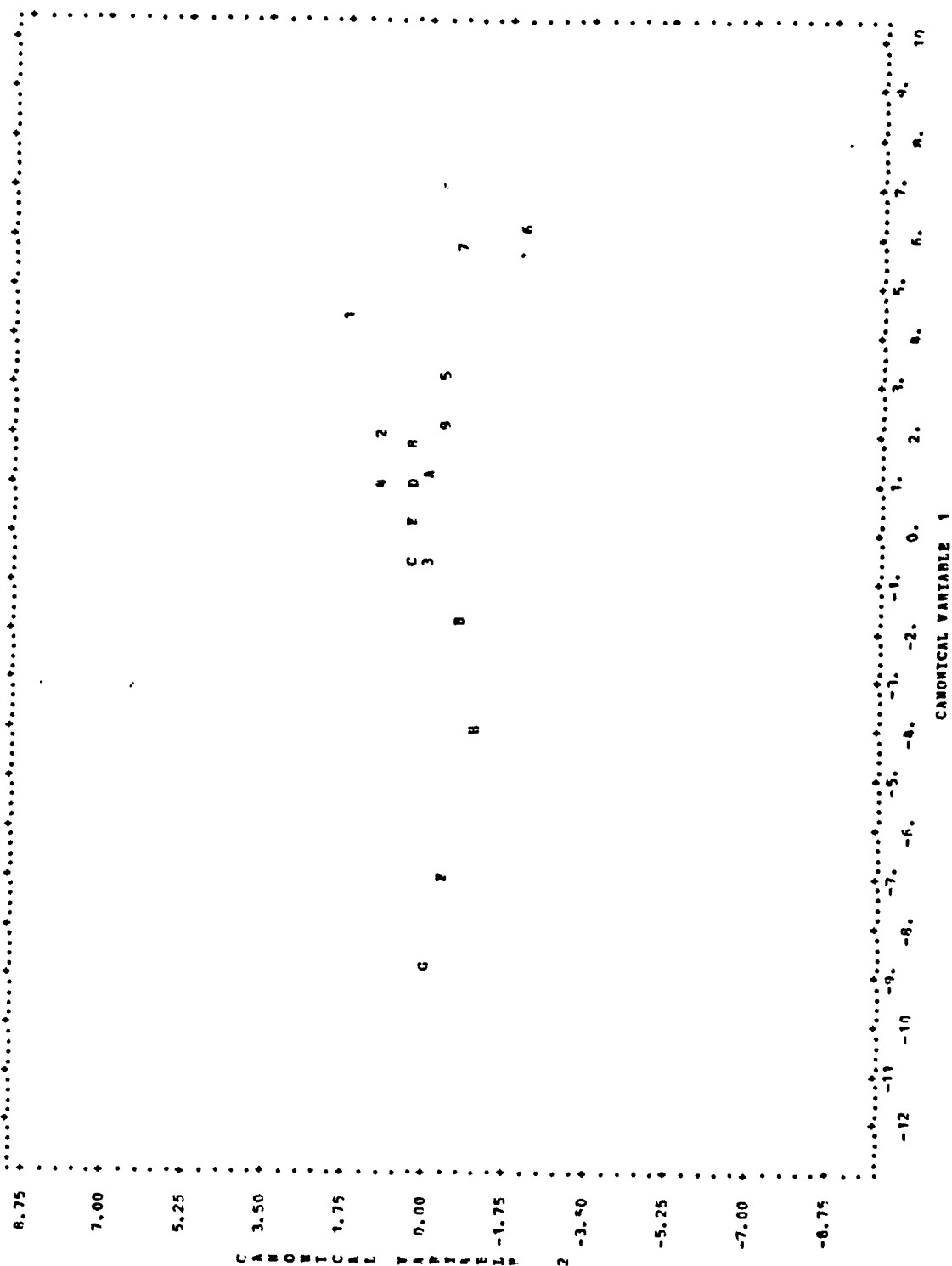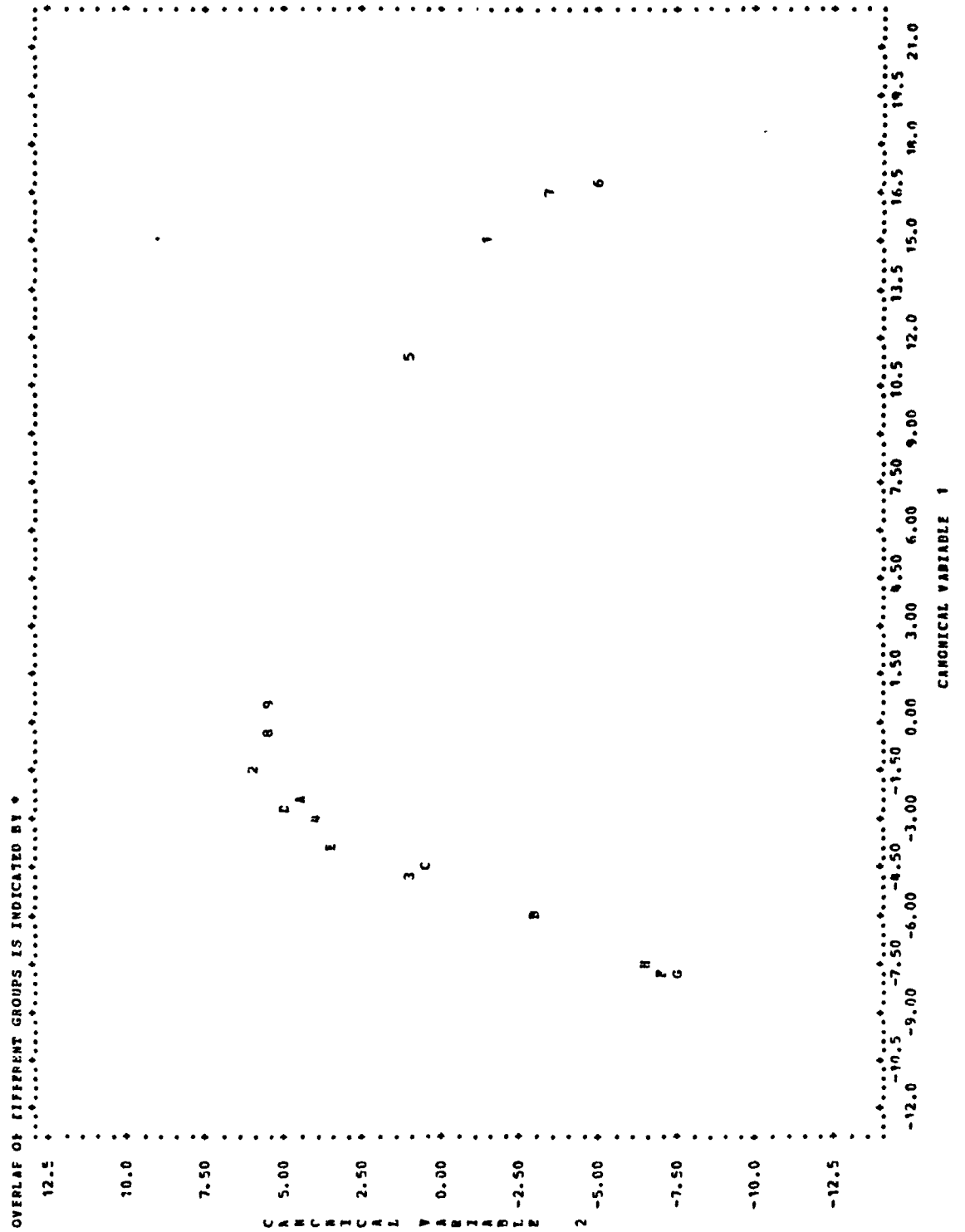   F, G, H - Spalls

OVERLAP OF DIFFERENT GROUPS IS INDICATED BY *

CANONICAL VARIABLE 1

Table 13. Classification matrix of lithologic categories using texture variables calculated from principal components axis 2.

CLASSIFICATION MATRIX

GROUP	PERCENT CORRECT	NUMBER OF CASES CLASSIFIED INTO GROUP –											
		G1	G2	G4	V1	V2	V3	V4	V5	P1	P2	P3	T1
G1	54.0	27	5	12	0	0	0	1	0	0	1	0	1
G2	72.9	13	35	0	0	0	0	6	0	0	0	0	0
G4	23.4	22	0	15	7	0	0	0	5	2	13	0	0
V1	27.0	7	9	30	17	0	0	7	7	1	2	0	1
V2	31.7					19							
V3	0.0	0	0	0	0	0	0	1	0	0	2	0	1
V4	17.0	0	0	3	1	2	0	7	3	1	3	0	0
V5	26.5	0	0	4	2	3	0	2	13	3	4	2	1
P1	7.8	0	0	5	1	6	0	9	8	5	6	0	1
P2	12.5	0	0	1	0	0	0	7	2	0	14	2	1
P3	12.5	1	0	0	0	5	0	2	8	0	6	1	1
T1	37.3	0	0	2	7	21	0	2	0	3	2	0	2
T2	32.7	1	0	1	0	8	0	13	5	3	8	0	2
T3	9.7	0	0	3	0	3	0	0	11	1	2	5	5
S1	14.5	0	0	0	2	0	0	0	12	1	0	4	9
S2	72.9	0	1	0	0	9	2	6	6	0	0	4	0
S3	42.9												
TOTAL	28.8	74	49	71	38	87	2	82	85	30	60	21	57

GROUP	PERCENT CORRECT	G1	G2	G4	V1	V2	V3	V4	V5	P1	P2	P3	T1
G1	54.0	0	0	0	0	0	0						
G2	72.9	0	0	0	0	0	0						
G4	23.8	0	0	0	0	0	0						
V1	27.0	0	0	0	5	0	0						
V2	31.7	7	2	0	1	1	0						
V3	0.0	6	2	0	6	8	0						
V4	17.0	18	0	6	0	0	0						
V5	26.5	0	3	1	0	4	0						
P1	7.8	4	3	0	0	1	0						
P2	17.5	2	2	3	1	1	0						
P3	2.3	8	4	1	2	1	0						
T1	37.3	17	7	0	0	0	0						
T2	32.7	16	0	1	0	3	0						
T3	9.7	0	0	7	8	25	0						
S1	14.5	0	1	12	51	11	0						
S2	72.9	0	0	4	3	24	0						
S3	42.9	0	0	5			0						
TOTAL	28.8	78	32	38	85	85	2						

Categories are:

G1, G2, G4 – Granite

V1, V2, V3, V4, V5 – Volcanics

P1, P2, P3 – Paleozoic sediments

T1, T2, T3 – Tertiary sediments

S1, S2, S3 – Spalls

Table 16. Classification matrix of Maine and Soviet granites.

GROUP	PERCENT CORRECT	NUMBER OF CASES CLASSIFIED INTO GROUP - RHYOL	SLGRAN	PLGRAN	G1	G2	G4	S1	S2	S3
RHYOL	13.2	31	42	40	19	8	94	0	0	0
SLGRAN	54.2	4	52	7	2	10	14	0	0	7
PLGRAN	54.1	1	13	53	19	12	0	0	0	0
G1	96.0	0	0	2	48	0	0	0	0	0
G2	100.0	0	0	0	0	48	0	0	0	0
G4	100.0	0	0	0	0	0	64	0	0	0
S1	44.6	0	5	0	0	0	0	37	30	11
S2	70.0	0	0	0	0	0	0	15	49	6
S3	48.2	0	4	0	0	0	2	15	8	27
TOTAL	51.2	36	116	102	88	78	174	67	87	51

Categories are:

RHYOL - Traveler Rhyolite
SLGRAN - Katahdin slope granite
P.GRAN - Katahdin plateau granite
G1, G2, G4 - Degelen granite
S1, S2, S3 - Degelen spall

Figure 35.   Scattergram of category means, lithologies of 12 May 1974
             Degelen area.   Texture variables calculated from PC axis 2.
             Symbols are:

                    1, 2, 3 - Granite
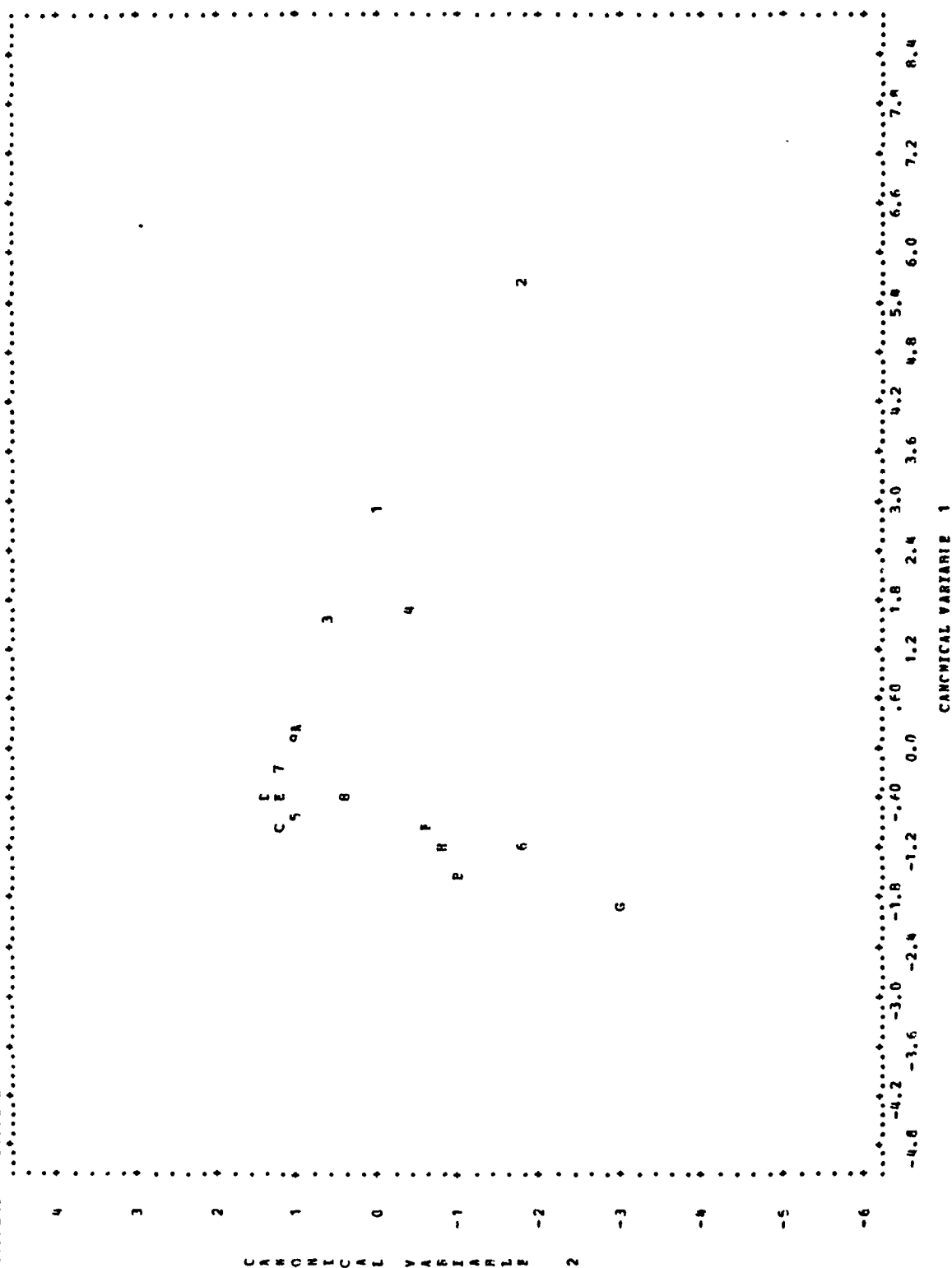
                  4, 5, 6, 7, 8 - Volcanics

               9, A, B - Paleozoic sediments

                C, D, E - Tertiary sediments

                   F, G, H - Spalls

OVERLAP OF DIFFERENT GROUPS IS INDICATED BY *

CANONICAL VARIABLE 1

-4.8 -4.2 -3.6 -3.0 -2.4 -1.8 -1.2 -.60 0.0 .60 1.2 1.8 2.4 3.0 3.6 4.2 4.8 5.4 6.0 6.6 7.2 7.8 8.4

is measured by the F-statistic which is given by the following formula:

$$F = \frac{(n. - g - p' + 1)n_i n_j}{p'(n. - g)(n_i + n_j)} \, D^2(G_i|G_j) \, ,$$

where

n. = total number of cases over all groups;

g = number of groups;

p' = number of variables entered into the analysis (including the one being entered in the current step);

ni = number of cases in group i;

nj = number of cases in group j;

and, where $D^2(G_i|G_j)$ is the squared distance between centroids of groups i and j. Table 14 lists the ranking of the variables used in the analysis. All four raw bands are used, but only nine of the texture variables were incorporated into the analysis. This is because the BMDP7M algorithm begins the analysis with the most discriminating variable and stops including them when the category separation begins to degrade. As one can see from Table 14, Band 5 (.6 - .7 micrometers) was the most important bandwidth in discrimination, followed by Bands 6, 7 and 4. Reasons for this ranking are made clearer when one examines the Degelen Massif false color composite of Plate 8. While Band 5 was more able to detect differences in visible color, Bands 6 and 7 sensed differences in vegetation cover. The texture variables most useful in rock type discrimination are also listed in Table 14. The best four are variables which relate category brightness to the datum planes of Table

Table 14. Ranking of variables in the stepwise discriminant analysis.

Type of Variable	Variable name	F-statistic
Raw bands	Band 4	723.0
	Band 5	229.0
	Band 6	141.1
	Band 7	102.4
Texture	MBDAT3	2377.1
	MADAT2	1445.6
	MADAT1	1018.4
	MBDAT2	817.6
	M1NCON	557.2
	SKEW	373.9
	M1NSQR	275.9
	KURTOSIS	217.1
	MDEVN	179.0

7. Apparently, for the Degelen categories, mean brightness relative to (below) 154 were most significant, followed by means above and below other datum planes. Mean first neighbor contrast (M1NCON) was next, followed by others as listed. Parker (1980) found texture variables 8, 12, and 13 (M1NCON, MADAT1 and MADAT2) to be the most powerful discriminators of granite, quartzite and colluvium. Both studies point to these variables, Parker's and those in Table 14, as consistently the best for distinguishing bedrock and colluvium categories.

Comparison of Katahdin and Degelen Granites

T-tests. The means difference test showed the categories studied to be quite different in most variables, but alike in some. Table 15 lists the categories, and the t-values calculated from the comparison of the most significant variables (variables with which most others were correlated). The slope granite categories of the two Maine scenes seemed to be alike in Band 5, and marginally similar in Band 6. They were, however, very distinct in Bands 4 and 7. When comparing a vegetation-free granite detritus category of the 12 May 1974 Soviet scene with the slope granite of 20 August 1976, the responses for Bands 6 and 7 appear close enough for these categories to be alike. In the visible spectrum, however, they are quite different. The Degelen granite detritus appears to also be similar to the 23 July 1973 slope granite in Band 6, but again, the other band responses are quite distinct. It should be noted, however, that all channels are brighter on the Soviet scene, and that the chlorophyll-caused rise in infrared response for the Katahdin granite is responsible for bringing the two

Table 15. t-values for most significant raw data and texture variables, Katahdin and Degelen granites.

Scene	Categories Tested	Variable	T
23 July 1973	Slope granite	Band 4	-31.42
		Band 5	1.27
20 August 1976		Band 6	2.27
		Band 7	-6.86
12 May 1974	Granite Detritus	Band 4	70.47
		Band 5	59.13
20 August 1976	Slope granite	Band 6	-1.22
		Band 7	-1.85
23 July 1973	Slope granite	Band 4	30.92
		Band 5	68.72
12 May 1974	Granite detritus	Band 6	1.89
		Band 7	-10.50
20 August 1976	Slope granite	MEAN	-1582.37
		STD	1344.59
12 May 1974	Granite detritus	SKEW	-42.03
		KURTOSIS	-1.34
		MPTREL	138.95
		MBDAT1	288.22

groups closer together.

A comparison of texture variables demonstrated the granites to be similar only in one variable. Table 15 shows KURTOSIS to be a common trait among the Maine and Soviet granites for these two scenes. The next most similar variable was skew, although the extent of comparability was limited, as indicated by its -42.0 value.

Texture transforms. Hsu's texture variables for the granite lithologies, calculated from the first principal component axis of the 20 August 1976 and 12 May 1974 scenes, were compared utilizing the classification matrix and scattergrams produced by the BMDP7M program. Table 16 is the classification matrix showing overlap of responses of the lithologic categories. A large amount of confusion exists between the rhyolite category (RHYOL) of the Katahdin scene and the granite detritus (G4) category of the Degelen scene. In fact, more rhyolite observations are assigned to the Degelen granite detritus category than to the other lithologic groups of the same scene. It would appear then that the surfaces of these outcrops, the Katahdin area rhyolite and the bare granites (G4) of the Degelen area, were texturally similar. The amount of overlap of the rhyolites with granites of the same areas is substantial, but much less than the overlap with the Russian granite detritus. It must be noted, however, that almost none of the Russian granite observations are classified into the Katahdin groups. This is probably due to a large variance of the Katahdin litholigic cover types as opposed to the low variance of the Degelen groups. The slope and plateau granite categories for the Katahdin area were, to a lesser degree, also classified as Degelen granites. Degelen spalls continued to be a distinct group. These findings can be summarized by stating

Figure 36. Scattergram of category means, granite and spall lithologies
           of 20 August 1976 and 12 May 1974 Maine and Soviet scenes.
           Symbols are:

                    1 - Traveler Rhyolite

                   2 - Katahdin slope granite

                 3 - Katahdin plateau granite

                    4 - Degelen Granite 1

                    5 - Degelen Granite 2

                 6 - Degelen granite detritus

                       7 - Degelen spall

                       8 - Degelen spall

                       9 - Degelen spall

Figure 36. Scattergram of category means, granite and spall lithologies
of 20 August 1976 and 12 May 1974 Maine and Soviet scenes.
Symbols are:

1 - Traveler Rhyolite

2 - Katahdin slope granite

3 - Katahdin plateau granite

4 - Degelen Granite 1

5 - Degelen Granite 2

6 - Degelen granite detritus

7 - Degelen spall

8 - Degelen spall

9 - Degelen spall

OVERLAP OF DIFFERENT GROUPS IS INDICATED BY •

```
   6.25 •

   5.00 •

   3.75 •

C  2.50 •
A
B
C
H
C        4
A  1.25 •
L            3
   A       6 1
   V  0.00 •     2
   A
   R
   I
   A
   B -1.25 •
   L                  9
   E
   2 -2.50 •      8 7

  -3.75 •                            5

  -5.00 •

  -6.25 •
        -9.750  -8.250  -6.750  -5.250  -3.750  -2.250  -.7500  .7500  2.250  3.750  5.250  6.750
           -7.500  -6.000  -4.500  -3.000  -1.500  0.000  1.500  3.000  4.500  6.000
```

CANONICAL VARIABLE 1
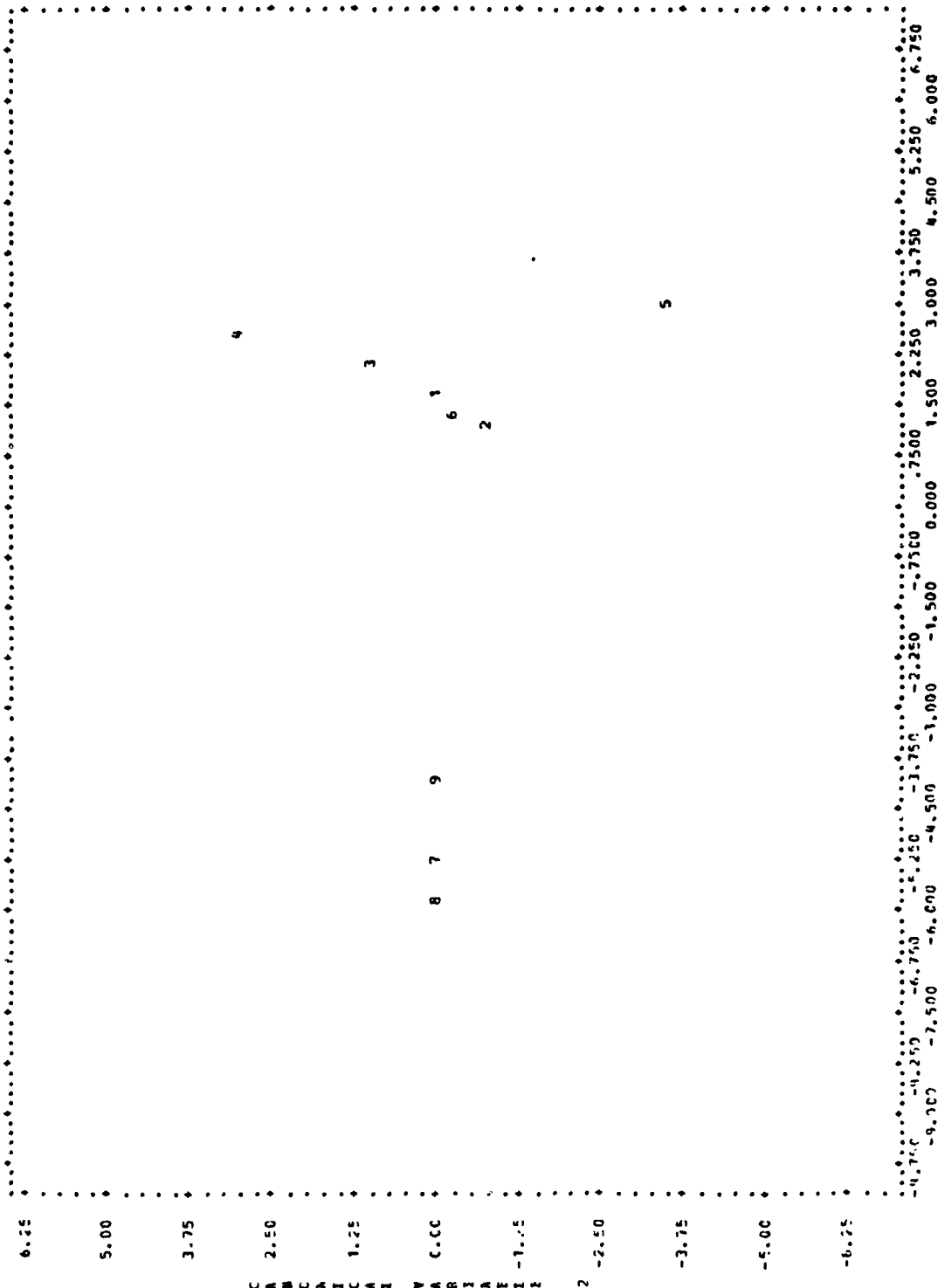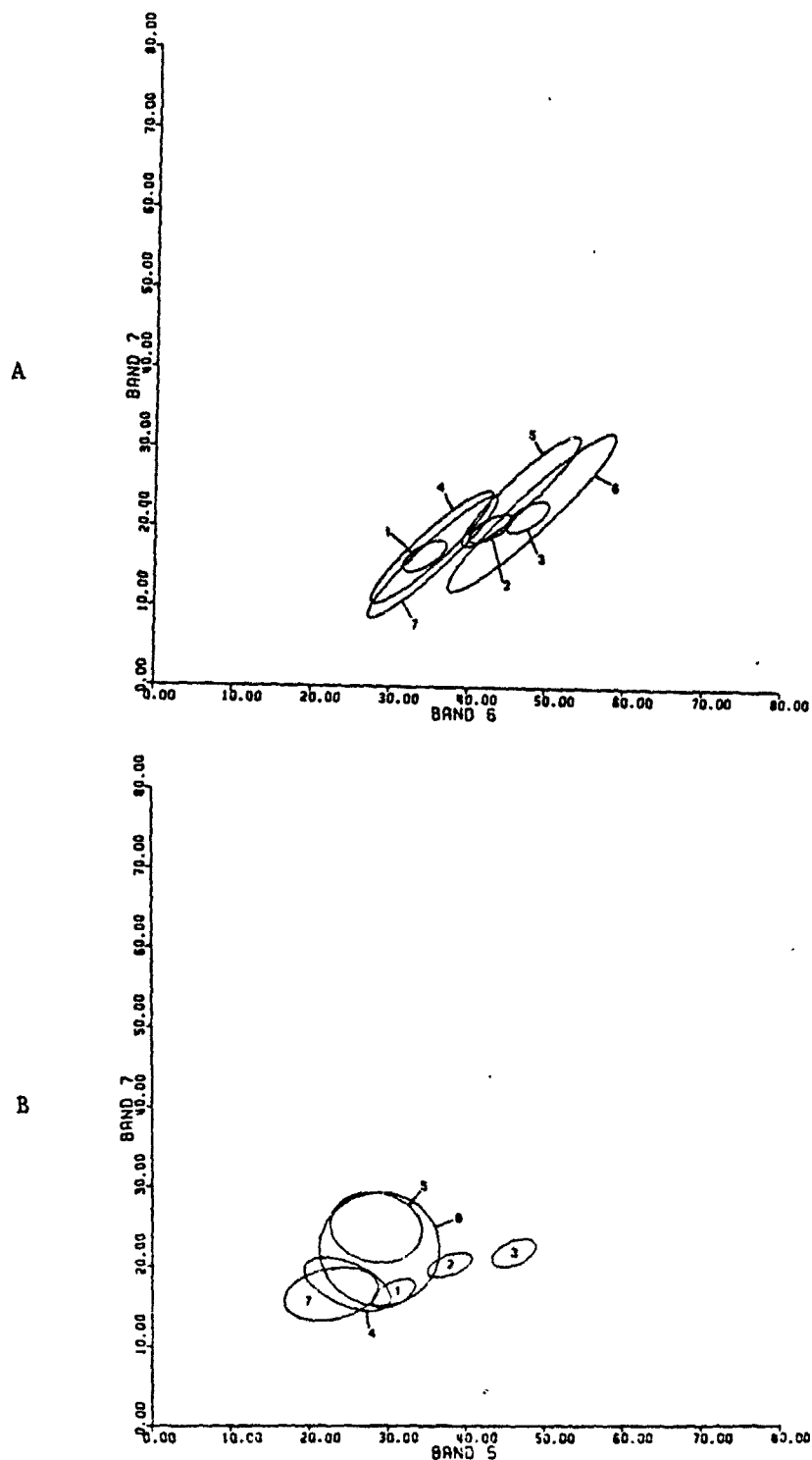
Figure 37. Two-channel plots of all granite categories. (A) Band 7 vs. Band 6; (B) Band 7 vs. Band 5. Categories: 1,2,3 are Granite 1, Granite 2 and Granite detritus of Degelen; 4, 5 are Katahdin granites of 23 July 1973, and 6 and 7 are 20 August 1976 Katahdin granites.
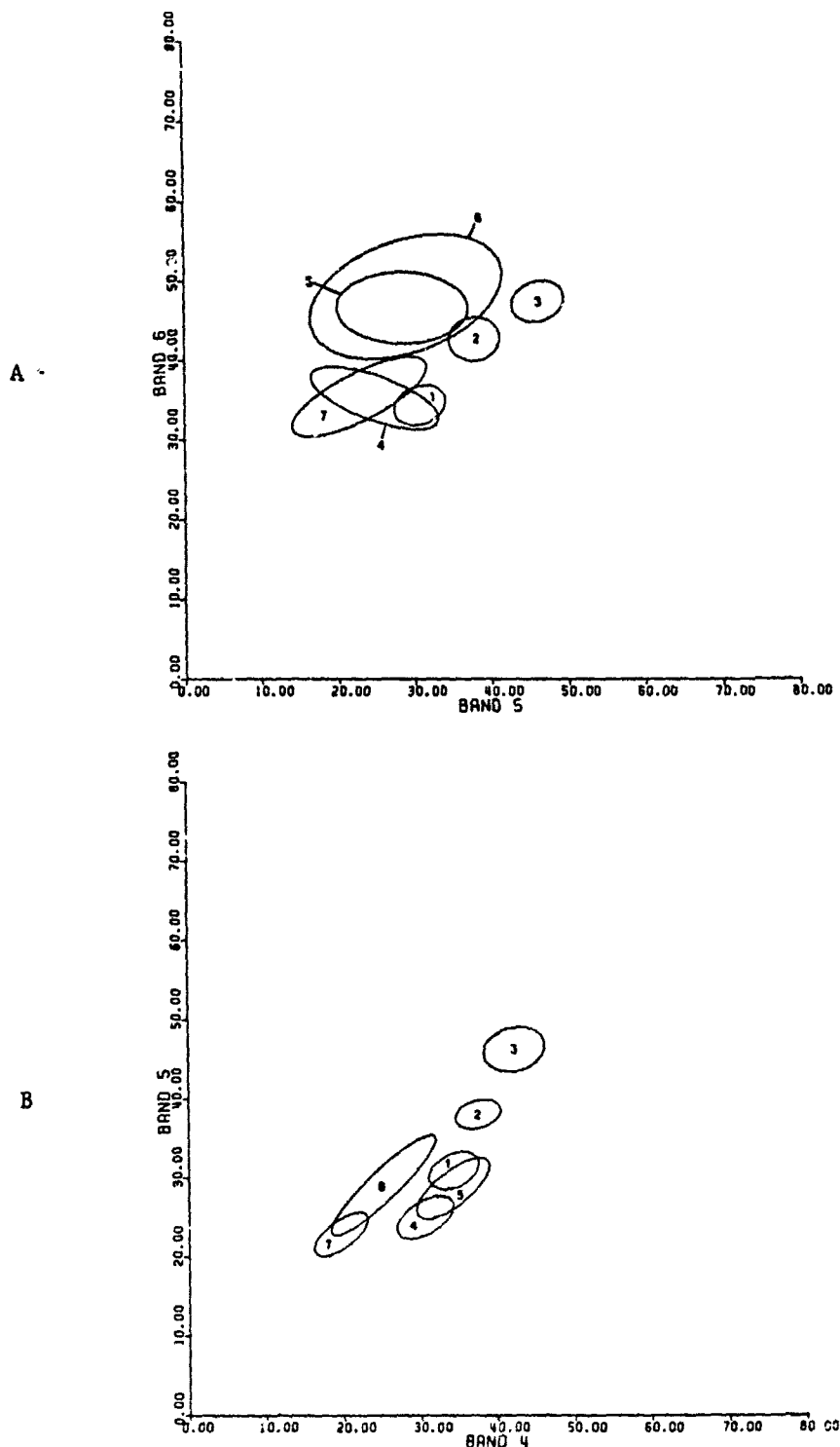
Figure 38. Two-channel plots of all granite categories. (A) Band 6 vs. Band 5; (B) Band 5 vs. Band 4. Categories: 1, 2, and 3 are Granite 1, Granite 2, and Granite detritus of Degelen; 4 and 5 are Katahdin granites of 23 July 1973, and 6 and 7 are 20 August 1976 Katahdin granites.

July 1973 granite stand out, as it does, although to a lesser degree, on the next plot (7/5). One will note, however, the consistent behavior of the 20 August 1976 and Degelen granites to either side. In the infrared, as indicated previously, the 20 August 1976 Maine and 12 May 1974 Degelen granites were alike, and that is borne out here. The granites then begin to diverge in the visible bands, as indicated by the Bands 7/5 graph in Figure 39B. Plots of 7/4 and 6/5 in Figure 40 show that the multiscene Maine granites converge somewhat. In the 6/5 plot, the Katahdin and Degelen granites behave quite differently, and again this points out the prevalence of the chlorophyll spectral effect on the Maine granites. The final two plots, shown in Figure 41, emphasize the differences between the Maine and Russian granites. On the Band 5/Band 4 plot, the 23 July 1973 and 20 August 1976 Maine granites are dissimilar and reasons for this are unclear. It is possible that atmospheric conditions were quite different on the two days, and that the atmospheric distortions of the granites' color is accentuated in these plots.

Interpretation of Enhanced Imagery

Degelen area. After a comparison of the imagery with the geologic map of the Semipalatinsk region (Figure 10), it was decided that the false-color composite (Plate 7) offered the most geological interpretability. The overlay on Plate 7 is an interpretation of lithologies shown on Figure 10. Faults marked on the geologic map are relatively easy to locate on the Landsat image, and others are conspicuous as well. For clarity, not all linear features have been

KATAHDIN AND DEGELEN GRANITES
BAND7/BAND6

A
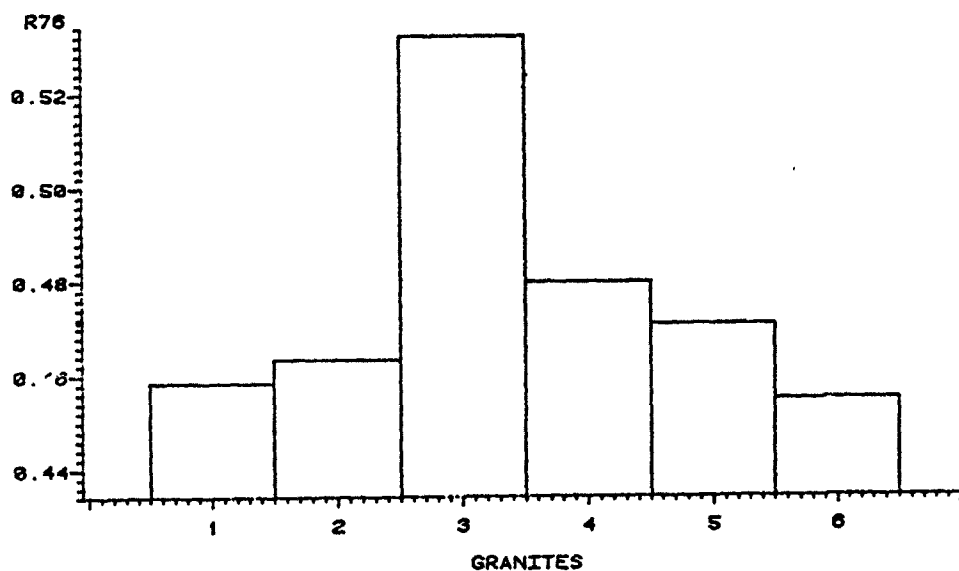
KATAHDIN AND DEGELEN GRANITES
BAND7/BAND5
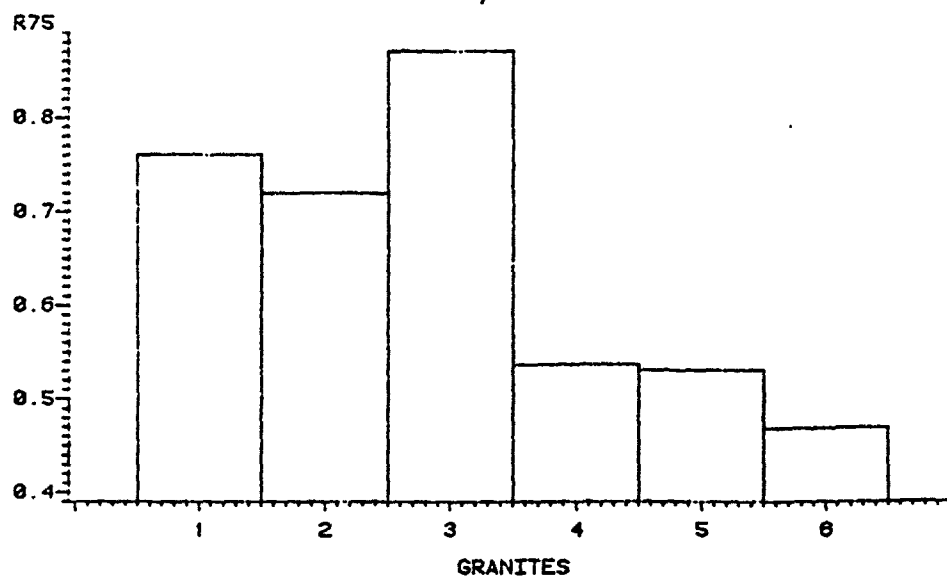
B

Figure 39. Band ratio plots, all granites. (A) Band 7/Band 6; (B) Band 7/Band 5. Categories are: 1, 2 - 20 August 1976 Katahdin granites; 3 - 23 July 1973 Katahdin granite; and 4, 5, 6 are Granite 1, Granite 2, and Granite detritus of 12 May 1974.
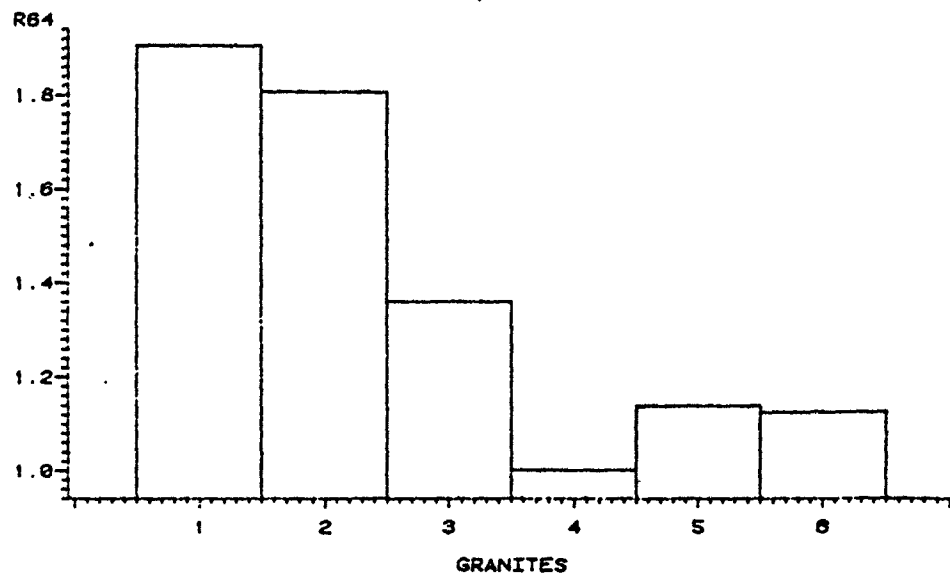
KATAHDIN AND DEGELEN GRANITES
BAND7/BAND4

GRANITES

A
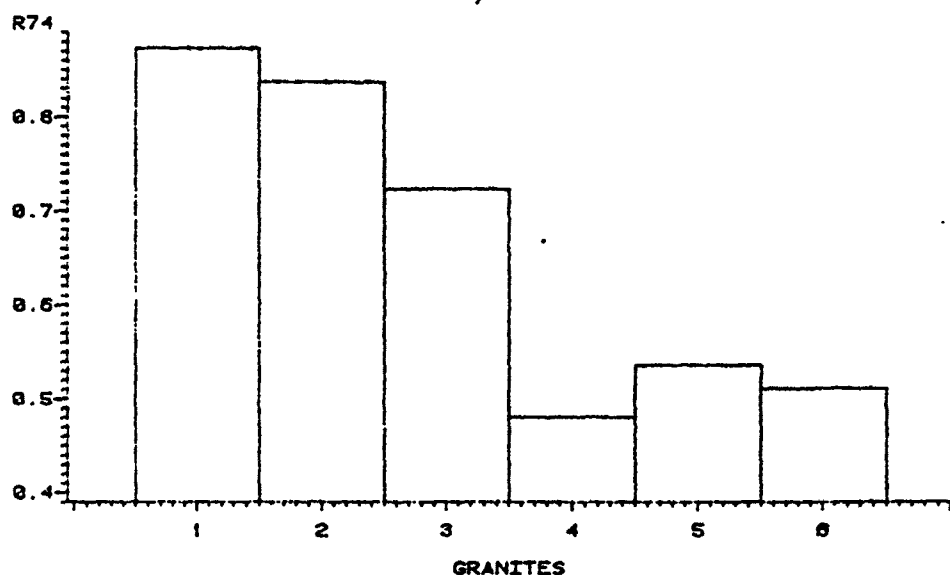
KATAHDIN AND DEGELEN GRANITES
BAND6/BAND5
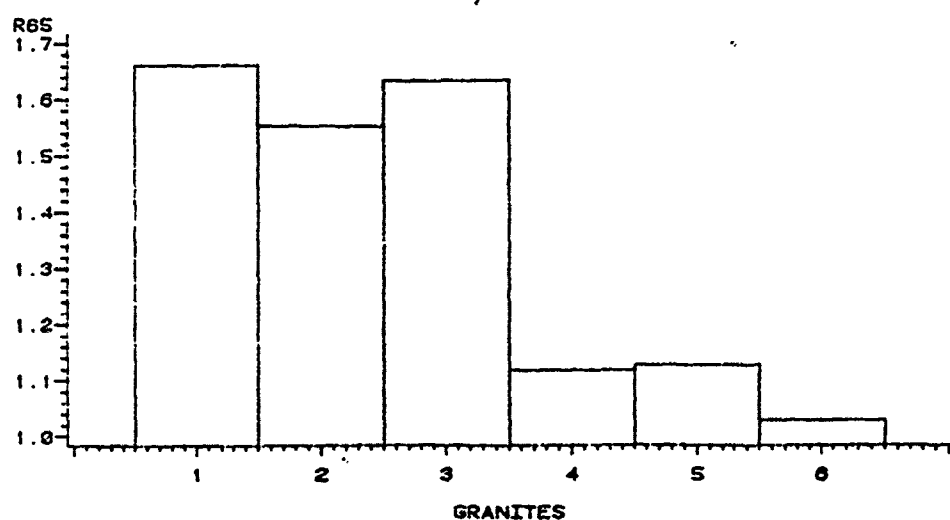
GRANITES

B

Figure 40. Band ratio plots, all granites. (A) Band 7/Band 4; (B) Band
6/Band 5. Categories are: 1,2 – 20 August 1976 granites; 3
– 23 July, 1973 granite; and 4, 5, 6 are Granite 1, Granite
2 and Granite detritus of 12 May 1974.

KATAHDIN AND DEGELEN GRANITES
BAND6/BAND4

A

KATAHDIN AND DEGELEN GRANITES
BAND5/BAND4
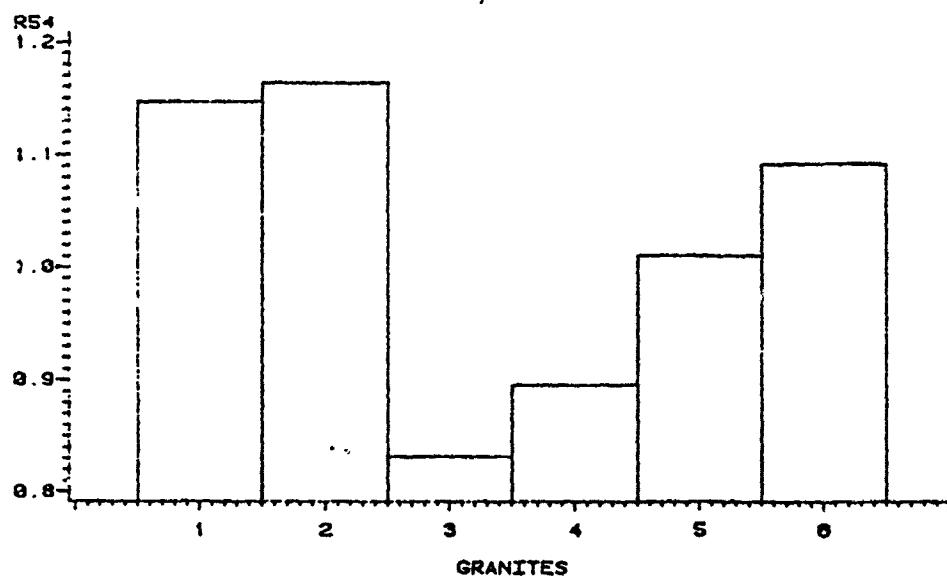
B

Figure 41. Band ratio plots, all granites. (A) Band 6/Band 4; (B) Band
5/Band 4. Categories are: 1, 2 - 20 August 1976 granites;
3 - 23 July 1973 granite; and 4, 5, 6 are G1, G2, and
Granite detritus of 12 May 1974.

marked on the overlay of Plate 7. The course of the Shagan River is very distinct. Of special interest is the conspicuousness of the granite plutons of the area, marked with the letter G on the overlay. The Degelen Massif is in the lower left corner of Plate 7, and has a prominent topographic expresssion, making it and others like it simpler to identify. Another reason for their prominence is a color difference due to a light vegetation covering. Such a growth stands out in this arid region. The pluton in the center of the image, however, is partially obscured by what appears to be unconsolidated Tertiary deposits. The contacts of the southernmost pluton are more difficult to identify, and are partly inferred here. Lithologic contacts in the immediate vicinity of the massif are conspicuous. The granite itself is a distinct feature, and contrasts with the Devonian volcanics adjacent to the east (V). The Silurian deposits (S) to the east of the volcanics are, once again, partly buried beneath Tertiary sediments. The large fault structure in the lower left corner of the image is a very discernable feature on all imagery of the area and is apparently still active. The large feature (A) just to the north of the Degelen Massif is a structure not directly in agreement with the Soviet geologic map. Denoted as two large masses of Silurian rock separated by an elongated body of Precambrian rocks, it appears much more homogeneous on the image. It could, perhaps, be an additional pluton, but the characteristic reddish hue of the others is absent. Also of interest on the image are several circular features, two of which are indicated by dashed lines on the image overlay. Although a total correlation is difficult, most contacts can be verified on the Landsat image, plus unmapped faults can be traced.

A more detailed mapping of faults and geologic analysis is possible on a larger image of the Degelen Massif itself (Plates 8 and 9). It is obviously a highly fractured intrusive body; most faults trend in a northeasterly direction, but there are a few that are nearly orthogonal to the rest. Such a dense network of fractures would certainly affect the coupling of a buried explosion and possibly control non-isotropic components of the seismic radiation field. The spall resulting from such blasts is quite noticeable as the bright features situated on central and southern ridge tops of the massif. Most of the blasting at Degelen has apparently occurred in the granite. Several circular features on the massif are visible, and have been marked with dashed lines. These could perhaps be related to the post-emplacement cooling of the ancient magma body.

The other image enhancements of the Semipalatinsk study area each add additional information to the analysis. On the ratioed scene (Plate 11), the Degelen massif stands out vividly as the bluish-violet body in the lower left corner of the scene. Spalls on it (A) are easily recognized by their yellow appearance. Another interesting feature on this image is the series of discrete, white blotches (B) on the northeastern sections of the volcanic rock adjacent to the pluton. These do not appear on a false color composite (Plate 8), but are most likely areas of complete defoliation, since the burned areas are white on this image also. These spots, however, are not black on the color composite. The barren granite areas, mapped as "granite detritus" and assigned the color yellow on the classification map of Plate 6, appear reddish-brown on this image (C). To the east of Degelen, parts of the elongated granite pluton there (marked with a 'C') appear red also. The

unmapped body just north of Degelen also has this color over parts of it. Directly to the north of that (also marked ´C´) in the upper left corner of the image, the color appears again, perhaps indicating the presence of another pluton. Spall peripheries are red also. At the locations denoted with the letter ´D´, cultivated fields (most of them barren at this time of year), assume the same reddish color. It perhaps is no coincidence that they are over or very near granite intrusions. Other fields commonly share an orange hue. Streams with associated vegetation, flowing approximately radially away from the pluton, are quite distinct on the ratioed image. Other vegetated areas have the same characteristic purple color. Two presumably productive fields in the upper right corner of the image are a deep purple. On the other hand, most bare areas are of a yellowish hue.

On the principal components image of the Semipalatinsk region, various features again are highlighted. The granites here take on a bluish tint, but bare granites and other non-vegetated surfaces are not differentiated, and assume a yellowish coloration. The dry lake beds (L) are all a distinctive pinkish hue.

The first of two principal components "2-´.-2" images (this one produced entirely with first principal component axes) contributed information mainly in the form of finer detail over the scene, since it was contrast stretched from 0 to 255 during processing. Despite this quality, the higher contrast of the raw data false color composite (Plate 7) was more useful in performing the geologic analysis.

The second of the two principal components "2-2-2" images, where a mixture of first and second axes were used, highlighted mainly the dry lake beds (L). These are distinct from dry or intermittent stream beds

and assume an orange color on the image. Once again, areas of slight vegetation cover are a light violet color, and non-vegetated areas are a white or yellow.

The principal components - ratio combination image (Plate 14) mainly emphasizes vegetation cover. Areas of relatively dense vegetation are a deeper red tint. These contrast with the white to blue barren areas, with blue being the color of areas of lowest reflectance.

Katahdin Area

During the analysis of the enhanced imagery of 20 August 1976 over the north-central Maine study area, the emphasis shifted from outcrop recognition to a recognition of forestation differences over the region. This is because there are very few outcrops in the area, and because vegetation varies readily with the soil type, drainage, and other factors that are directly dependent upon the underlying lithology.

This dependency is well illustrated by an analysis of Plate 16, a ratioed image of the Mount Katahdin region. Whereas the non-contrast stretched false-color composite of the same area (Plate 15) shows little forest differentiation, the ratioed scene demonstrates very recognizable patterns of forest growth. These can be grouped into coniferous (light hues) and deciduous trees (darker tones). A geologic interpretation of the ratioed image, made using the geologic map of Figure 42, is shown on Plate 17. The Katahdin Pluton, marked Dg on the image and map, is located in the lower right corner of Plate 17. This contact is easily traceable onto the ratioed image, as is the general outline of the Traveler Rhyolite (Dr on the map and image). The Ordovician volcanics

Blank

Figure 42. Geology of northern Maine. The area depicted in Plates 15 -
18 is outlined. Relevant geology:

Ds - Devonian cyclically bedded dark gray slate
     and sandstone.

Du - Devonian metamorphosed shale, siltstone,
     sandstone and conglomerate.

Dg - Devonian biotite and biotite-muscovite
     granite and quartz monzonite.

Dr - Felsic volcanic rocks.

Ov - Metamorphosed felsic to mafic volcanic
     rocks with interbedded metasedimentary
     rocks.

(After Doyle, 1967).
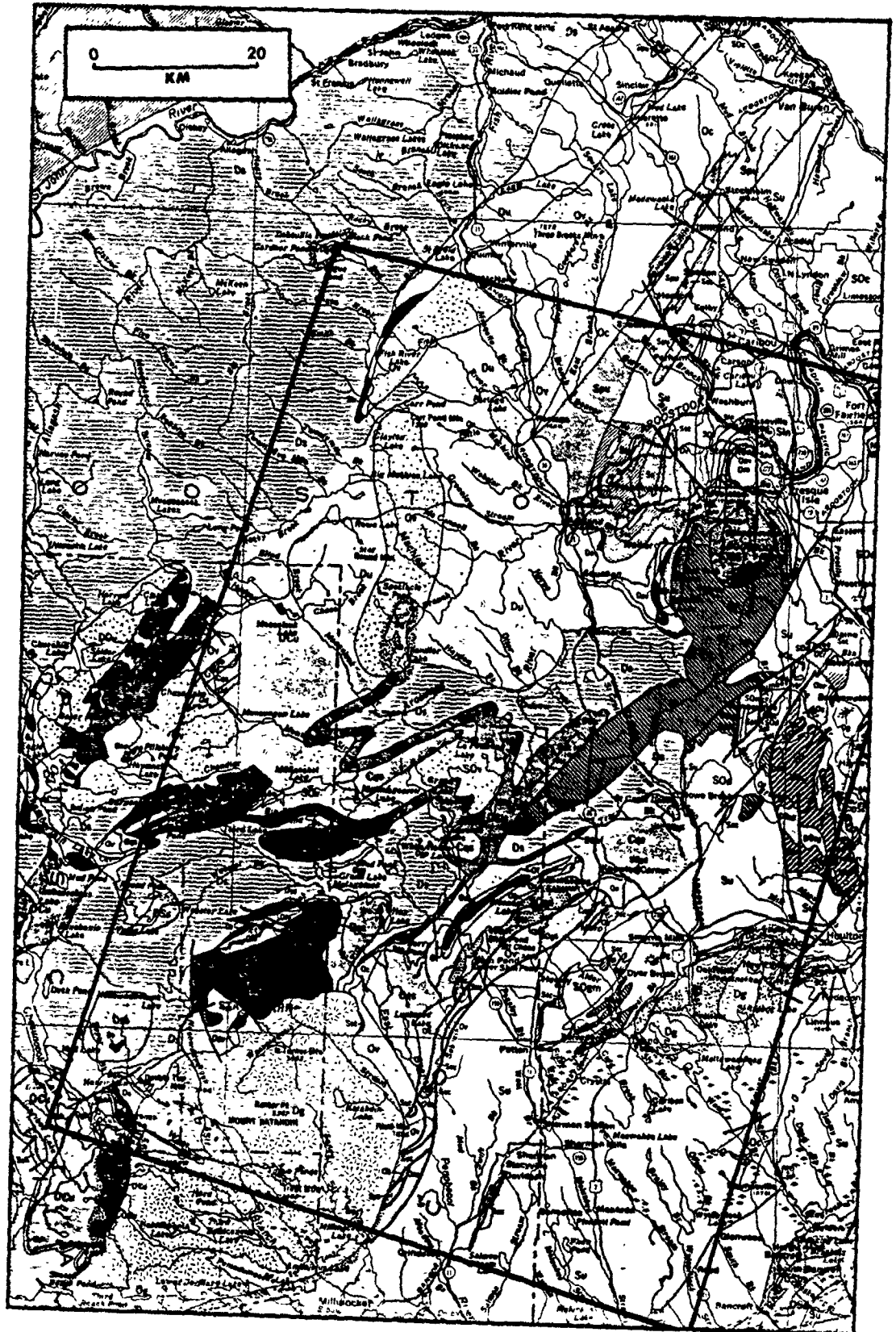
(Ov) are similar to the Traveler Rhyolite, but otherwise very distinct. The network of faults adjacent to the volcanics is recognizable on the image and more have been marked on the ratioed image. The Ordovician volcanics to the north of the Traveler Rhyolite (also Ov) is very discernable, and it appears that these volcanics are continuous across the undifferentiated region marked DCu, undifferentiated Cambrian and Devonian, on the geological map. The presence of the cloud over that strategic area raises a problem until one looks at the corresponding area on the principal component image of Plate 18. Here, the growth patterns are not completely obscured by the cloud. The bright yellow areas on the ratioed scene are areas clear of forest cover, and examples of this are the logged areas in the northeast, the series of logging roads toward the bottom right of the image, and the slopes of Mount Katahdin and Traveler Mountain.

The principal components image (Plate 18) highlights various other features. For example, all clearings are red in this image. Mt. Katahdin and Traveler Mountain, marked on the image, stand out conspicuously as do the logging roads. On the principal components image, the deciduous trees appear as the light hues, and the coniferous growth takes on a blue coloration.

After examination of both the ratioed and principal components Katahdin scenes, a few generalizations can be made. First, these processes, aided by the contrast-stretching included in processing, easily distinguish deciduous and coniferous forest growth. Second, this differentiation is a guide to location of geologic contacts, as soil types and soil drainage affecting plant growth are directly linked to the soil parent material.

Geologic and Tectonic Comparisons. An analysis of the enhanced imagery of the Degelen and Katahdin regions (Plates 7 and 17), offers a comparison of their respective tectonic histories. Fault patterns are of a higher density in the Degelen area (Plate 7) and seem to be of greater length. Most are parallel or nearly parallel, although a few cross-cutting structures are visible. A dominant feature is the large active fault located in the lower left corner of Plate 7. Stresses associated with this fault may be partly responsible for the intense fracturing of the Degelen Massif (Plate 9). The Katahdin plutonic intrusion, being a late tectonic event of the Appalachian Orogeny, contrasts sharply with the Degelen Massif with regard to the amount of fracturing it has undergone. Widespread jointing of the Maine pluton, a phenomenon of the magmatic cooling process, is the most notable small scale textural characteristic of this otherwise homogeneous granite body. The regional pattern of faulting in northern Maine, some of it visible on Plate 17, is more subparallel than the Soviet patterns. These faults have been inactive or only occasionally active in recent geologic history.

CHAPTER V

DISCUSSION AND CONCLUSIONS

Discussion

Characteristics of the study areas. The usefulness of Landsat
multispectral data in the spectral characterization and thematic mapping
of lithologies over two study areas has been investigated. Interest in
the Soviet Union study area, and in the Degelen Massif in particular,
has arisen by virtue of its role as an active nuclear test site. The
Mount Katahdin region of north-central Maine was chosen by other
investigators as a site geologically and tectonically analogous to the
Soviet area. Investigation of the Maine area is useful for the proper
understanding of the tectonic setting of the Degelen region, which is
necessary for improved quantitative interpretation of seismic signatures
from seismic monitoring of buried nuclear explosions in that area.

The Katahdin and Degelen areas are both located in tectonic fold
belts, where Paleozoic (and some Mesozoic in the USSR region) sediments
and interbedded volcanics have been folded, faulted, and subsequently
intruded by granites. The Katahdin and Degelen granites are themselves
similar in that they are both biotite granites high in quartz and
feldspar, and are broken by numerous aplitic dikes (Hon, 1980 and
Kropotkin, 1945). Surrounding lithologies are similar, with sediments
and volcanics of Silurian, Devonian and Cambrian age occurring (Figures
10 and 41).

However, there are differences, some of which play an important

part in lithologic discrimination and comparison of categories between these two areas. Climatic differences are readily apparent on Landsat imagery. The Degelen region (Plate 7) is a comparatively arid one, and seemingly devoid of vegetation over large areas. Signs of mechanical weathering are numerous, for example the alluvial fan on the eastern border of the Degelen massif (Plates 8 and 10). The Maine imagery (Plates 2 and 3) exhibits a much more temporate climate with fairly dense forestation prevalent. Both chemical and mechanical weathering have played a role in influencing the topography of that area. The coarse-grained granite facies of the Katahdin Batholith and others like it are relatively easily eroded and form topographic lows over the region, some now occupied by lakes. However, the fine-grained Summit facies of the Katahdin Granite has remained prominent.

Glacial process have carved the face of the mountain creating the sharp ridges and steep slopes it presently exhibits. Varying thickness of glacial till blanket the area (Caldwell, 1972). Topography of the Degelen Massif, although prominent, is much more fault-controlled as evidenced by Plates 8 and 9. There are no readily visible signs of glaciation in the latter region.

The number of lithologic exposures in the two areas differs greatly for the above reasons. Large expanses of the Degelen region (appearing blue on Plate 7) are apparently free of vegetation, and presumably fresh exposures of both bedrock and unconsolidated material are widespread. On the other hand, the only exposures of any kind in the Katahdin region are mountain peaks above treeline (Mount Katahdin, Traveler Mountain, and others) and man-made clearings. Many of the mountain slopes, moreover, possess a surficial lichen encrustation.

These climatically induced features pose a significant problem in
comparing the two areas using Landsat spectral bands. However, there
are several common characteristics of the responses for the granitic
bodies in the two areas.

Use of Landsat MSS data. A number of ramifications for the use of
Landsat multispectral data must be understood prior to its use in a
project similar to this one. The four banks of sensors, each collecting
data over a separate spectral region (Figure 4) average the spectral
response over an area approximately one acre in size on the Earth's
surface. Objects smaller than that which contrast sharply with their
surroundings will influence the response for the entire picture element.
Only the very surface of the Earth is observed, and these observations
are a function of several factors. For soils, humus, iron, and moisture
content greatly influence the reflectance (Verstappen, 1977).
Vegetation over the soil obviously alters the appearance, and this in
turn is influenced by the chlorophyll content of the vegetation. Rock
exposures vary in spectral response with the degree of alteration by
chemical and physical processes, with lichen encrustation, and with
grain size (Salisbury and Hunt, 1974).

Certain problems are encountered when performing a detailed
analysis of these multispectral data. The sensors aboard Landsat detect
fairly wideband radiation in a spectral region which is not the most
favorable for lithologic discrimination. One of the principal uses for
which the satellite was originally intended is presumably the mapping of
vegetation, as the sharp inflections of the chlorophyll spectral curve
in the 0.5 to 1.1 micrometer region (Figure 3) coincide with the sensor
bandwidths chosen for Landsat (Figure 4). The spectral responses of

many lithologies are not diagnostic in this region. Bandwidths

identified as better suited for the differentiation of exposed rocks

are, arranged by capability, the 1.18 to 1.30, 4.50 to 4.75, 0.46 to

0.50, and 1.52 to 1.73 micrometer regions (Siegrist and Schnetzler,

1980). Even if these more favorable bands were available, rock surfaces

may be obscured by glacial till, a soil horizon, vegetation, or some

material totally unrelated to the composition of the underlying

lithology. With the addition of complex topographic conditions, further

perturbations of the reflectances of the material in question come into

play.

The scenes, as a result of these conditions, were analyzed in

slightly different manners. In the Maine regions, the Landsat sensors

viewed mainly the effect of chlorophyll, therefore rock outcrops and

similar clearings were plainly visible, although still spectrally

tainted by the photosynthetic agent. Other areas had both a covering of

till and vegetation and since the forest types mapped fairly

distinctively, a geobotanical analysis was useful in delineating several

geologic contacts (Plates 16 to 18). Deciduous growth, apparently more

sensitive to lithologic variation, appears purple on Plate 17 and light

gray on Plate 18.

Over the Soviet region, chlorophyll played less important, but

still noticeable, role. Although its effect on response means of the

categories chosen was far less (compare Tables 7, 9 and 10), granite

plutons in the region were highlighted by their reddish hue on the false

color composite (Plate 7), an indication of at least light vegetation

cover. Granites 1 and 2 of Table 10 demonstrate the mild chlorophyll

spectral influence, which may be more properly gauged by the

"vegetation" group statistics in that same table.

Thematic mapping. The thematic mapping performed on the Maine scenes illustrated the strengths and limitations of the Landsat sensor and of the classification procedure used. Forest types, divided into deciduous and two coniferous categories, mapped in a distinctive manner, demonstrating sensitivity of the Landsat sensors to chlorophyll reflectance. Rock types, although easily distinguishable from forest and most other categories, were confused with each other and occasionally with forest clearings of uncertain surface type. One example of this was the area to the south of Mount Katahdin on Plate 5, which is perhaps the Baxter State Park headquarters location. The limit on category numbers for the classification resulted in seemingly different targets being cross-classified. Slope granite and cloud were an example of this, and the problem stemmed from the brightest group of responses being classified into the closest group, which was slope granite. An additional problem was the high population variance of the bright granite categories, which at times would have caused the population to encompass cloud picture elements.

In the Degelen scene, classification success was gauged in a different manner due to the less prevalent vegetation cover. Granites were separable from other lithologic categories, partly on the merit of a sparse vegetation cover (see Granites 1 and 2, Table 10). Detritus distributed around the massif was linked to its probable parent material by the classificaton, and the volcanics were easily distinguishable from the granites mainly due to the volcanics' low albedoes. However, these were confused with other low-albedo deposits to the west of the massif (Plate 6). Burned areas and dark volcanics were also confused, but it

is possible that similar conditions existed at both sites.

Texture transforms. Due to limitations in the use of tonal characteristics in the discrimination of cover types, and to the common non-normality of pixel populations (which inhibits classification accuracy), a number of texture measures have been devised (Hsu, 1978). Quite often, the human eye distinguishes an object by the spatial variability of surface point reflections from that object, and not merely by its color. It stands to reason, therefore, that a textural transformation should aid in the discrimination of lithologies that may be of a similar hue, but different surface texture.

Problems encountered in enlisting texture were twofold in this study. First, the coarse spatial resolution of the Landsat sensors precludes a sufficiently characteristic measurement of the true textural qualities of a target surface. Second, to maintain proper fidelity of the textural measurements, which may differ slightly from category to category, it was necessary to utilize transformed data in a large integer format. This made a classification of texture data using the ORSER software impractical.

Textural differences between lithologic types were successfully enhanced by these transforms. Bedrock and Tertiary deposits, to a first order distinguishable by the eye, were further separated by a textural transformation, as demonstrated by a stepwise discriminant analysis. The variables most useful for discriminating groups were identified on the basis of their F-statistic and compared with those identified in a similar manner by another researcher (Parker, 1980).

A comparison of texture variables of the Katahdin and Degelen granites and spalls using the BMDP7M classification matrices and

scattergrams demonstrated certain similarities between these groups. The Traveler Rhyolite and Degelen granite detritus groups were found to be overlapped, as were a smaller proportion of the Katahdin and Degelen granites. Spalls were shown by the same tests to be a distinct group. It is very possible, therefore, that the rhyolite slopes, and to a lesser degree, the granite slopes of the Maine region share similar textural characteristics with the granite detritus surfaces of the Degelen Massif. That is, surface "roughness" on the scale of one acre is comparable in the two areas.

Statistical tests. The BMDP7M stepwise discriminant analysis program was a useful tool in judging category separation, whether the variables used were raw data, or texturally transformed data. From these tests, it was possible to detect an improvement in discrimiration between bedrock and colluvium categories. The t-test was also useful for determing the comparability of groups based upon one variable.

Digitally enhanced imagery. The use of digitally enhanced color imagery offered an improvement over simple classification in three primary ways. One obvious advantage is the number of color tones available as opposed to distinguishable gray tones on a black and white image. Many more than just eight categories could be seen on the color imagery and gradational changes between features were visible. Overall scene contrast could be raised or lowered, depending on the analysis chosen (Plates 1 and 7). Secondly, the images incorporated a very large area, so that an understanding of the spatial distribution of identifiable features was feasible, as well as a correlation with previously mapped geology. Thirdly, the ability to combine three

preliminary images into one final composite was very useful. An example of this was the ratioed data, which was demonstrated by the DISCRIM classification matrix tests to be of little statistical help in lithologic differentiation. However, the combination of three ratioed images produced final images of both study areas that offered some of the best correlation with known geology. This was especially the case for the Mount Katahdin area.

Geophysical implications. Regional gravity data over northern Maine demonstrates a characteristic behavior over felsic intrusions, of which Mount Katahdin is an example (Figure 9). Gravity lows are located over these plutons because of the relatively low density of their constituent minerals. Mafic plutons, however, exhibit a higher density thereby producing positive anomalies. Magnetic anomalies over the intrusive bodies are more irregular and respond mainly to the magnetite content of the metamorphosed country rock adjacent to the batholiths, and to tabular volcanics interbedded with steeply dipping sediments of the region (Figure 16).

The lack of comparable geophysical data for the Soviet site prompts us to postulate theoretical responses of the similar lithologies of that area. Gravity lows would probably be found over the Degelen Massif and its counterparts, as their constituent minerals are similar to those comprising the Maine igneous bodies. Analogous magnetic anomaly patterns perhaps can be inferred, since regional lithologies are comparable with some volcanic bodies around the plutons. Linear magnetic features should follow the trend of fold axes. Specifically, at Degelen they should trend in a southeast-northwest direction. The magnetic response over the Degelen Massif itself would most likely be

dominated by the Devonian volcanics on its eastern margin (Figure 10). A magnetite deposit, worked in the last century (Kropotkin, 1945) would, of course, highly influence magnetic patterns near the pluton. Magnetic and gravity profiles together likely could be used to infer the geometry of the plutons at depth, if they become available in the future.

Analysis of enhanced imagery demonstrated some regional similarity between the two sites, but there are important differences between the Katahdin and Degelen granites. Fault patterns in the Degelen area are of higher density, with at least one currently active. Fault patterns in Maine are sparser and apparently inactive. The Degelen Massif exhibits widespread fracturing which can affect source coupling of nuclear detonations occurring in the granite. The Katahdin pluton, on the other hand, shows a relative lack of faulting although jointing of the granite is a predominant feature. The regional lithologic variability defined by this remote sensing analysis, coupled with gravity and magnetic data over similar features in Maine, provides some constraints on the lateral variability of geophysical and geological properties at depth.

Conclusions

Results of this study have shown that:

1) Remote sensing data are useful in detecting regional
   geologic variations in the Semipalatinsk region of
   the USSR and the Mount Katahdin area in Maine.

2) Enhanced imagery (e.g. density-sliced band combinations, band ratios, principal component transformations, and contrast-stretched bands) produced a visual contrast between surface terrains that aided greatly in mapping the location of Soviet plutons and in delineating faults and regional geologic contacts in both the Semipalatinsk and Maine area.

3) Analyses demonstrated a textural similarity between Katahdin and Degelen igneous rock outcrops, but also showed the Degelen spall to possess distinctive textural characteristics different from surrounding parent rock units.

4) Regional fault patterns are comparable for the two regions; however, fracturing is a feature more characteristic of the Degelen Massif than the Katahdin Pluton.

5) Geophysical, geological, and tectonic parallels between the Degelen and Katahdin fold belt regions, substantiated by remote sensing observations, provide some constraints upon expected geophysical and geological variability of the subsurface of the Degelen area.

PLATES

Plate 1. Study area, Kazahkstan, USSR. Image produced with principal components "2-2-2" method.

Plate 2.   False color composite, July 23, 1973 study area, Mount
           Katahdin area.

N

0 ——— 5
KM
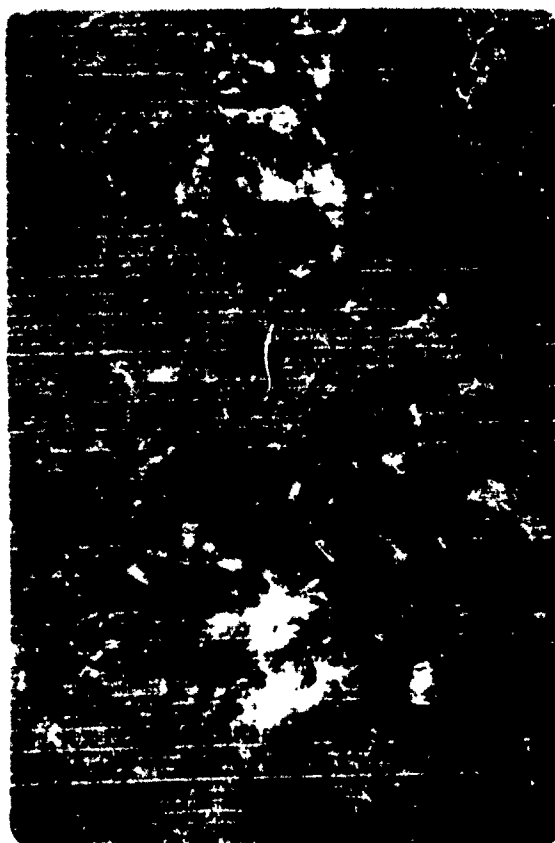
Plate 3. False color composite, August 20, 1976 study area, Mount Katahdin area.
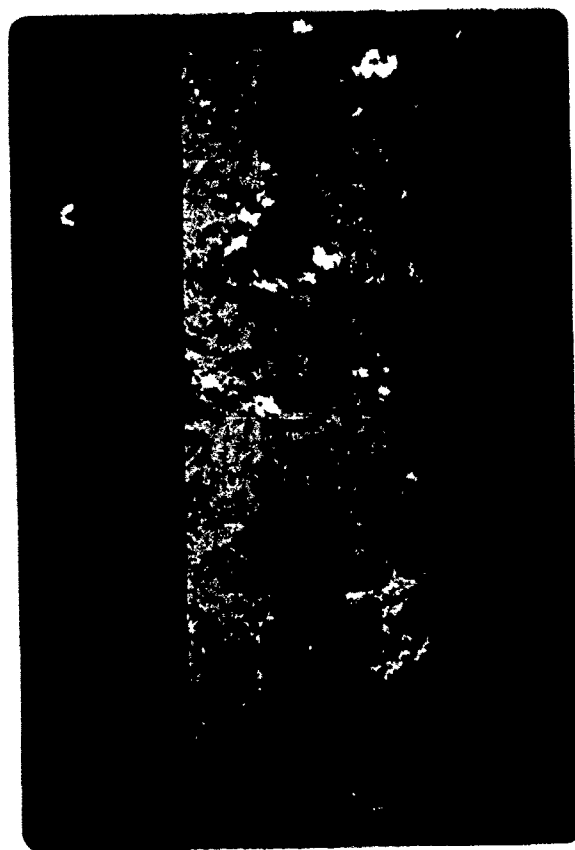
Plate 4. Classification map, July 23, 1973 scene.

Plate 5. Classification map, August 20, 1976 scene.
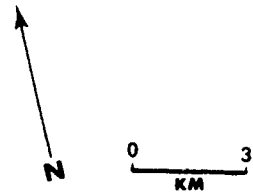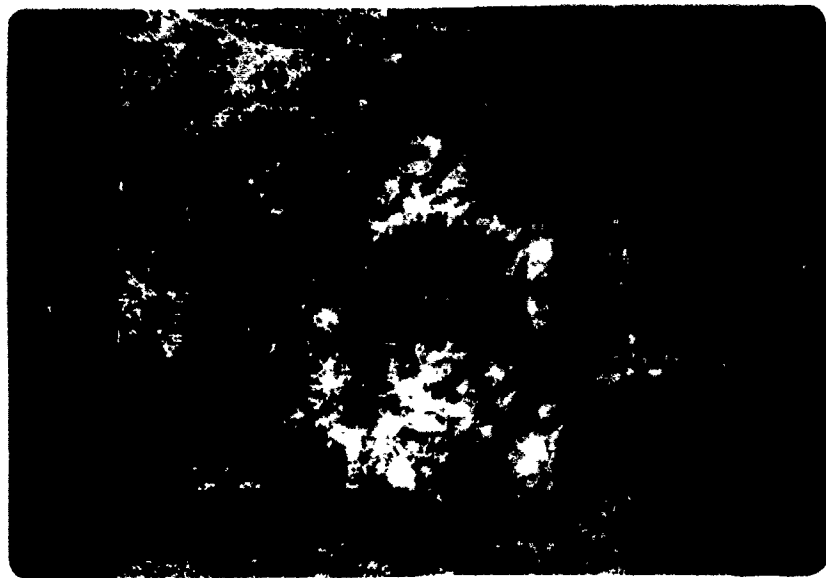
Plate 6. Classification map, May 12, 1974 Degelen area.

N

0 _____ 15
KM
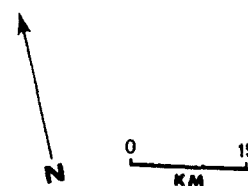
Plate 7. False color composite with overlay of geological
          interpretation, Degelen region. See text for explanation.
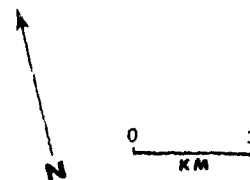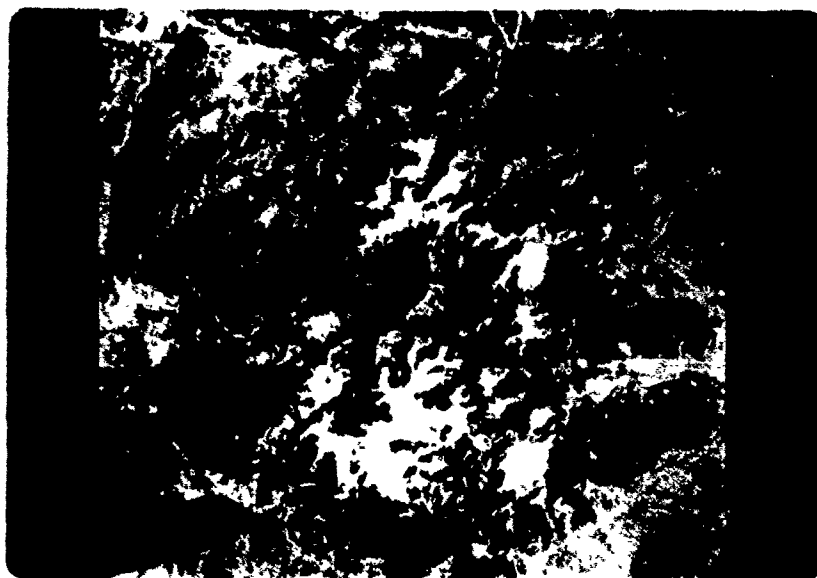
Plate 8. False color composite, Degelen massif, May 12, 1974.
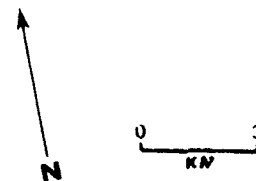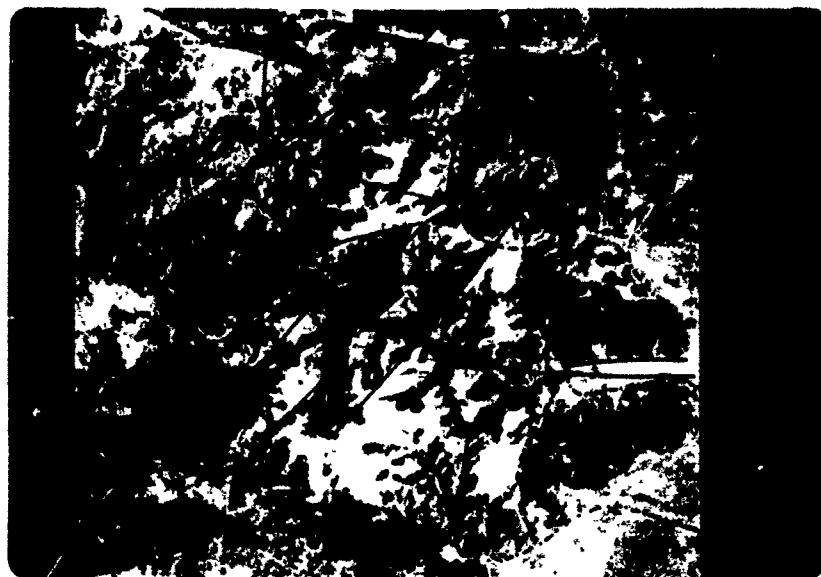
Plate 9. False color composite, Degelen massif, with faults marked.
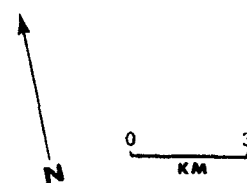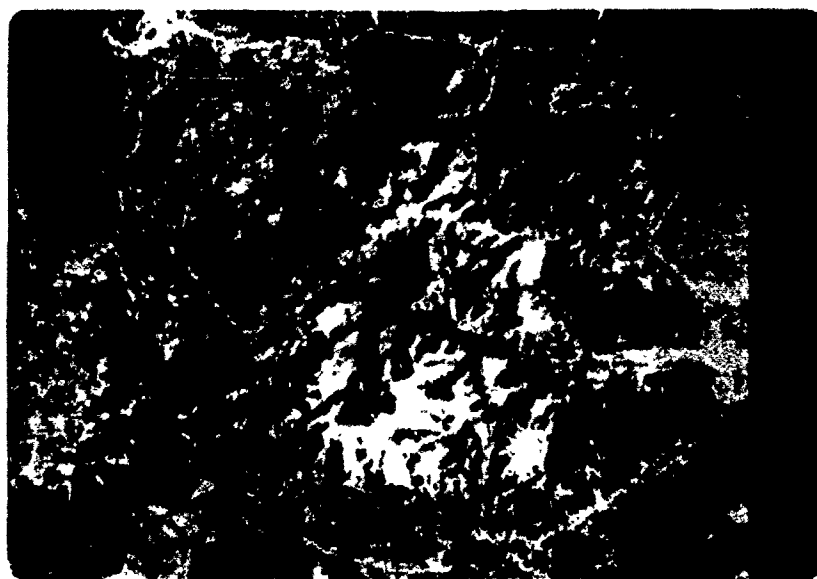
Plate 10. False color composite, May 11, 1976 Degelen Massif.

N

0 ─────── 15
    KM

Plate 11. Ratioed image, Semipalatinsk region. See text for explanation of symbols.
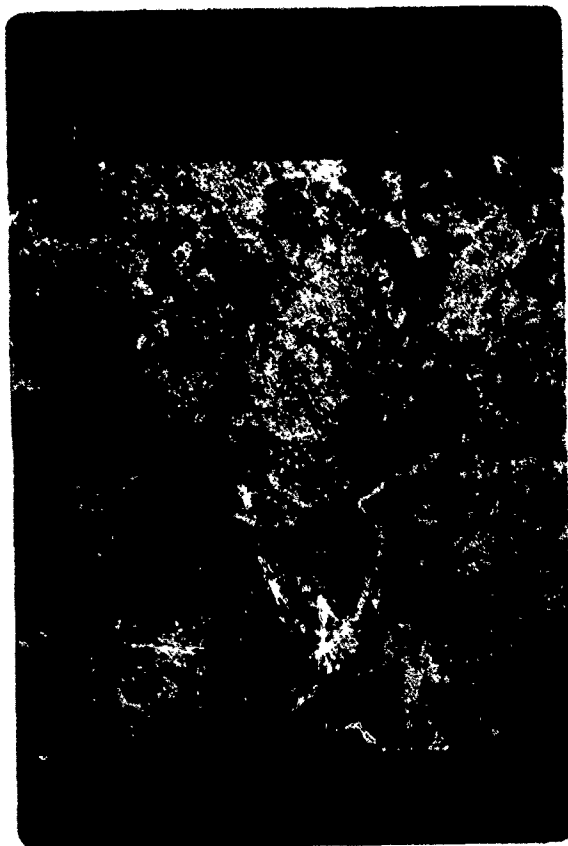
Plate 12. Principal component image, Semipalatinsk region. L - Dry lake beds.

0 _____ 15
KM

N
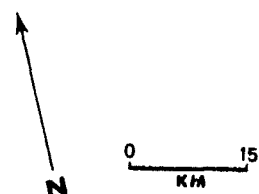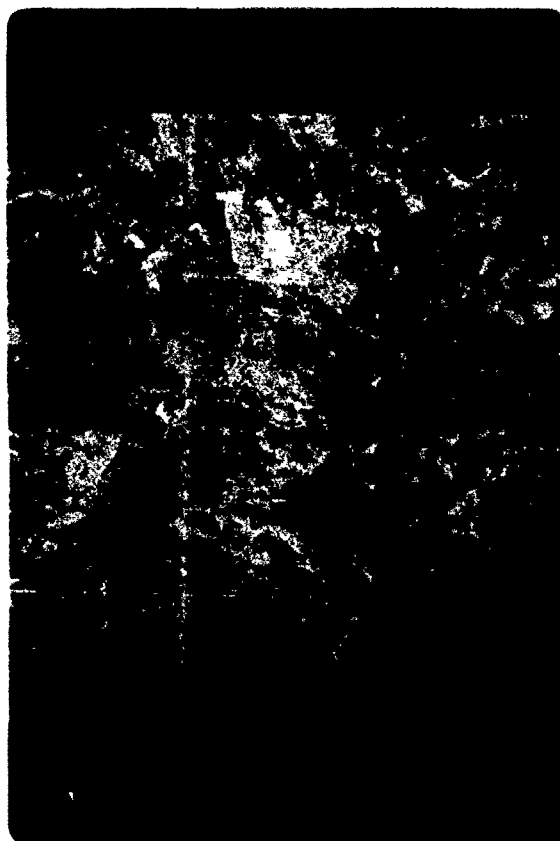
Plate 13. Principal component "2-2-2" image, first and second axes used, Semipalatinsk region. L - Dry lake beds.
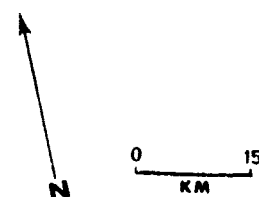
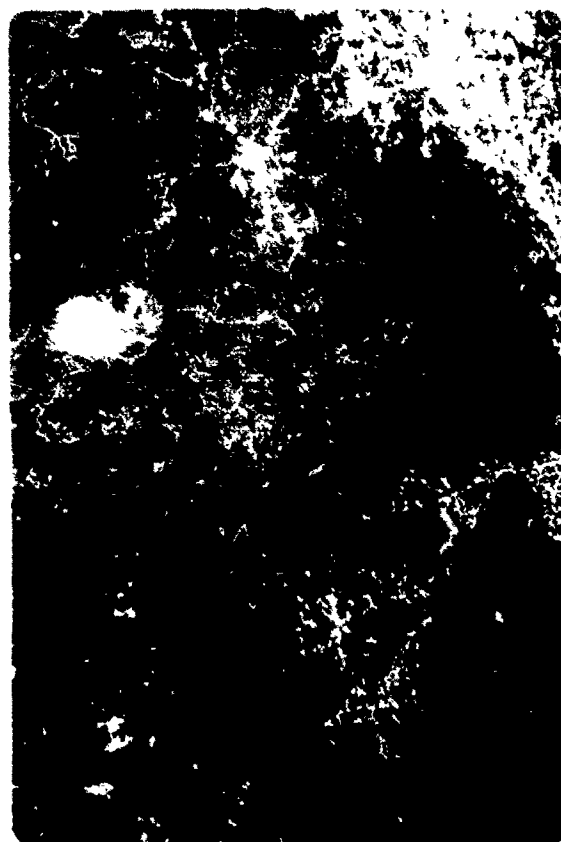Plate 14. Principal component and ratio combination image, Semipalatinsk region.
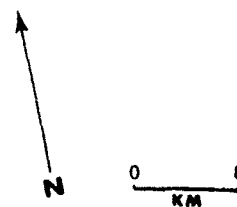
Plate 15.   False color composite, Katahdin study region, August 1976
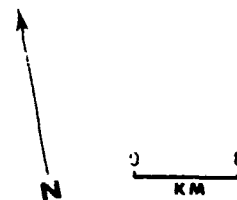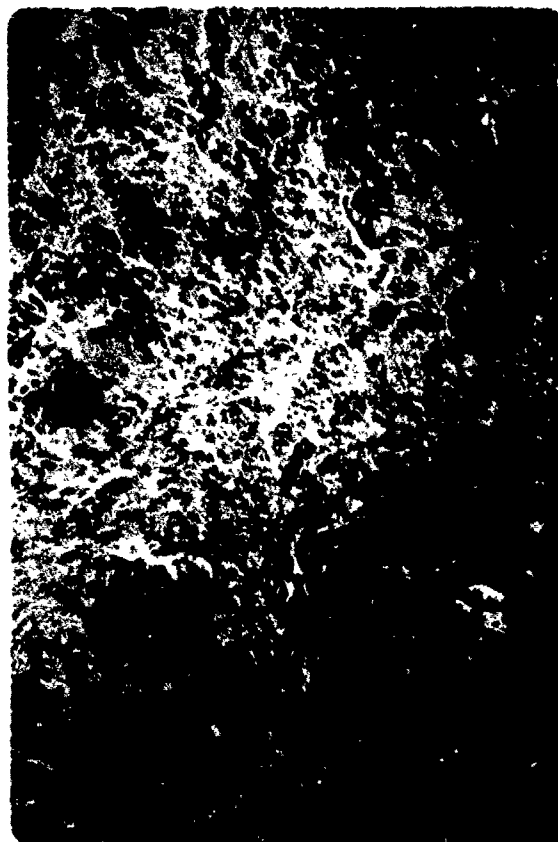scene.

N

0 — 8
KM

Plate 16.   Ratioed scene, August 1976 Mount Katahdin region.   Mount
Katahdin location indicated.

Plate 17. Rationed scene, Mount Katahdin region with geological interpretation. See text for explanation.
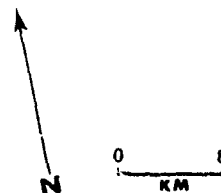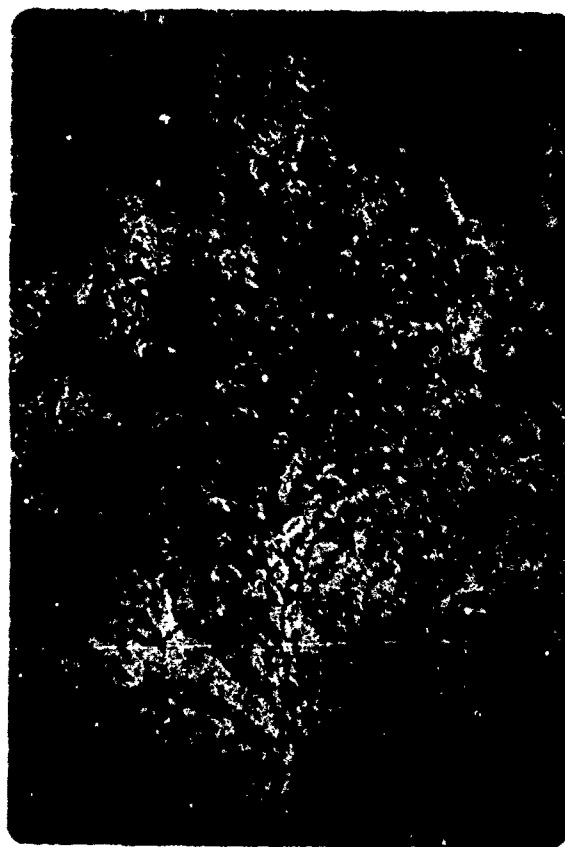
Plate 18. Principal components image, Mount Katahdin region. Locations of Traveler Mountain and Mount Katahdin indicated.

BIBLIOGRAPHY

Abotteen, R. et al. 1977. Performance test of signature extension algorithms. Proc. Intl. Symp. on Remote Sensing of Environment, 11th, pp. 1-10. Ann Arbor, Mich.: Environmental Research Institute of Michigan.

Abrams, Michael J. 1980. Lithologic mapping. In Remote Sensing in Geology, pp. 381-418. Edited by Barry S. Siegal and Alan R. Gillespie. New York: John Wiley & Sons.

Allingham, John 1964. Geologic and magnetic map of northern Maine. U. S. Geol. Survey Geophysical Investigations Map GP-312.

Ayuso, Robert A. and Wones, David R. 1980. Geology of the Bottle Lake Complex. In A Guidebook to the Geology of Northeastern Maine and Neighboring New Brunswick, pp. 32-48. Edited by D. Roy and R. Naylor. New England Intercol. Geol. Conf.

Ballew, Gary 1977. Alteration mapping at Goldfield, Nevada, by cluster analysis and discriminant analysis of Landsat digital data. Proc. Intl. Symp. on Remote Sensing of Environment, 11th, pp. 783-785. Ann Arbor, Mich.: The Environmental Research Institute of Michigan.

Blodget, H. W.; Gunther, F. J.; and Podwysocki, M. H. 1978. Discrimination of rock classes and alteration products in southwestern Saudi Arabia with computer-enhanced Landsat data. NASA Technical Paper 1327.

Boucot, Arthur J. 1959. Stratigraphy of the Moose River Synclinorium, Maine. U. S. Geol. Survey Bulletin 1111-E.

Caldwell, Dabney W. 1972. The Geology of Baxter State Park and Mt. Katahdin, rev. ed. Augusta: Maine Geological Survey, Dept. of Forestry.

_____ 1980. Alpine glaciation of Mt. Katahdin. In A Guide to the Geology of Northeastern Maine and Neighboring New Brunswick, pp. 80-82. Edited by D. Roy and R. Naylor. New England Intercol. Geol. Conf.

Dave, J. V. 1980. The effect of atmospheric conditions on remote sensing of a surface nonhomogeneity. Photogrammetric Engineering and Remote Sensing, 46, pp. 1173-1180.

Dixon, W. J. et al. 1981. BMDP Statistical Software 1981. Berkeley: The University of California Press.

EROS Data Center 1982. Landsat Data Users Notes. Sioux Falls, S. D.: U. S. Geological Survey. Issue No. 22. March, 1982.

Espenshade, G. H. and Boudette, E. L. 1967. Geology and petrology of the Greenville Quadrangle, Piscataquis Counties, Maine. U. S. Geol. Survey Bulletin 1241.

Espenshade, G. H. 1972. Geology of the Moxie Pluton in the Moosehead Lake-Jo-Mary Mountain area, Piscataquis County, Maine. U. S. Geol. Survey Bulletin 1340.

Eyton, J. Ronald 1982a. Hybrid Image Classification Instructional Package. Photogrammetric Engineering and Remote Sensing (in review).

Eyton, J. Ronald 1982b. Personal communication.

Fraser, Robert S. 1969. Effect of the Atmosphere on Electromagnetic Sensing of the Earth's Resources from a Remote Platform. Redondo Beach, California: TRW Systems.

Gaydos, Leonard and Newland, Willard L. 1978. Inventory of land use and cover of the Puget Sound region using Landsat digital data. U. S. Geol. Survey Jour. Research, 6, pp. 807-814.

Genes, Andrew N. 1980. Outline of the Pleistocene glaciation of northern Maine and adjacent Canada. In A Guidebook to the Geology of Northeastern Maine and Neighboring New Brunswick, pp. 23-31. Edited by D. Roy and R. Naylor. New England Intercol. Geol. Conf.

Gillespie, Alan R. 1980. Digital techniques of image enhancement. In Remote Sensing in Geology, pp. 139-226. Edited by Barry S. Siegal and Alan R. Gillespie. New York: John Wiley & Sons.

Goetz, Alex F. H. and Rowan, Lawrence C. 1981. Geologic remote sensing. Science, 211, pp. 781-791.

Helwig, Jane and Council, Kathryn A. 1979. SAS User's Guide. Cary, North Carolina: The SAS Institute.

Hoffer, R. M.; Fleming, M. D.; and Drebs, P. V. 1974. Use of Computer-aided Analysis Techniques for Cover-type Mapping in Areas of Mountainous Terrain. West Lafayette, Ind.: Lab. for Appl. of Rem. Sensing, Purdue University.

Holben, Brent H. and Justice, Christopher 1980. The topographic effect on spectral response from nadir-pointing sensors. Photogrammetric Engineering and Remote Sensing, 46, pp. 1479-1485.

Hon, Rudolph 1980. Geology and petrology of igneous bodies within the Katahdin Pluton. In A Guidebook to the Geology of Northeastern Maine and Neighboring New Brunswick, pp. 65-79. Edited by D. Roy and R. Naylor. New England Intercol. Geol. Conf.

Ministry of Geology of the USSR. 1968. Geology of the USSR. Leningrad.

Morrison, O. F. 1976. Multivariate Statistical Methods. New York: McGraw-Hill (2nd Edition).

Pavlides, Louis; Griscom, Andrew; and Kane, Martin F. 1965. Geology of the Bridgewater Quadrangle, Aroostook County, Maine. U. S. Geol. Survey Bulletin 1206.

Raines, Gary L. and Canney, Frank C. 1980. Vegetation and geology. In Remote Sensing and Geology, pp. 365-380. Edited by Barry S. Siegal and Alan R. Gillespie. New York: John Wiley & Sons.

Rankin, Douglas W. 1968. Volcanism related to tectonism in the Piscataquis Volcanic Belt, an island arc of Early Devonian age in north-central Maine. In Studies of Appalachian Geology, Northern and Maritime, pp. 355-369. Edited by E-an Zen, et al. New York: Interscience Publishers.

_____ 1980. The Traveler Rhyolite and its Devonian setting. In A Guidebook to the Geology of Northeastern Maine and Neighboring New Brunswick, pp. 98-113. Edited by D. Roy and R. Naylor. New England Intercol. Geol. Conf.

Ravenhurst, Casey E. 1980. Utility of Digitally Merged Seasat-A SAR, Landsat MSS, and Magnetic Field Data Sets for Mapping Lithology and Structure in a Vegetated Terrain. Unpublish Master's Thesis. University Park, Pa.: The Pennsylvania State University.

Rowan, L. C. et al. 1974. Discrimination of rock types and detection of hydrothermally altered areas in south-central Nevada by the use of computer-enhanced ERTS images. U. S. Geol. Survey Prof. Paper 883.

Roy, David C. 1980. Tectonics and sedimentation in northeastern Maine and adjacent New Brunswick. In A Guidebook to the Geology of Northeastern Maine and Neighboring New Brunswick, pp. 1-21. Edited by D. Roy and R. Naylor. New England Intercol Geol. Conf.

Salisbury, John W. and Hunt, Graham R. 1974. Remote sensing of rock type in the visible and near-infrared. Proc. Intl. Symp. on Remote Sensing of Environment, 9th, pp. 1953-1958. Ann Arbor, Mich.: Environmental Research Institute of Michigan.

Siegal, Barry S. and Abrams, Michael J. 1976. Geologic mapping using Landsat data. Photogrammetric Engineering and Remote Sensing, 42, pp. 325-337.

Siegal, Barry S. and Goetz, A. F. H. 1977. Effect of vegetation on rock and soil discrimination. Photogrammetric Engineering and Remote Sensing, 43, pp. 191-196.

Siegrist, Alicia and Schnetzler, Charles C. 1980. Optimum spectral bands for rock discrimination. Photogrammetric Engineering and Remote Sensing, 46, pp. 1207-1215.

Slater, Philip N. 1979. A re-examination of the Landsat MSS. Photogrammetric Engineering and Remote Sensing, 45, pp. 1479-1485.

Smith, J. A.; Lin, Tzeu Lie; and Ran, K. J. 1980. The Lambertian assumption and Landsat data. Photogrammetric Engineering and Remote Sensing, 46, pp. 1183-1189.

Taranik, James V. 1978. Principles of computer processing of Landsat data for geologic applications. U. S. Geol. Survey Open File Report 78-117.

Turner, B. J.; Baumer, G. M. and Myers, W. L. 1982. The ORSER Remote Sensing Analysis System: A User's Manual. The Pennsylvania State University: The Office for Remote Sensing of Earth Resources. Research Publication 109/OR.

Turner, Robert E. 1975. Signature variations due to atmospheric effect. Proc. Intl. Symp. on Remote Sensing of Environment, 10th, pp. 671-675. Ann Arbor, Mich.: Environmental Research Institute of Michigan.

Verstappen, H. Th. 1977. Remote Sensing in Geomorphology. Amsterdam: Elsevier Scientific Publishing Co, pp. 11-14.

White, Walter S. 1968. Generalized geologic map of the northern Appalachian region. U.S. Geological Survey Open-File Map. In Studies of Appalachian Geology, Northern and Maritime, pp. 452. Edited by E-an Zen et al. New York: Interscience Publishers.

Wong, Kam W. 1976. Automatic terrain mapping. FCP Research Review Conference. University Park, Pennsylvania: The Pennsylvania State University.

Zietz, Isidore et al. 1980. Magnetic anomaly map of the Appalachian Orogen. St. John's: The Memorial University of Newfoundland.